

AD A 052026

DNA 4155F

# ALUMINUM RING THERMOSTRUCTURAL RESPONSE STUDY

12

Physics International Company  
2700 Merced Street  
San Leandro, California 94577

November 1977

Final Report for Period March 1976—September 1976

CONTRACT No. DNA 001-76-C-0246

AD No.   
DDC FILE COPY

APPROVED FOR PUBLIC RELEASE;  
DISTRIBUTION UNLIMITED.

THIS WORK SPONSORED BY THE DEFENSE NUCLEAR AGENCY  
UNDER RDT&E RMSS CODE B342076464 N99QAXAA12115 H2590D.

Prepared for  
Director  
DEFENSE NUCLEAR AGENCY  
Washington, D. C. 20305

DDC  
RECEIVED  
MAR 30 1978  
B

**Best  
Available  
Copy**

(18) DNA, SBTIF

(19) +155F

UNCLASSIFIED

AD-E300 129

SECURITY CLASSIFICATION OF THIS PAGE (When Data Entered)

REPORT DOCUMENTATION PAGE		READ INSTRUCTIONS BEFORE COMPLETING FORM	
1. AUTHOR	2. GOVT ACCESSION NO.	3. REPORT NUMBER	4. REPORT DATE
DNA 41551		12 102p-1	
5. TITLE (and Subtitle)	6. AUTHOR	7. TYPE OF REPORT & PERIOD COVERED	8. PERFORMING ORGANIZATION NAME AND ADDRESS
ALUMINUM RING THERMOSTRUCTURAL RESPONSE STUDY	V./Buck J./Shea	Final Report for Period Mar - Sep 76	Physics International Company 2700 Merced Street San Leandro, California 94577
9. MONITORING AGENCY NAME & ADDRESS (if different from Controlling Office)	10. PROGRAM ELEMENT PROJECT, TASK AREA & WORK UNIT NUMBERS	11. REPORT DATE	12. SECURITY CLASS (of this report)
	Subtask N99QAXAA121-15	Nov 77	UNCLASSIFIED
13. DISTRIBUTION STATEMENT (of this Report)	14. NUMBER OF PAGES	15. DECLASSIFICATION DOWNGRADING SCHEDULE	
Approved for public release; distribution unlimited.	108		
16. DISTRIBUTION STATEMENT (of the abstract entered in Block 20, if different from Report)			
17. SUPPLEMENTARY NOTES			
This work sponsored by the Defense Nuclear Agency under RDT&E RMSS Code B342076464 N99QAXAA12115 H2590D.			
18. KEY WORDS (Continue on reverse side if necessary and identify by block number)			
Thermostructural Response Radiation Heating Electron Beams			
19. ABSTRACT (Continue on reverse side if necessary and identify by block number)			
The response of aluminum rings subjected to sudden radiation heating was experimentally investigated using pulsed electron beams. The DNA OWL II generator, operating at a nominal mean voltage of 1.0 MeV, provided the radiation environment. Transport of the electron beam from the diode to the target was achieved using a longitudinal magnetic field. The aluminum rings were 8 inches in diameter, 2-inches wide, and 0.12 inch thick.			

DD FORM 1 JAN 73 1473 EDITION OF 1 NOV 65 IS OBSOLETE

UNCLASSIFIED

SECURITY CLASSIFICATION OF THIS PAGE (When Data Entered)

282 760

File

UNCLASSIFIED

SECURITY CLASSIFICATION OF THIS PAGE (When Data Entered)

20. ABSTRACT (Continued)

1085 The rings were rigidly clamped over a 10 degree segment opposite from the irradiated side. Circumferential strain data were obtained on the inner surface of the rings at 0°, 45°, 90°, 135°, and 170° with respect to the axis of the electron beam. Transverse strain data were also obtained at 0°. Quartz gauge stress measurements were performed on flat aluminum specimens simultaneously with the ring experiments. The response was also observed with fast motion pictures (4000 frames/sec). Data were obtained at fluences that varied between 5 cal/cm<sup>2</sup> (elastic response) and 20 cal/cm<sup>2</sup> (elastic-plastic response).

ACCESSION for	
NTIS	White Section <input checked="" type="checkbox"/>
DOC	Buff Section <input type="checkbox"/>
UNANNOUNCED	<input type="checkbox"/>
JUSTIFICATION _____	
BY _____	
DISTRIBUTION/AVAILABILITY CODES	
Dist. AVAIL. and/or SPECIAL	
A	

UNCLASSIFIED

SECURITY CLASSIFICATION OF THIS PAGE (When Data Entered)

# CONTENTS

	<u>Page</u>
PREFACE	3
SECTION 1 INTRODUCTION	5
SECTION 2 EXPERIMENTAL APPARATUS AND TECHNIQUES	7
2.1 Experimental Configuration	7
2.2 Electron Beam Diagnostics	9
2.3 Structural Response Diagnostics	16
SECTION 3 EXPERIMENTAL RESULTS	19
3.1 Calorimetry Data	19
3.2 Structural Response Data	25
SECTION 4 CONCLUSIONS AND RECOMMENDATIONS	30
REFERENCES	31
APPENDIX A FLUENCE MAPS	33
APPENDIX B MEASURED AND CALCULATED DEPOSITION PROFILES IN CARBON	57
APPENDIX C-1 CALCULATED DEPOSITION PROFILES IN ALUMINUM NORMAL INCIDENCE	61
APPENDIX C-2 CALCULATED DEPOSITION PROFILES IN ALUMINUM ASSUMING 30° ANGLE OF INCIDENCE AND TUBE VOLTAGE INCREASED BY 7 PERCENT	67
APPENDIX C-3 CALCULATED DEPOSITION PROFILES IN ALUMINUM ASSUMING 60° ANGLE OF INCIDENCE AND TUBE VOLTAGE INCREASED BY 7 PERCENT	71
APPENDIX D STRAIN GAUGE RECORDS--OSCILLOSCOPE DATA	75
APPENDIX E QUARTZ GAUGE RECORDS	95

## ILLUSTRATIONS

<u>Figure</u>		<u>Page</u>
1	Electron Beam Test Geometry	8
2	Target Configuration Showing Aluminum Ring with Curved Carbon Calorimeters on Each Side	10
3	Detail of Aluminum Ring Showing Clamp on Right and Strain Gauge Installations	11
4	Flat Graphite Calorimeter	14
5	Depth Dose Calorimeter Showing 0.020-inch- Graphite Foils and 1.125-inch Aperture	15
6	Block Diagram of Strain Gauge Instrumentation	17
7	Bridge Circuit Schematic	17
8	Fluence Uniformity on OWL II Thermostructural Response Experiments	21
9	Normalized Fluence Versus Distance from Cathode	23
10	Variation in Fluence with Angular Position for Cylindrical Targets	24
11	Permanent Change in the Diameter of 8-inch- Aluminum Rings Produced by Irradiation with 1.0 MeV Electrons	28

## PREFACE

The work described in this report was performed by Physics International Company for the Defense Nuclear Agency under contract DNA001-76-C-0246. The principal investigator at Physics International was Mr. E. V. Buck, who was assisted by Mr. C. Felts and Mr. A. York. The project supervisor was Dr. James Shea. The efforts were coordinated with Dr. A. O. Burford of Lockheed Missiles and Space Company and Mr. P. G. Underwood of the Lockheed Palo Alto Research Laboratory. The project monitor was Mr. Donald Kohler, DNA, SPAS Division.

## SECTION 1

### INTRODUCTION

This report describes thermostructural response testing performed for the Defense Nuclear Agency (DNA), utilizing pulsed electron beams to induce thermal loads in aluminum rings. The pulsed electron beams were generated by the DNA OWL II Facility at Physics International Company. The aluminum rings were 2-inches wide, 8 inches in diameter, and 0.121-inch thick. The primary response data consisted of measurements of dynamic strain in the circumferential and transverse directions on the inner surface of the rings.

The objectives of the program were to measure the response generated in these rings at two thermal loading conditions. The first condition was pulsed heating just below the level required to produce permanent deformation of the ring. The second condition was heated substantially above the threshold for permanent deformation. Data were successfully obtained for both these conditions and for two additional levels above the threshold for permanent deformation.

The structural response data collected in this program will be used by Lockheed Missiles and Space Company (LMSC) for modeling studies and comparison with computer code predictions under Contract DNA001-75-C-0175. Lockheed personnel (Dr. A. O. Burford and P. G. Underwood) participated in the design of the experiments and selection of test conditions. Test specimens were provided by LMSC as well.

*Preceding Page BLANK -*



Description of the Experimental Apparatus, Techniques, and Procedures is presented in Section 2. The Experimental Results are described in Section 3, and the Conclusions and Recommendations are given in Section 4.

## SECTION 2

### EXPERIMENTAL APPARATUS AND TECHNIQUES

#### 2.1 EXPERIMENTAL CONFIGURATION

The OWL II electron beam generator was used to produce rapid thermal loading of the aluminum rings. The accelerator is a pulse charged system, consisting of an oil immersed, 1/3 MJ Marx generator and a water-insulated coaxial transmission line pulse transformer, which provides the pulseforming network (Reference 1). The accelerator configuration employed for the testing reported here utilized a 120 nsec pulseforming line, a 1.8 ohm output impedance transformer, and a 9-inch diameter circular cathode.

The electron beam test geometry is shown schematically in Figure 1. The electron beam is generated by a field emission cathode and passes through a transmission anode (0.0005-inch thick titanium) into the experimental chamber. A graphite aperture with an 8-inch-inside diameter and a second 0.0005-inch-thick titanium foil are located just behind the anode. The graphite absorbed the intense portion of the beam that originates at the perimeter of the cathode and effectively prevented anode material from reaching the test specimen. A magnetic lens was used to control and transport the electron beam from the cathode emission surface to the target. This produces an electron beam that retains the cross-sectional shape of the cathode, but the area of the beam varies inversely with the magnetic lens ratio; hence the beam fluence is directly proportional to the magnetic lens ratio. Fluence uniformity is controlled to first order by dish-ing the cathode to compensate for the bow of the anode produced by the 1 torr gas pressure in the test chamber.

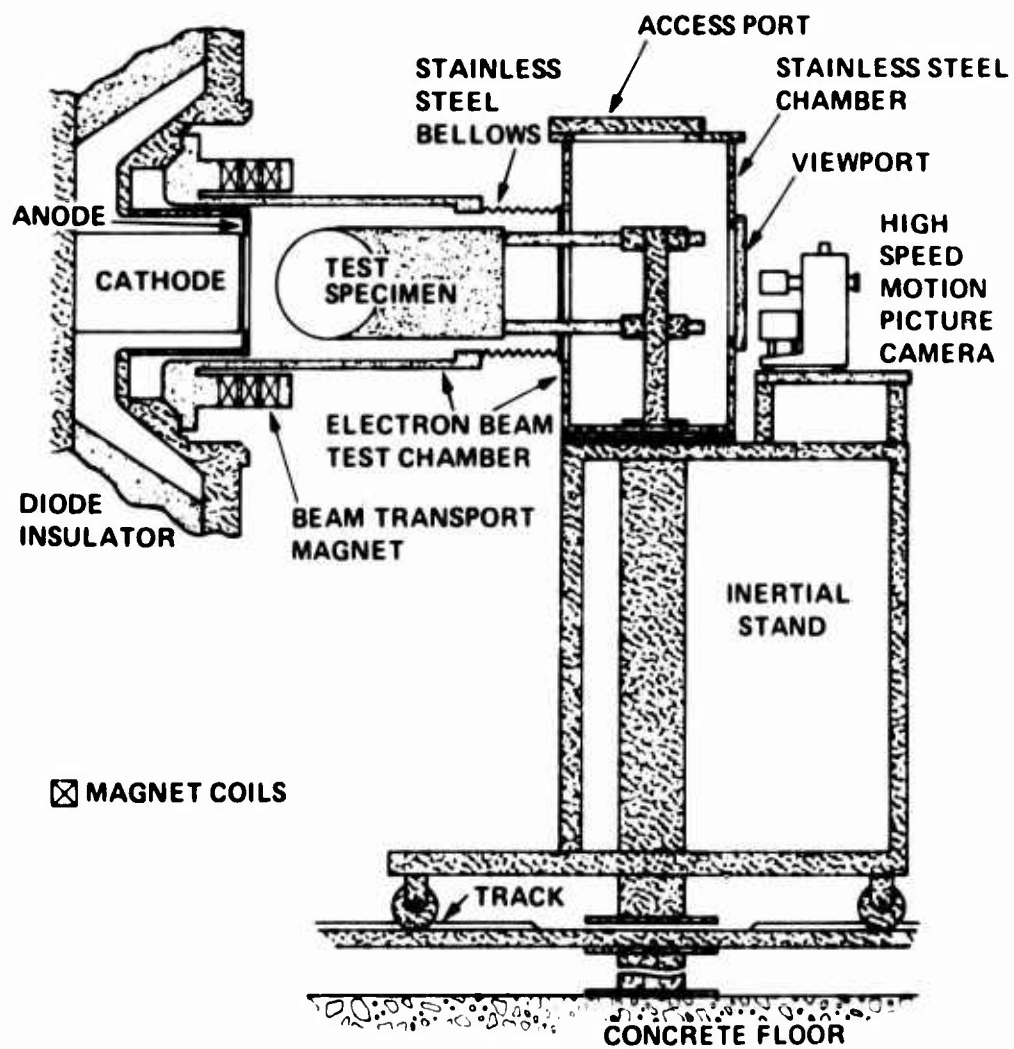


Figure 1 Electron beam test geometry.

The target holder details are shown in Figures 2 and 3. The rings were clamped rigidly over a 0.5 inch segment (7.2 degrees of arc) centered at the 180 degree position (0 degree position faces cathode). The clamping apparatus, in turn, was mounted on an inertial stand bolted to the concrete floor. This arrangement is necessary to prevent shock waves generated in the machine from affecting the experiment. A curved calorimeter was mounted on each side of the ring. The central blocks of the calorimeter on the left side were replaced by a mount for a flat coupon of the test material. The coupon was instrumented with a quartz pressure transducer for simultaneous stress-time measurements. The curved calorimeter blocks were one inch wide and each encompassed a 20 degree segment of arc, except for those immediately adjacent to the quartz gauge, which comprised a 15 degree segment of arc. An arm on one side of the ring specimen held the light source and a mirror for photographic coverage of the test specimens.

## 2.2 ELECTRON BEAM DIAGNOSTICS

Diagnostics used in characterization of the electron beam were employed both in the diode and at the target location. The diode diagnostics consisted of a voltage monitor, a set of  $\dot{B}$  probes, and a set of current monitors. The voltage monitor is a capacitive voltage divider embedded in the diode insulator. The  $\dot{B}$  probes are magnetic field sensors that have an output proportional to the time rate of change of the magnetic field associated with the diode current. The diode current monitors consist of Rogowski coil segments that are  $\dot{B}$  probes with built-in integrators so that the output is directly proportional to diode current. Four  $\dot{B}$  probes and two Rogowski coil segments were on the anode plate located on a diameter just inboard of the inside diameter of the diode insulator. Two full Rogowski coils surrounded the cathode: one was in the anode plate, and the other was in the anode extension near the cathode tip.

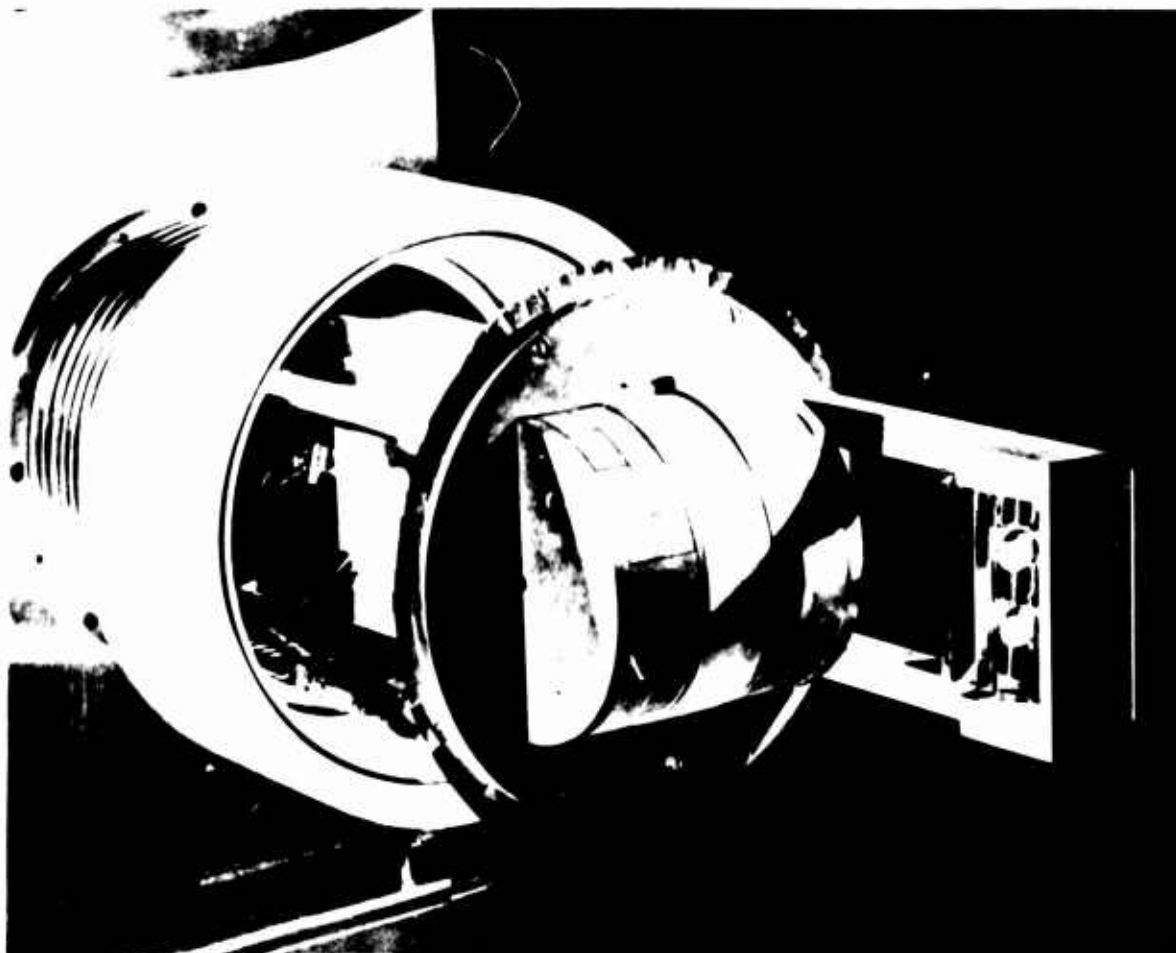


Figure 2 Target configuration showing aluminum ring with curved carbon calorimeters on each side. Lights and mirror are to the right: Quartz gauge in center of left calorimeter.



Figure 3 Detail of aluminum ring showing clamp on right and strain gauge installations.

The diode diagnostics were recorded with fast oscilloscopes (typically 150 MHz bandwidth). The oscilloscope data were digitized and analyzed on the Physics International Interactive Data Reduction Facility. The facility includes a digitizing tablet, a keyboard and graphics display unit, a hard copy unit, a 64K word mini-computer, and a code which interactively receives, analyzes, and plots the data. The data analysis includes correction of the input data for any RC and L/R slumps inherent in the monitors, calculation of the accelerator voltage, and calculation of quantities such as the total beam energy and mean electron energy.

The accelerator voltage,  $V_{acc}$ , was determined from the equation:

$$V_{acc} = V_{monitor} - L \frac{dI}{dt}$$

or

$$V_{ac} = V_{monitor} - L \times \left( \text{constant} \times \frac{dB}{dt} \right)$$

where

$V_{monitor}$  is the voltage measured by the voltage monitor after correction for RC slump

$L$  is the diode inductance

$I$  is the diode current

and the constant is the ratio  $I/B$  at the location of the  $\dot{B}$  probe. The product  $L \times \text{constant}$  was determined by comparing  $V_{monitor}$  to the  $B$  probe when the cathode was shorted to the anode (i.e.,  $V_{ac} = 0$ ).

The acceleration voltage and diode current waveforms were used directly in the PIED Monte Carlo Code (Reference 2) to calculate electron beam energy deposition profiles for correlation with measurements.

The beam diagnostics used at target location consisted of fluence and deposition profile calorimeters. On data shots the primary diagnostic used at target location was the peripheral curved calorimeter array (Figure 2). A complete calorimeter array, shown in Figure 4, was used for initial fluence mapping and determining fluence uniformity. The calorimeters are constructed of ATJ graphite blocks mounted on fiberglass boards with aluminum screws. Each block was instrumented with an iron-constantan thermocouple. The thermocouple signals were recorded by a scanning digital voltmeter. Fluences were calculated with a PI mini-computer program, using polynomial fits to handbook enthalpy curves for ATJ graphite and aluminum.

The electron beam energy deposition profile was investigated with a graphite foil stack calorimeter, shown in Figure 5. The foils were 0.020-inch-thick ATJ graphite foils held in position by polyethylene blocks. The foils were instrumented with iron-constantan thermocouples, which were clamped against a copper tab attached to an edge of each foil. The thermocouple signals were read out with the same scanning digital voltmeter system described previously. The deposition profiles were calculated with a PI mini-computer program using polynomial fits to the enthalpy curves for ATJ graphite and copper.



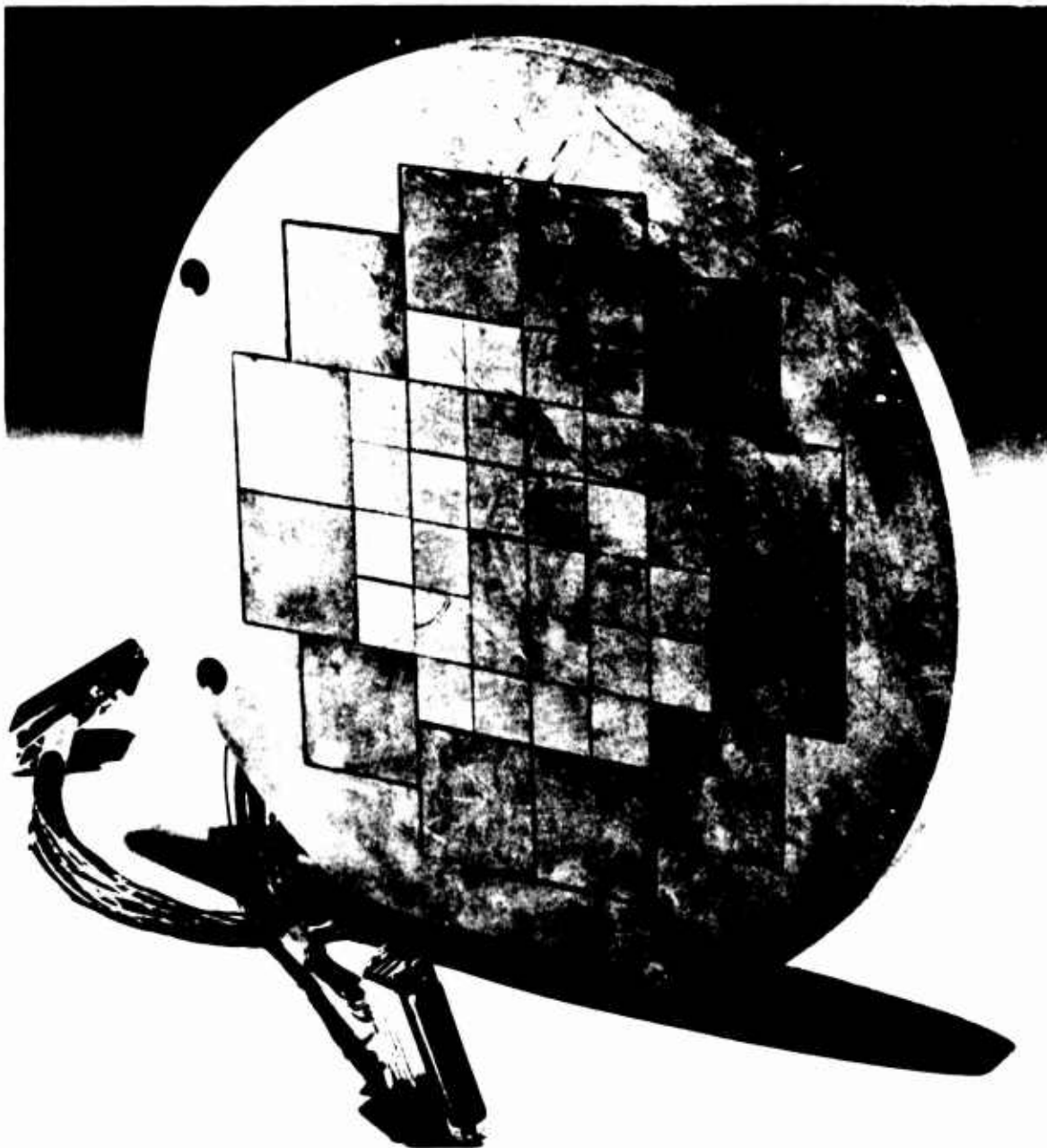


Figure 4 Flat graphite calorimeter. Central blocks are 1-inch square. Peripheral blocks are 2-inch square.

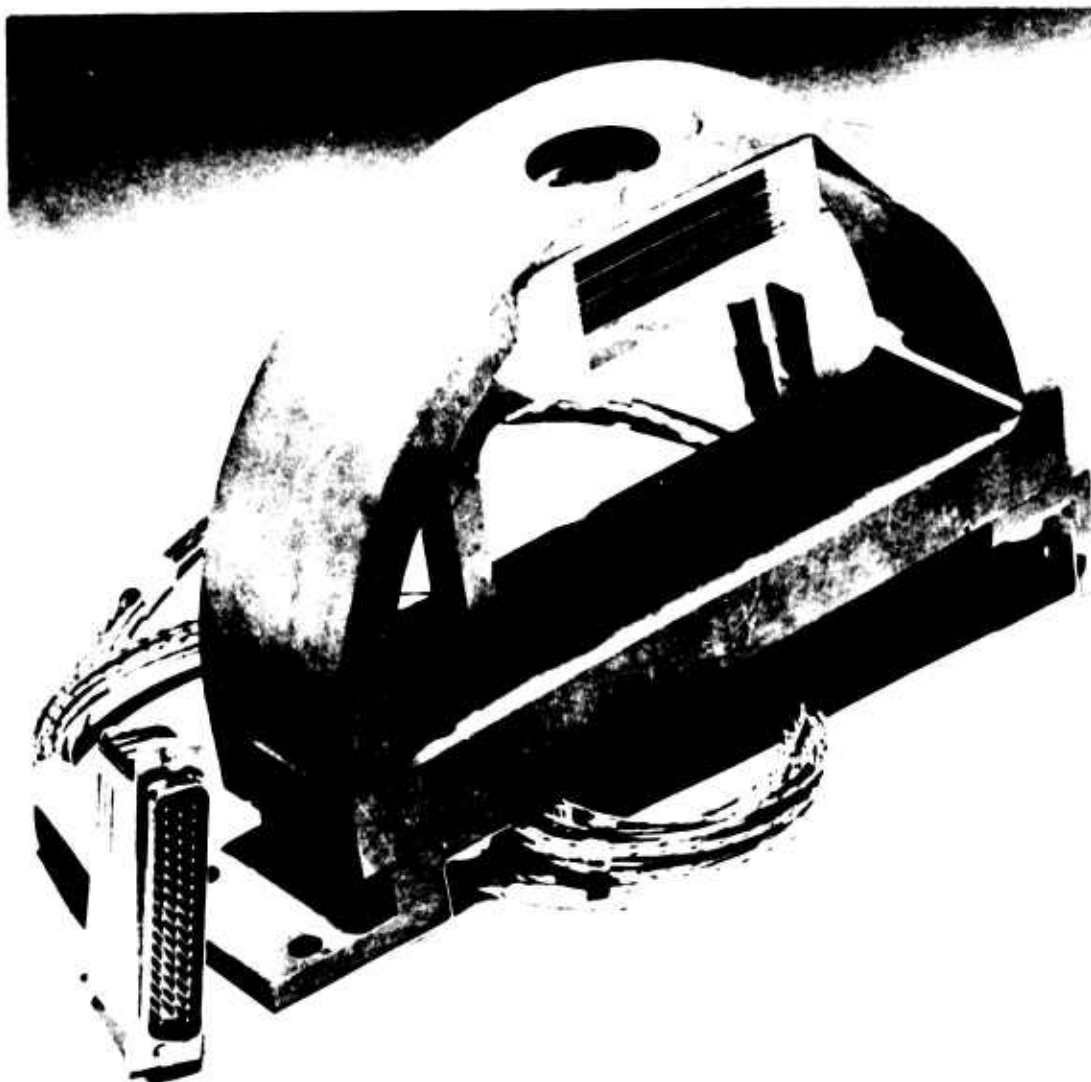


Figure 5 Depth dose calorimeter showing 0.020-inch-graphite foils and 1.125-inch aperture.

### 2.3 STRUCTURAL RESPONSE DIAGNOSTICS

Structural response induced by pulsed electron beam irradiation of the aluminum rings was measured using strain gauges and high speed motion pictures. The strain gauge data acquisition system was essentially the same as used during previous experiments on cantilevered beams (Reference 3). The system was expanded to six channels as part of this program. A block diagram of one channel of this system is shown in Figure 6. A schematic of the basic bridge circuit is shown in Figure 7. A common dc power supply was used to set up and balance each bridge circuit; individual pulsed power supplies were used during data collection. Considerable attention was paid to noise reduction. Double shielding was used wherever possible, with the inner shield of each channel single-point grounded to the amplifier chassis. The outer shield, which enclosed all six channels, extended from the ring itself to the electronics rack.

A set of small magnetic field compensation loops located close to the ring were used to tune out signals induced by the pulsed magnetic beam guide. These tuning loops were enclosed in a Faraday cage which was designed to shield the electrical noise from the electron beam but remain transparent to the magnetic beam guide. This is feasible because the relevant frequencies differ by at least five orders of magnitude (hence the skin depths differ by more than two orders of magnitude).

The recording instrumentation consisted of Preston Model 83C0XWB-B differential amplifiers, a Hewlett-Packard Model 3924B tape recorder, and various oscilloscopes. The bandwidth of oscilloscope data was limited to about 100 kHz by the Preston amplifiers and the bandwidth for the tape recorder data was limited to about 20 kHz by the tape recorder amplifiers.

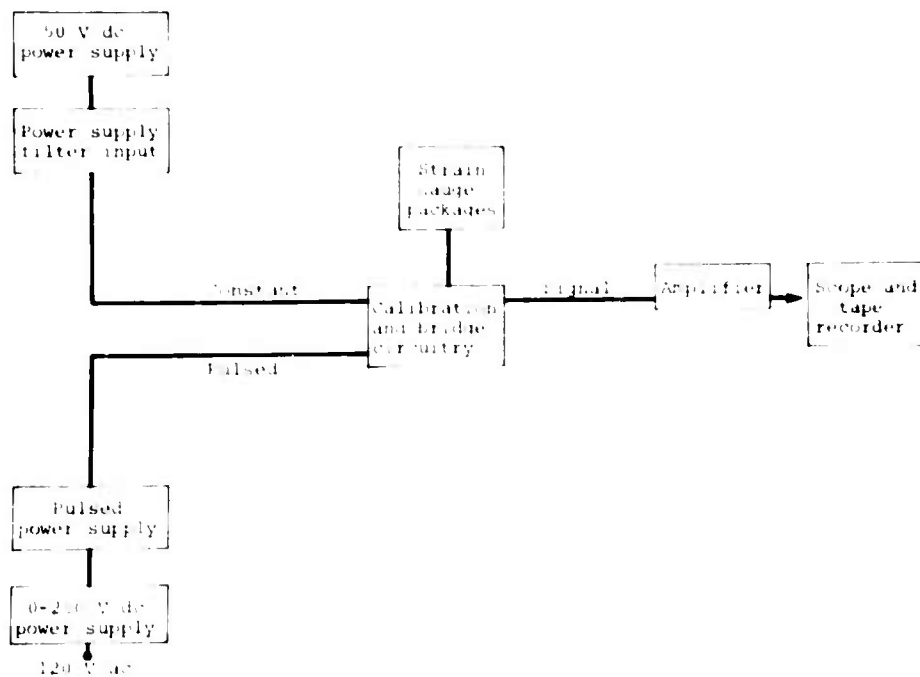


Figure 6 Block diagram of strain gauge instrumentation.

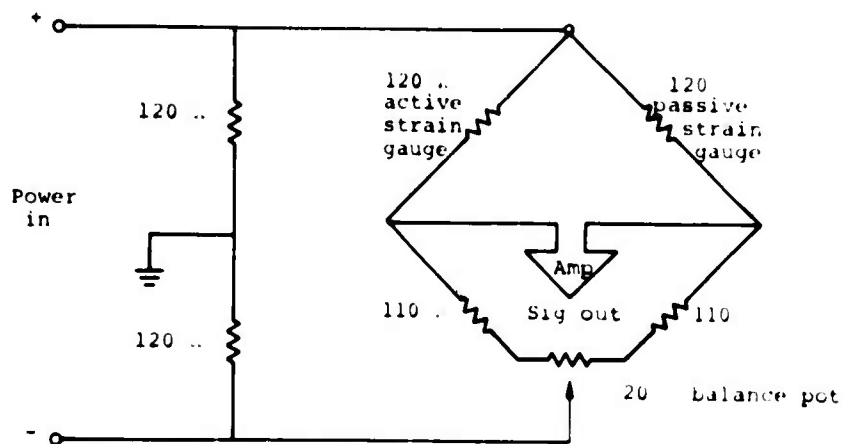


Figure 7 Bridge circuit schematic.

The strain gauges were located on the inner surface of the ring at 0, 45, 90, 135, 170, and -45 degrees. (0 degree is closest to the cathode). All gauges were oriented to measure circumferential strain, except that on some experiments the -45 degree gauge was replaced by a transversely oriented gage at -10 degrees. Each strain gauge package consisted of two gauges, an active gauge bonded to the cantilevered beam and a passive gauge mounted directly above the active gauge, mechanically decoupled from the ring with a styrofoam pad. The passive gauge comprised one leg of the bridge circuit and served to cancel spurious signals induced in the active gauge by the pulsed magnetic field used to guide the beam and the pulsed electron beam itself. The gauges directly behind the volume of irradiation were Micromasurements Type EA13 125AV-120 (option B64) strain gauges; the other gauges were Micromasurements Type EA13 125AD-120 strain gauges. The active elements of both types of gauges are identical. The difference between the gauges is that the gauges used behind the volume of irradiation have long foil leads that allow the solder tabs to be acoustically decoupled from the ring. This reduces the probability that gauge failure will be induced by the thermomechanical stress pulse.

Gauges were bonded to the rings with Micromasurements Type M-Bond 610 adhesive. The cure cycle employed was approximately 45 minutes warm-up, followed by approximately 60 minutes at 300°F, followed by approximately 45 minutes cool-down.

Motion of the front region of the ring was recorded with a high speed motion picture system mounted at the rear of the test chamber. The photographic record was taken with a Red Lakes Lab Model 1C 2051E "Hycam" operating at a framing rate of about 4000 frames per second. The camera was enclosed by a 1-inch-thick lead box in order to minimize X-ray fogging of the high speed film.

## SECTION 3

### EXPERIMENTAL RESULTS

#### 3.1 CALORIMETRY DATA

The fluence maps collected on this program are presented in Appendix A. The data are summarized in Table 1. For the flat calorimeter, the tabulated average fluence is for the 32 central 1-inch-square blocks. The mean square deviation (MSD) from the average value is included to indicate the degree of fluence uniformity. For the curved calorimeter, the tabulated average fluence is the average of the two blocks at the 0 degree position. Also tabulated in Table 1 are the mean energy per electron and the total beam energy, calculated from diode diagnostics, and the cathode to target distance.

The fluence uniformity is shown graphically in Figure 8, where the calorimeter block (flat array) readings are plotted for four pulses as a function of the distance from the center of the array. For the higher fluence levels, some fall-off is seen at the outer edges, which is due to the fact for these levels the outmost blocks were only partially illuminated by the beam. The two outermost sets of blocks extend to 5.4 inches and 5.6 inches respectively from the center of the array.

In Figure 9 the average fluence, normalized by the total beam energy, is shown as a function of the cathode to target distance. Superimposed on the data points is a plot of the

TABLE 1 SUMMARY OF FLUENCE MAP DATA

Pulse Number	Cathode-Target Distance (in.)	Target <sup>*</sup> Type	Average Fluence (cal/cm <sup>2</sup> )	M.S.D. (cal/cm <sup>2</sup> )	Total Energy (kJ)	Mean Electron Energy (MeV)
2834	21.1	C	2.4	0.4	61	1.07
2835	16	C	3.9	0.5	45	0.97
2836	15	C	5.4	0.4	56	1.02
2838	15	DD	5.1		56	1.03
2839	15	R			64	1.16
2840	15	C	5.9	0.7	56	0.99
2841	15	R	4.6		54	0.72
2845	15	DD	7.4		60	0.86
2846	15	DD	6.7		58	0.86
2847	15	R	7.0		58	0.95
2848	13.5	C	7.8	0.6	56	0.86
2849	10	C	14.7	1.0	60	0.98
2851	10	C	14.8	1.1	57	0.93
2852	10	R	14.3		53	0.96
2853	10	R	15.0		55	0.97
2854	12.5	C	10.5	0.7	57	0.92
2855	12.5	R	10.2		58	0.98
2856	12.5	DD	8.2		55	0.95
2857	12.5	R	11.0		56	0.95
2858	7.5	C	21.5	1.6	58	0.94
2859	7.5	R	17.5		48	0.98
2860	7.5	R	23.2		54	0.93
2861	8.5	R	18.5		57	0.91
2862	8.5	C	16.8	1.5	56	0.93

\* C Flat calorimeter

DD Depth dose measurement

R Ring irradiation

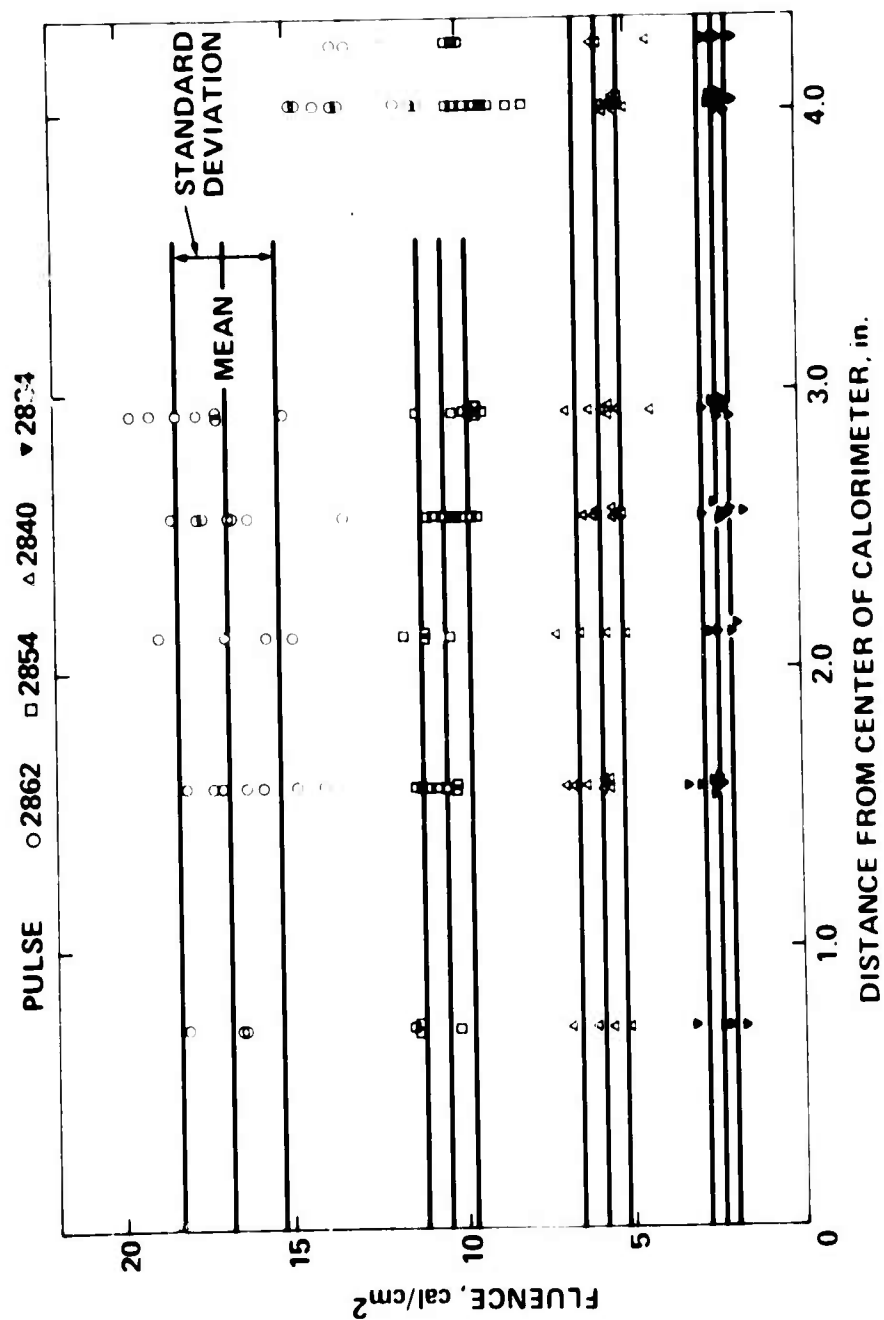


Figure 8 Fluence uniformity on OWL II thermostructural response experiments.



beam guide magnetic field strength, in arbitrary units, versus cathode to target distance. The normalized fluence is seen to follow the field strength quite closely, confirming the results of an earlier study of this experimental configuration (Reference 4).

In a previous ring program (Reference 5) it was found that the fluence over the surface of the ring varied as the cosine of the angle. In that program the maximum fluence was approximately  $115 \text{ cal/cm}^2$  and the beam guide magnetic field was essentially paraxial (i.e., no divergence). Data from the curved calorimeters are shown in Figure 10 for two of the data pulses. The predicted fluence and its angular dependence, assuming a cosine variation, are shown for each pulse in the figure. The predictions are based upon the calculated diode energies and include the variation in fluence with distance from the cathode. The variation for a cosine dependence only is shown for comparison purposes for Pulse 2861. Comparing the data to the predictions, it is seen that the observed falloff with angular position is somewhat greater than the cosine variation. The reason for this behavior is not presently understood.

The electron beam energy deposition profile measurements are shown in Appendix B. These data are compared to electron beam energy deposition profiles calculated from the acceleration voltage and diode waveforms. The calculations assume normal incidence and are shown for the diode voltage as measured, and for the diode voltage increased by a factor of 1.07 which gives somewhat better agreement. A 7 percent correction to the voltage calibration of the monitor is not considered to be beyond the uncertainty limits of the calibration technique. Albedo

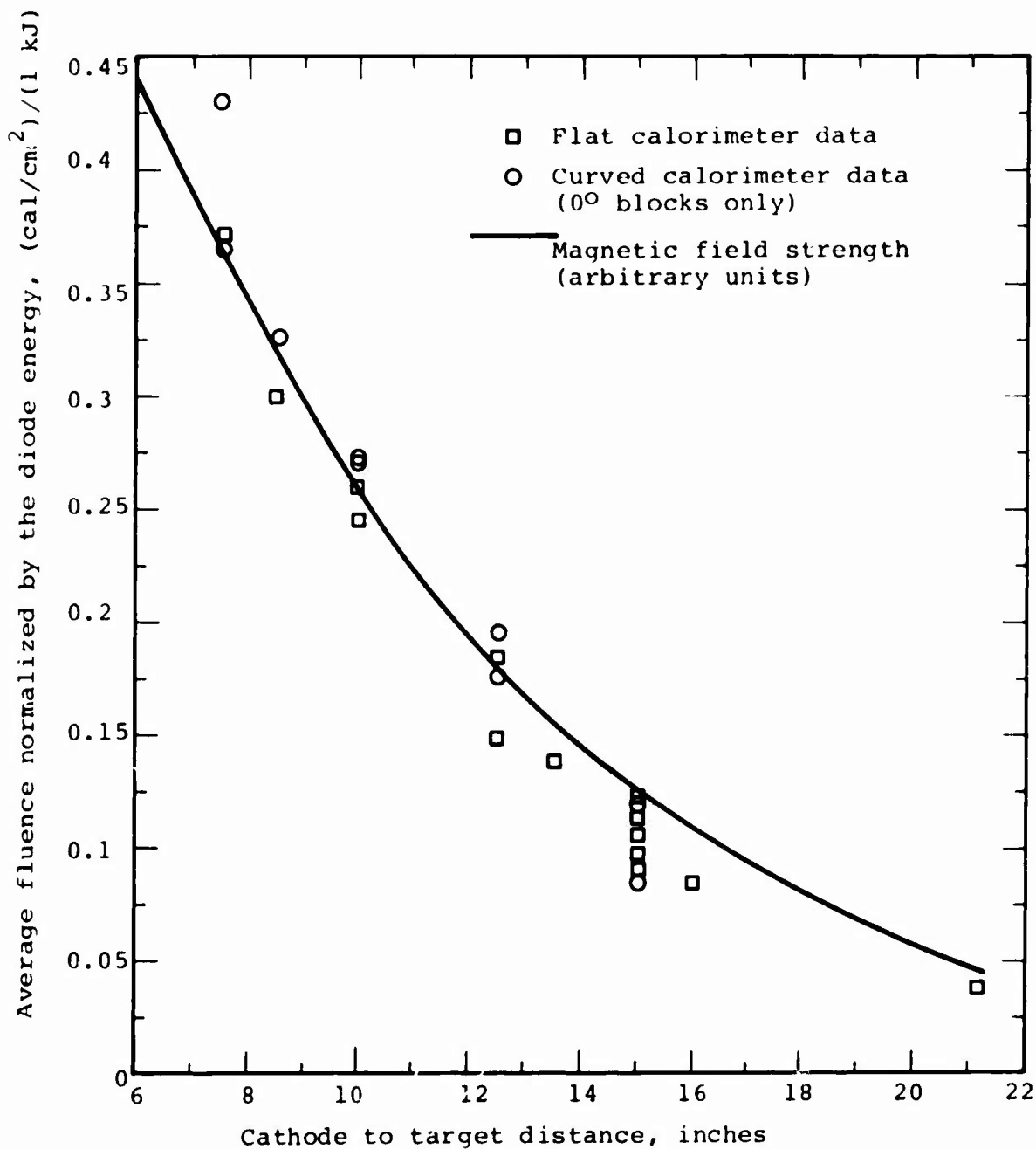



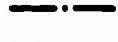



Figure 9 Normalized fluence versus distance from cathode.

Pulse 2861	{		Calorimeter data, Pulse 2861
			Computed from Figure 9, multiplied by cosine "
			Zero degree fluence from Figure 8, multiplied by cosine "
Pulse 2855	{		Calorimeter data, Pulse 2855
			Computed from Figure 9, multiplied by cosine "

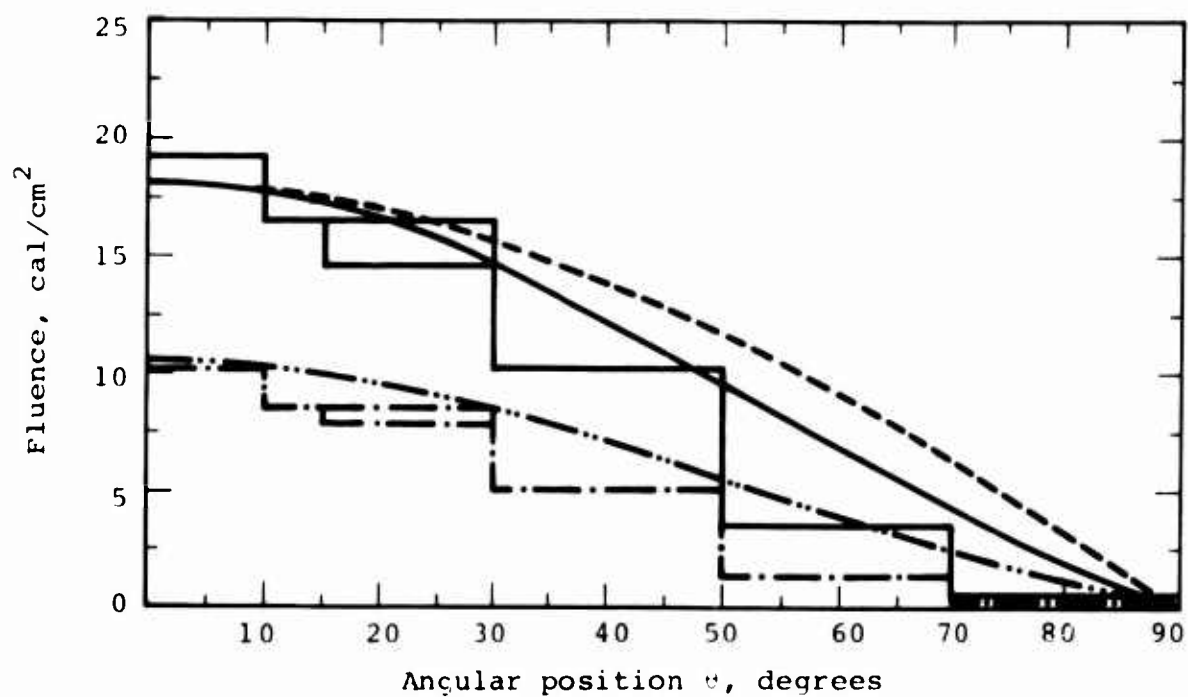


Figure 10 Variation in fluence with angular position for cylindrical targets.

suppression was not considered for these calculations since only 3 to 4 percent of the incident energy is reflected for this beam condition. Deposition profile calculations for the ring experiments are presented in Appendix C. These were calculated in the same manner as for Appendix B.

### 3.2 STRUCTURAL RESPONSE DATA

The structural response data pulses are summarized in Table 2. The magnetic tape records have been forwarded to LMSC under separate cover. The oscilloscope data are presented in Appendix D. The data are, in general, of excellent quality. Due to the failure of an oscilloscope channel, the slow sweep rate data for channel 2 could not be obtained. These data were, however, subsequently recovered from the magnetic tape records. Strain records were not obtained for Pulse 2859 due to a premature crowbar of the bridge power supplies.

Motion pictures were obtained of all but the three highest dose level pulses. For these three, the mirror and light fixture had to be removed in order to position the ring close to the diode. Motion of the ring is clearly discernable in each of the records obtained. Although primarily intended for qualitative information only, the motion picture records provide confirmation of the trends in the strain gauge records. In particular, the vibrations are seen to damp much more quickly as the amount of plastic deformation increases. The films confirmed that no material impacted the test specimens that could introduce spurious effects.

The quartz gauge records are presented in Appendix E. Records were obtained for all except two pulses, 2855 and 2860, for which faulty gauges are suspected. The signals were very clear and noise free and should provide quantitative information on ring loading conditions.

TABLE 2 SUMMARY OF STRUCTURAL RESPONSE DATA

Pulse Number	Ring S/N	Strain Gauge Configuration	Maximum Fluence (cal/cm <sup>2</sup> )	Data Recovered		
				Strain	Quartz	Film
2839	9	Standard	*	X		X
2841	7	Standard	4.6	X	X	X
2847	2	Transverse	7.0	X	X	X
2852	8	Standard	14.3	X	X	X
2853	3	Transverse	15.0	X	X	X
2855	10	Standard	10.2	X		X
2857	4	Transverse	11.0	X	X	X
2859	1	Transverse	17.5		X	
2860	6	Transverse	23.2	X		
2861	5	Transverse	18.5	X	X	

\* Magnetic beam guide failure--extensive front surface damage to ring.

Measurements of pre-test and post-test ring dimensions are presented in Table 3. The change in diameter is plotted as a function of fluence in Figure 11. A threshold fluence for permanent deformation of about  $6 \text{ cal/cm}^2$  is clearly appropriate for 1.0 MeV electrons. The data suggest that for pulse 2860 the fluence determined from the two 0 degree calorimeters ( $23 \text{ cal/cm}^2$ ) is higher than that indicated by the deformation. If the diode energy is used in conjunction with Figure 9 to estimate the fluence, the data would shift as shown on the figure.

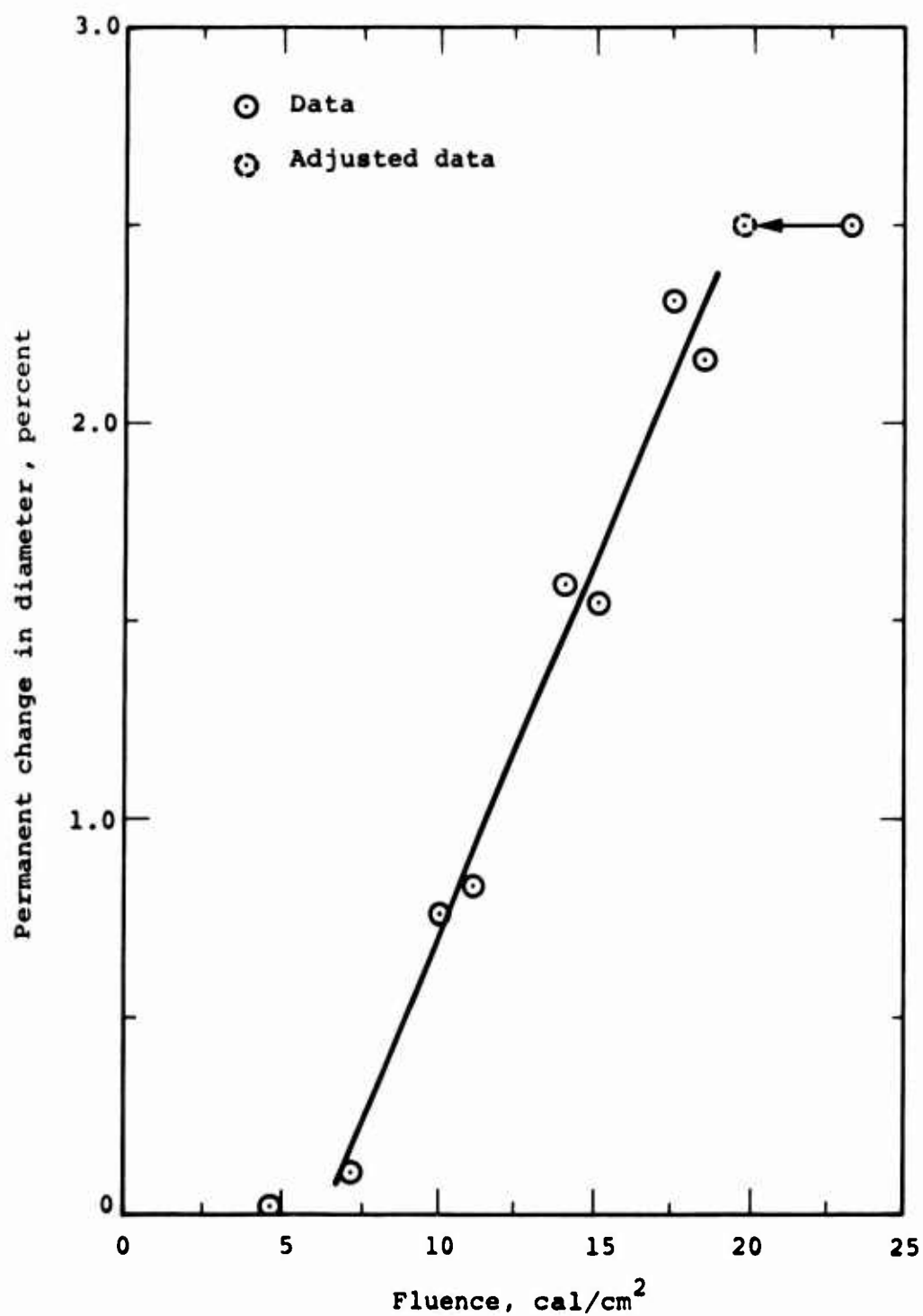


Figure 11 Permanent change in the diameter of 8-inch-aluminum rings produced by irradiation with 1.0 MeV electrons.

TABLE 3 MEASUREMENTS OF RING DIMENSIONS

Pulse Number	Ring S/N	Pre-Test Diameters		Post-Test Diameters		Warp* at 0° (inch)
		0° (inch)	90° (inch)	0° (inch)	90° (inch)	
2839	9	7.994	7.994	7.808	8.098	0.020
2841	7	7.994	7.994	7.992	7.994	0.0
2847	2	7.993	7.993	7.982	8.000	0.002
2852	8	7.990	7.994	7.851	8.103	0.008
2853	3	7.995	7.993	7.861	8.109	0.010
2855	10	7.996	7.995	7.927	8.048	0.004
2857	4	7.995	7.996	7.920	8.054	0.004
2859	1	7.994	7.994	7.792	8.162	0.014
2860	6	7.994	7.994	7.780	8.180	0.015
2861	5	7.997	7.996	7.820	8.166	0.013

\* The warp represents the difference between the diameter at the edge of the ring and the center; it indicates the residual curvature of the ring (at the 0 degree point) in the transverse direction.



## SECTION 4

### CONCLUSIONS AND RECOMMENDATIONS

Dynamic strain gauge data and high speed motion pictures were successfully obtained on 8-inch diameter by 2-inches wide by 0.121-inch-thick aluminum rings that had been irradiated by 1.0 MeV electrons at fluences from 5 to 24 cal/cm<sup>2</sup>. Circumferential strains were measured at six locations on the inner surface of the rings. Transverse strains were measured in the irradiated region on some experiments. Measurements of the stress pulse were obtained concurrently with a quartz pressure transducer bonded to a coupon of the test material. Electron beam diagnostics consisted of diode monitors, flat and curved carbon calorimeters, and carbon foil dosimeters.

Improvements in experimental techniques have resulted in good accelerator reliability and an exceptionally high rate of data recovery. This program has substantially increased the data base available for correlating analytical predictions of thermostructural response. With this background it is appropriate to begin investigations of more complex geometries such as cylinders or frustra, and other materials, such as fiber-reinforced composites. Hence, such experiments are recommended.

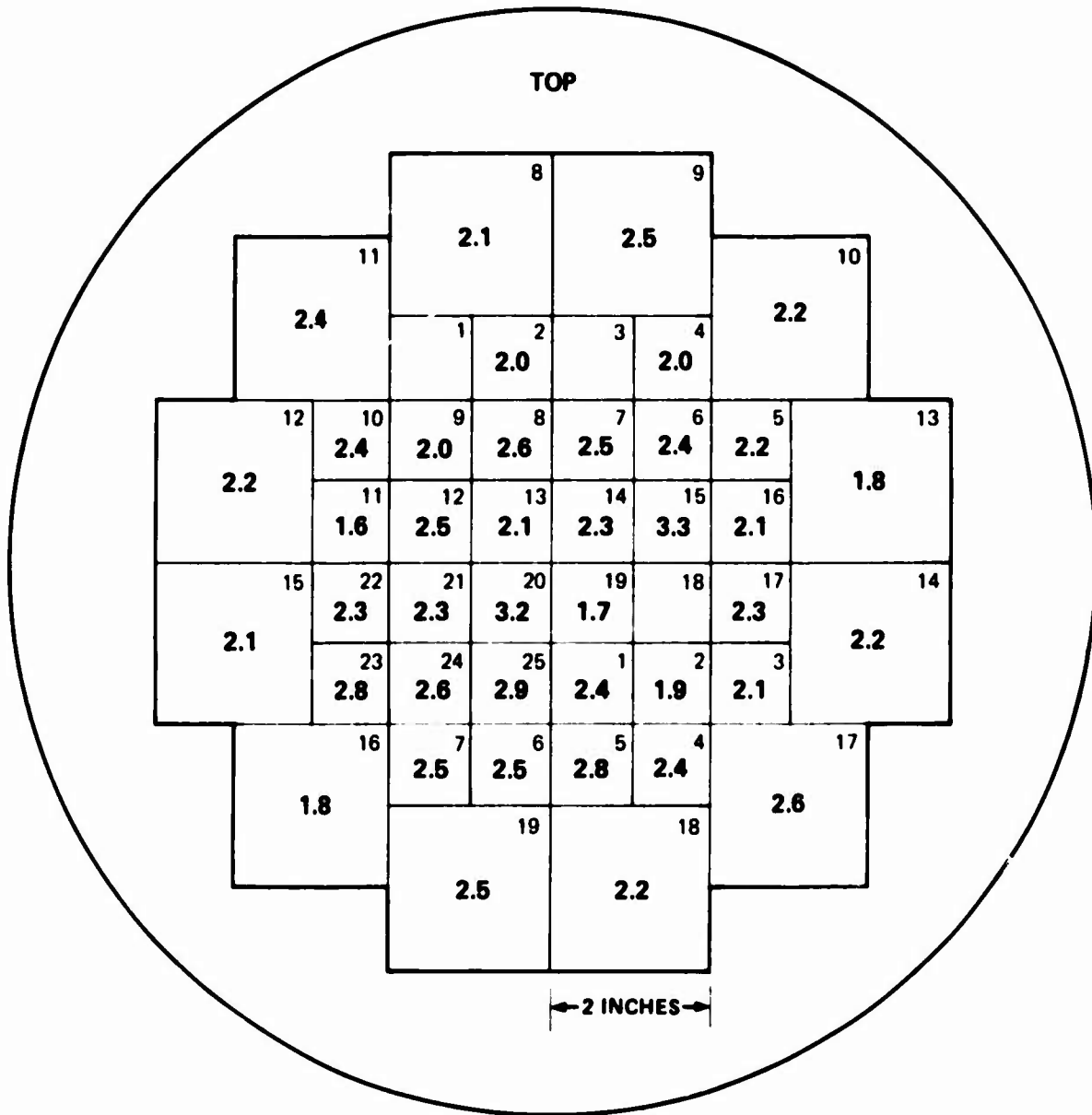
## REFERENCES

1. G. Frazier, K. Nielsen and P. Spence, "OWL II Generator Enhancement and Electron Beam Characterization." (Private Communication.)
2. PIELD Monte Carlo Code, Physics International Company, San Leandro, California.
3. K. Childers, V. Buck, and J. Shea, "Thermostructural Response of Cantilevered Titanium Alloy Beams Subjected to Pulsed Radiation Heating," PIFR-836, Physics International Company, San Leandro, CA., February (1976).
4. K. Childers and J. Shea, "OWL II Diode Study," PIFR-788, Physics International Company, San Leandro, CA., June (1975).
5. K. Childers, V. Buck, and J. Shea, "Carbon-Carbon Thermal Structural Response Testing," AFWL-TR-74-330, Air Force Weapons Laboratory, Kirtland Air Force Base, NM, October (1975).

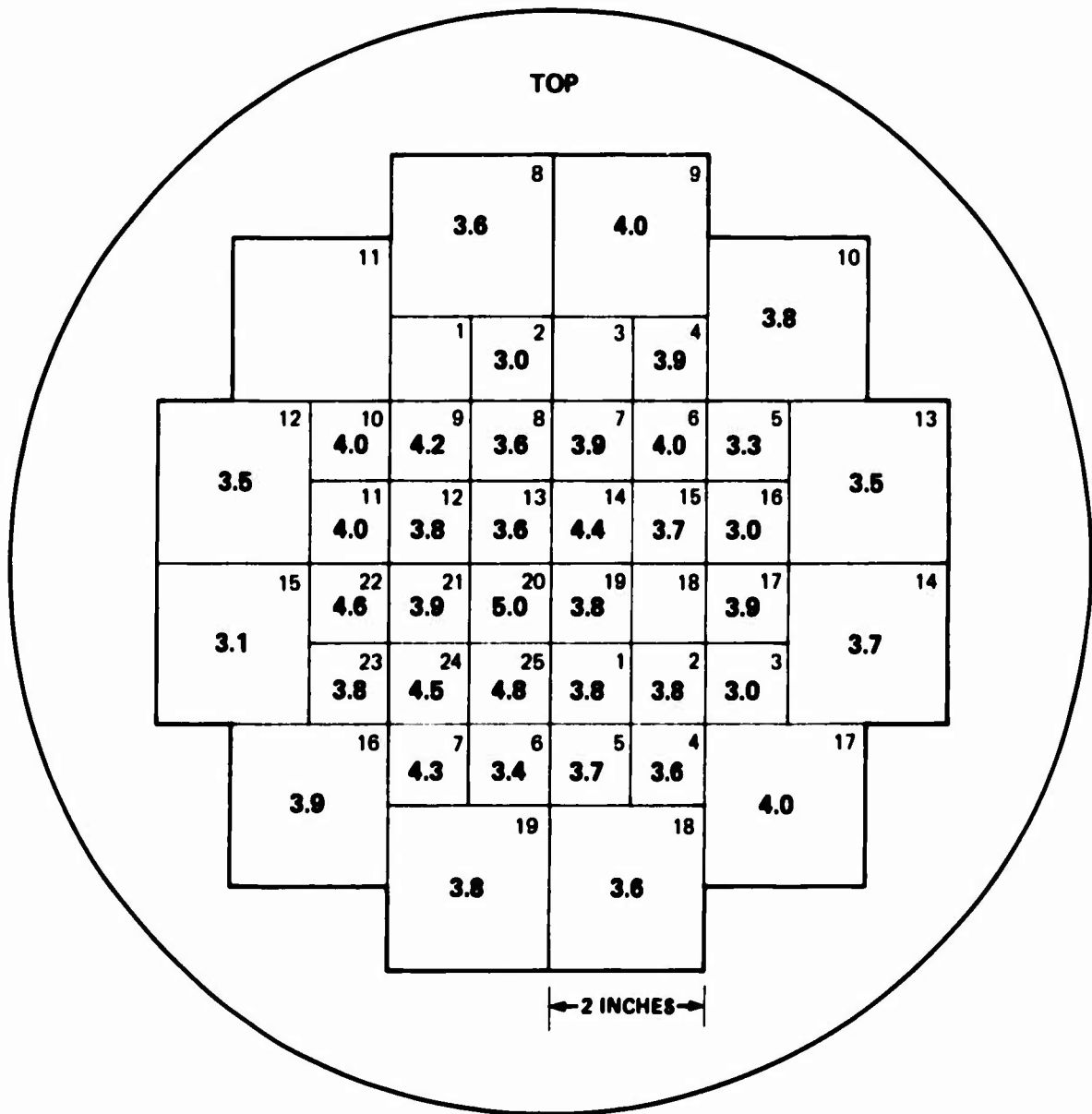
APPENDIX A  
FLUENCE MAPS  
(ALL FLUENCES IN CAL/CM<sup>2</sup>)

*Preceding Page BLANK*

SHOT #2834

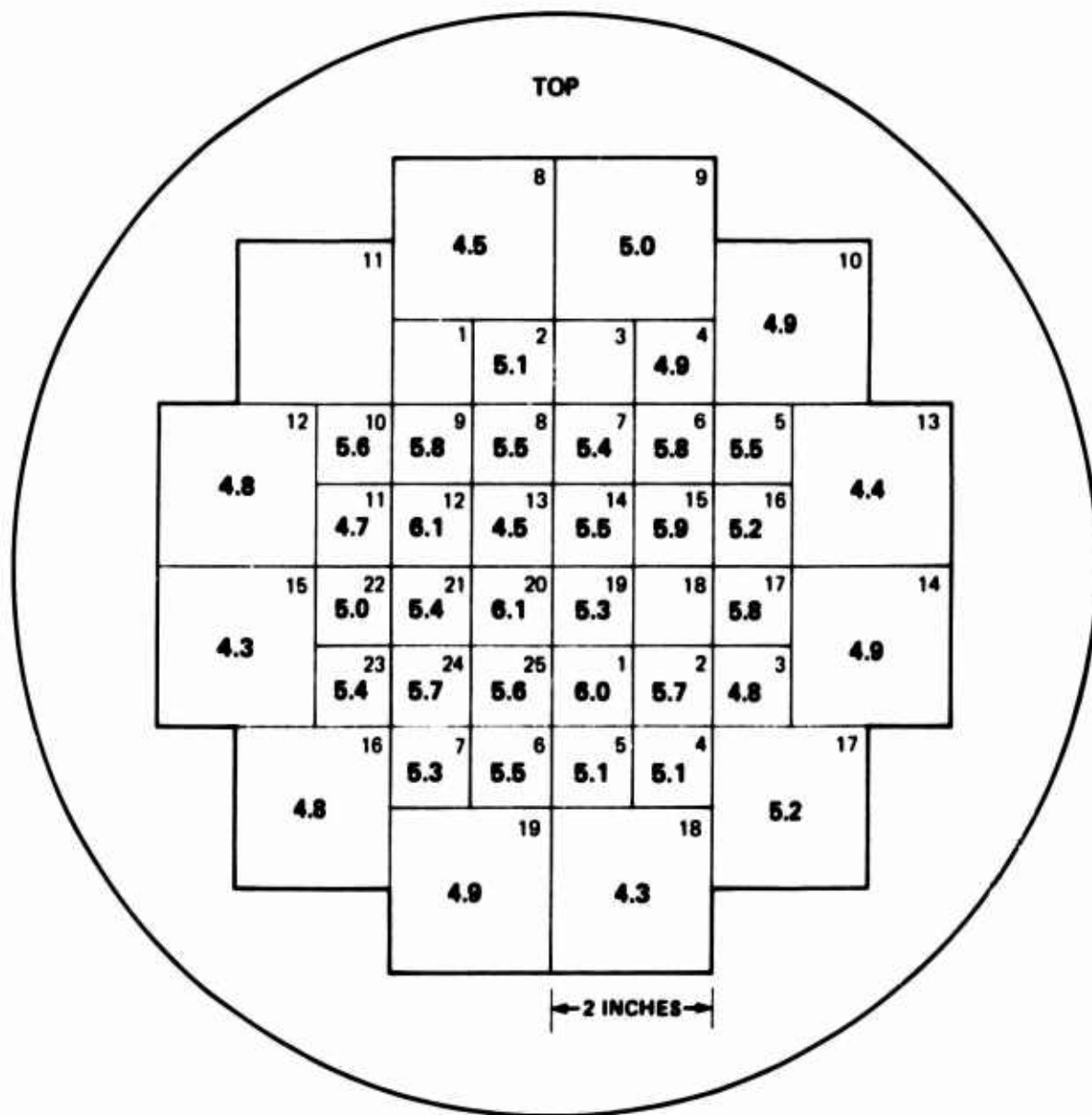


SHOT NO. 2835



SHOT NO. 2836

DATE: 6/25/76



PULSE NO. 2838

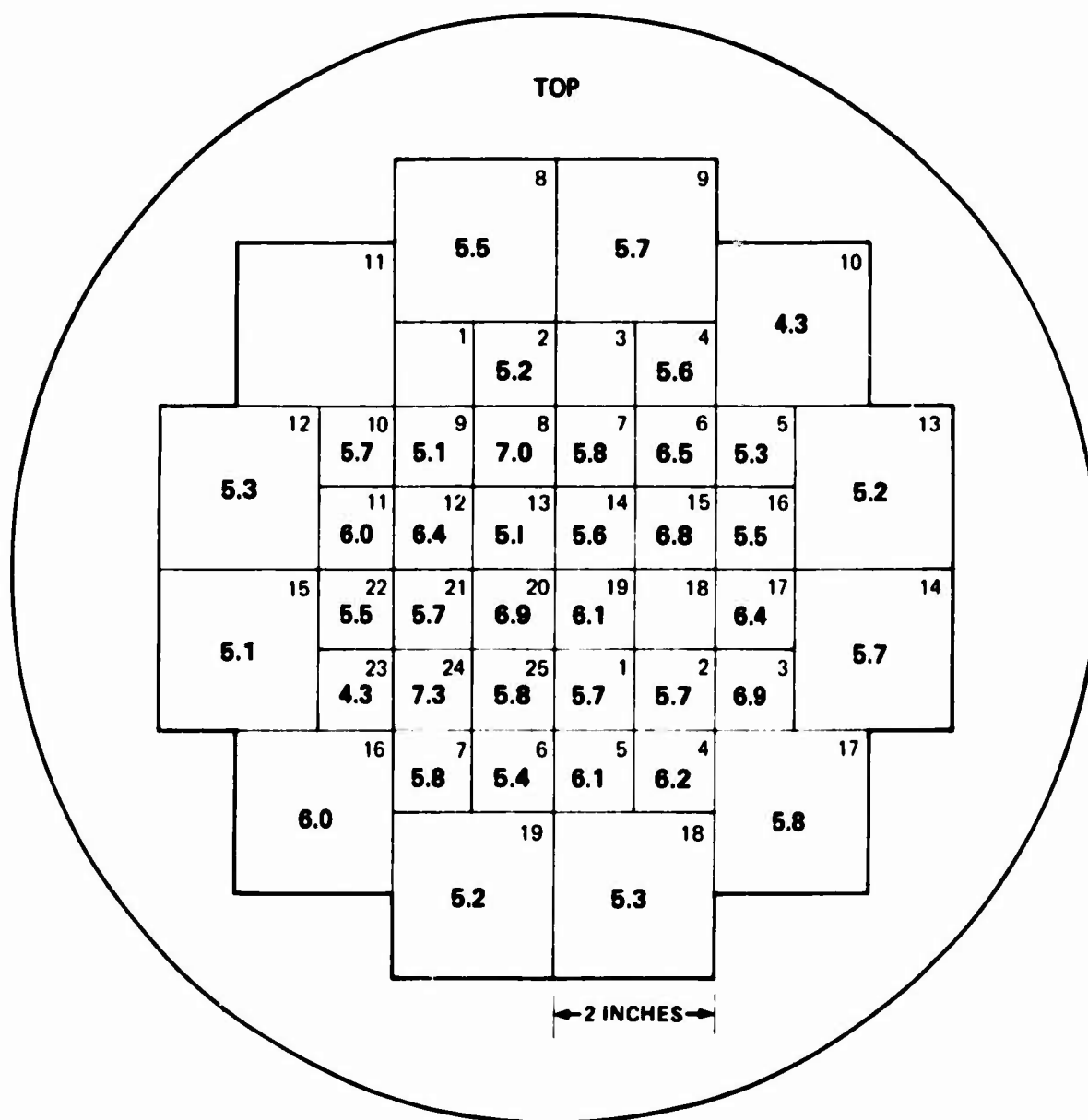
DATE: 6/25/76

1	9
2	10
3	11
4	12
4.7	
5	13
6	14
7	15
8	16

	0.16
1	10
0.87	0.84
2	11
2.40	2.61
3	12
4.2	3.8
4	13
4.7	5.4
5	14
4.3	
6	15
2.3	2.8
7	16
0.94	0.42
8	17
0.12	
9	18

SHOT NO. 2840

DATE: 6/25/76





**PULSE NO. 2841**

**DATE: 6/25/76**

1	0.10	9	0.14
2	0.68	10	
3	2.05	11	2.42
4	3.3	12	3.9
5	3.6	13	4.0
6	1.42	14	
7	0.47	15	
8	0.14	16	0.14

1		10	0.15
2	0.76	11	0.66
3	2.51	12	2.52
4	4.6	13	4.0
5	4.4	14	4.8
6	3.9	15	
7	2.51	16	1.97
8	0.61	17	0.33
9	0.11	18	

PULSE NO. 2845

DATE: 6/25/76

1	9
2	10
3	11
4	12
6.2	
5	13
6	14
7	15
8	16

	0.17
1	10
1.02	0.95
2	11
3.6	3.6
3	12
5.3	5.9
4	13
7.5	7.3
5	14
6.3	
6	15
3.2	3.5
7	16
1.18	0.64
8	17
0.20	
9	18

**PULSE NO. 2846**

**DATE: 6/25/76**

1	9
2	10
3	11
4	12
6.2	
5	13
6	14
7	15
8	16

	0.12
1	10
0.93	0.79
2	11
3.3	3.3
3	12
5.8	5.3
4	13
7.0	6.3
5	14
6.1	
6	15
3.5	2.95
7	16
0.92	0.56
8	17
0.13	
9	18

PULSE NO. 2847

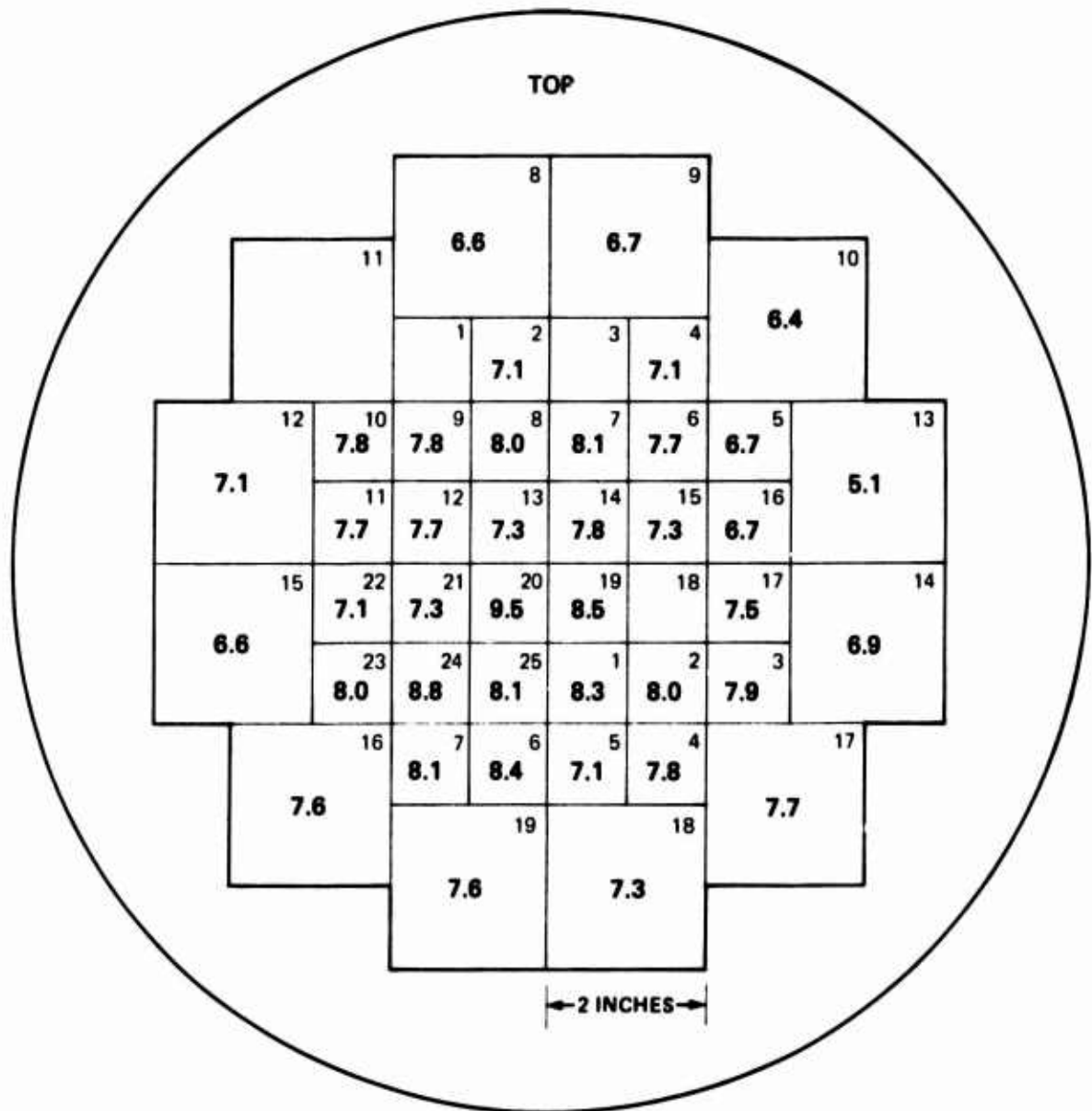
DATE: 6/25/76

1	0.15	9	0.19
2	0.80	10	0.49
3	3.3	11	3.6
4	5.0	12	5.5
5	5.4	13	5.1
6	2.1	14	
7	0.64	15	
8	0.13	16	0.14

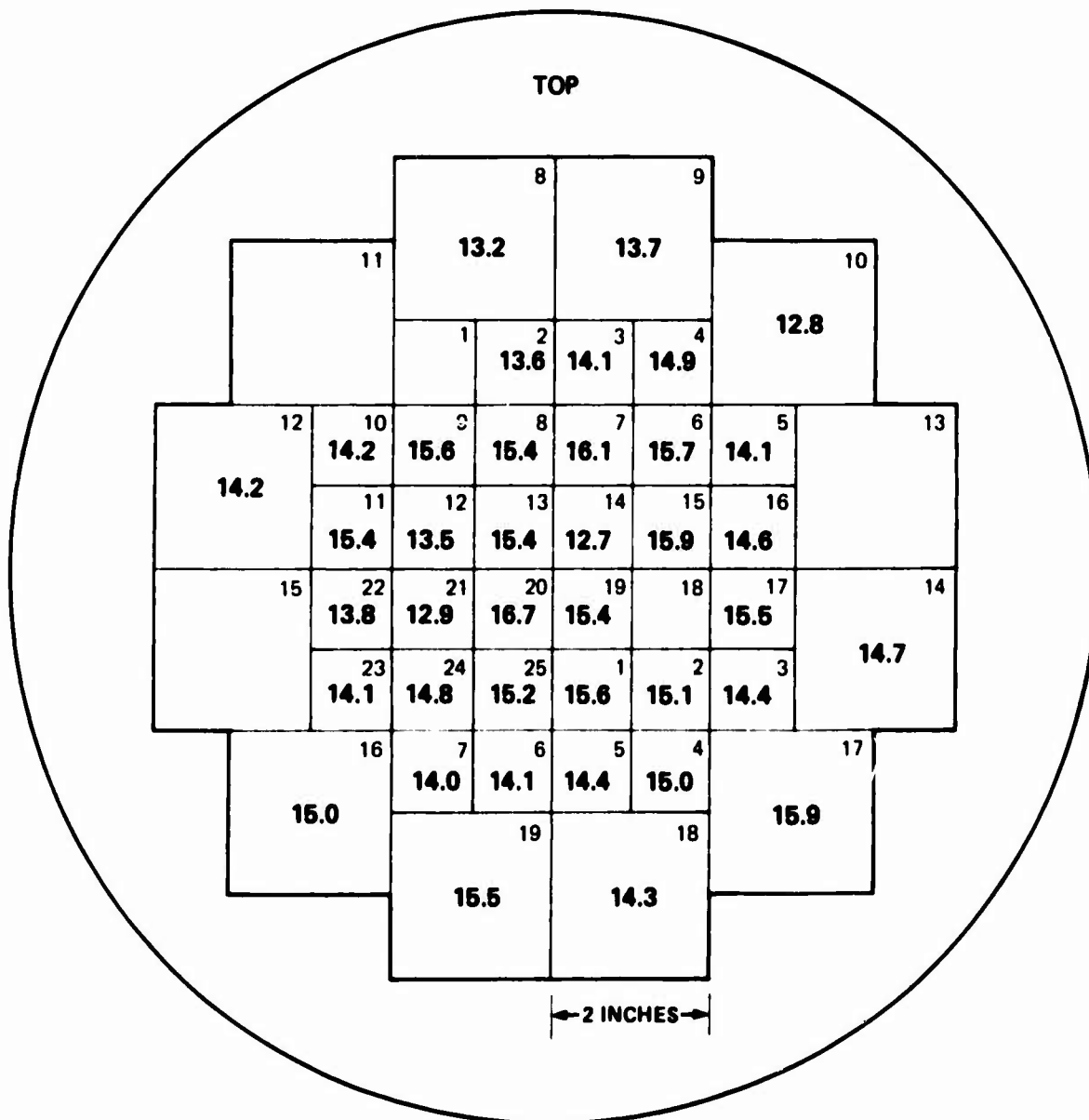
1		10	0.13
2	1.00	11	0.89
3	3.2	12	3.3
4	5.6	13	5.9
5	7.3	14	6.7
6	6.1	15	
7	3.1	16	2.8
8	0.96	17	0.48
9	0.16	18	

SHOT NO. 2848

DATE: 6/25/76

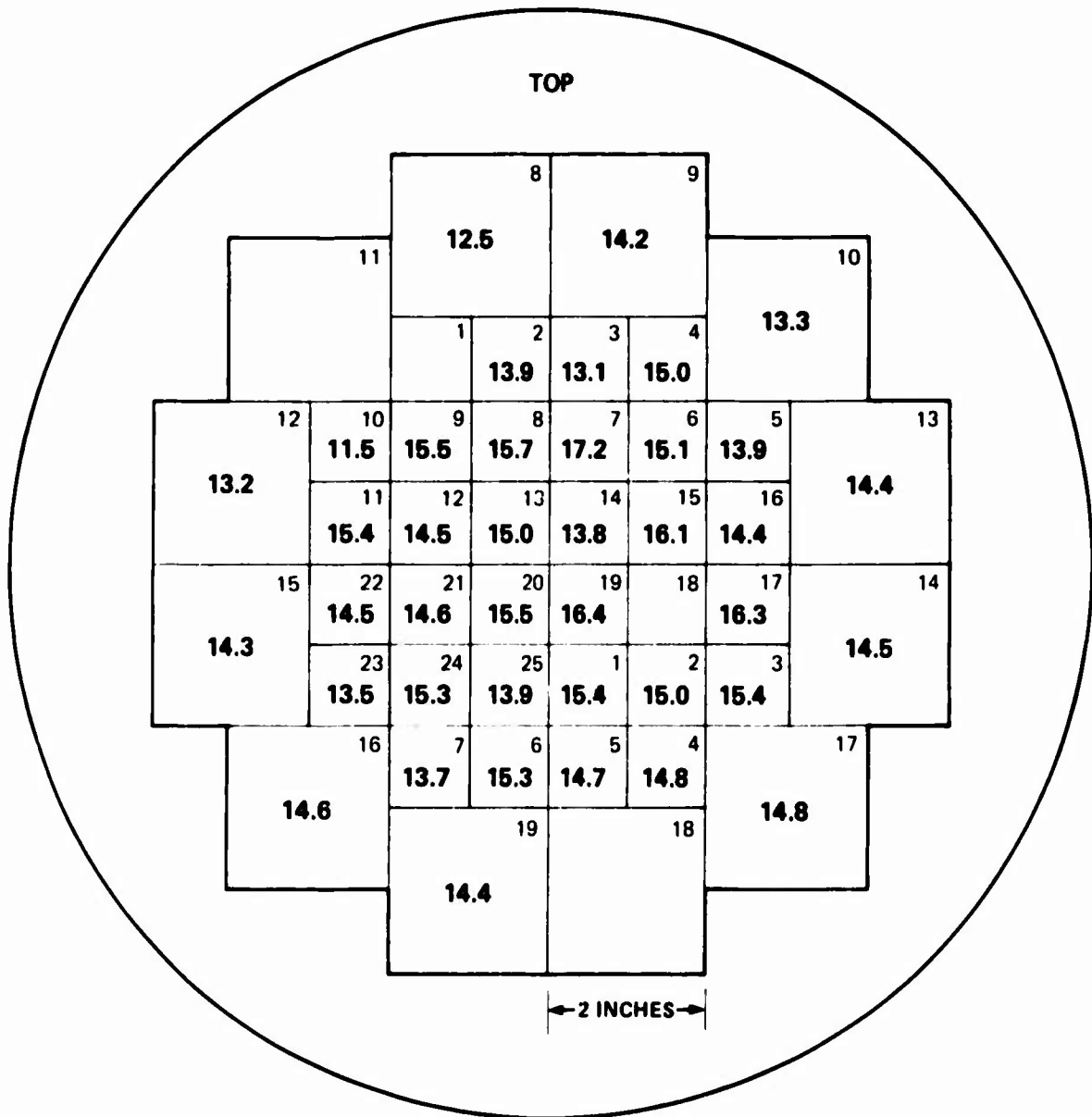


**DATE: 6/25/76**



SHOT NO. 2851

DATE: 6/25/76



TOTAL: 6491

PULSE NO. 2852

DATE: 6/25/76

1	0.29	9	0.30
2	2.25	10	
3	7.2	11	6.8
4	11.1	12	11.0
5	10.8	13	11.1
6	4.5	14	
7	1.53	15	
8	0.32	16	0.31

1		10	0.33
2	2.71	11	2.73
3	7.1	12	7.8
4	12.9	13	12.1
5	13.5	14	15.1
6	13.3	15	
7	7.5	16	6.3
8	2.18	17	1.19
9	0.31	18	



PULSE NO. 2853

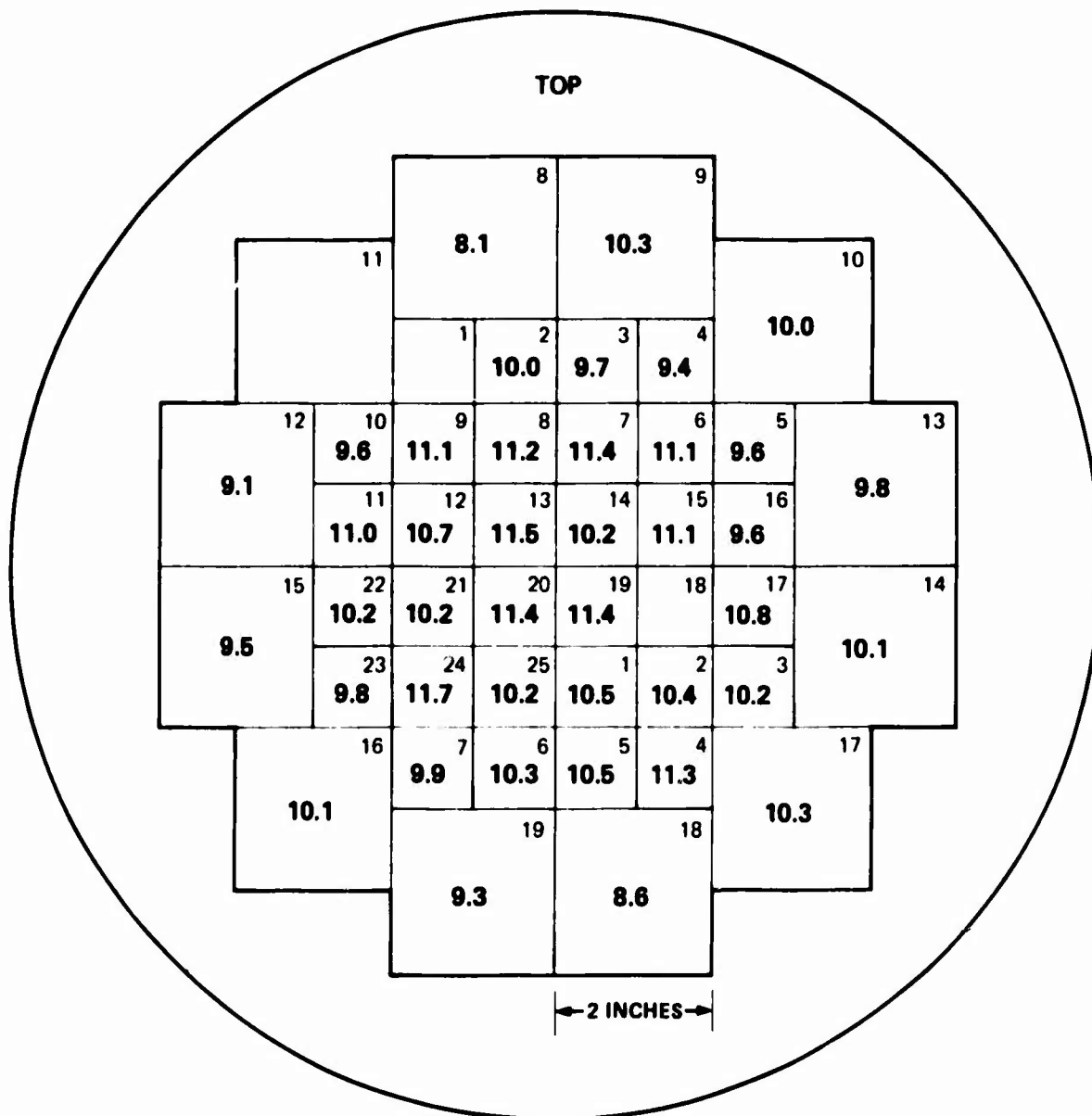
DATE: 6/25/76

1	0.32	9	0.37
2	2.48	10	1.29
3	7.4	11	8.0
4	11.1	12	10.1
5	11.7	13	12.4
6	4.9	14	
7	1.69	15	
8	0.38	16	0.35

1		10	0.31
2	2.50	11	2.38
3	7.6	12	8.0
4	13.2	13	12.5
5	14.6	14	15.3
6	12.8	15	
7	7.4	16	7.2
8	2.93	17	1.38
9	0.31	18	

SHOT NO. 2854

DATE: 6/25/76



PULSE NO. 2855

DATE: 6/25/76

1	0.29	9	0.32
2	1.59	10	
3	6.3	11	5.5
4	5.5	12	8.3
5	8.7	13	8.8
6	3.1	14	
7	0.88	15	
8	0.20	16	0.18

1		10	0.22
2	1.51	11	1.45
3	5.4	12	5.8
4	7.2	13	8.3
5	9.2	14	11.1
6	9.9	15	
7	5.6	16	4.1
8	1.66	17	0.80
9	0.24	18	

PULSE NO. 2856

DATE: 6/25/76

1	9
2	10
3	11
4	12
9.1	
5	13
6	14
7	15
8	16

	0.20
1	10
1.22	1.57
2	11
4.8	5.2
3	12
5.5	7.9
4	13
7.1	9.3
5	14
8.3	
6	15
4.6	4.5
7	16
1.39	0.84
8	17
0.14	
9	18

PULSE NO. 2857

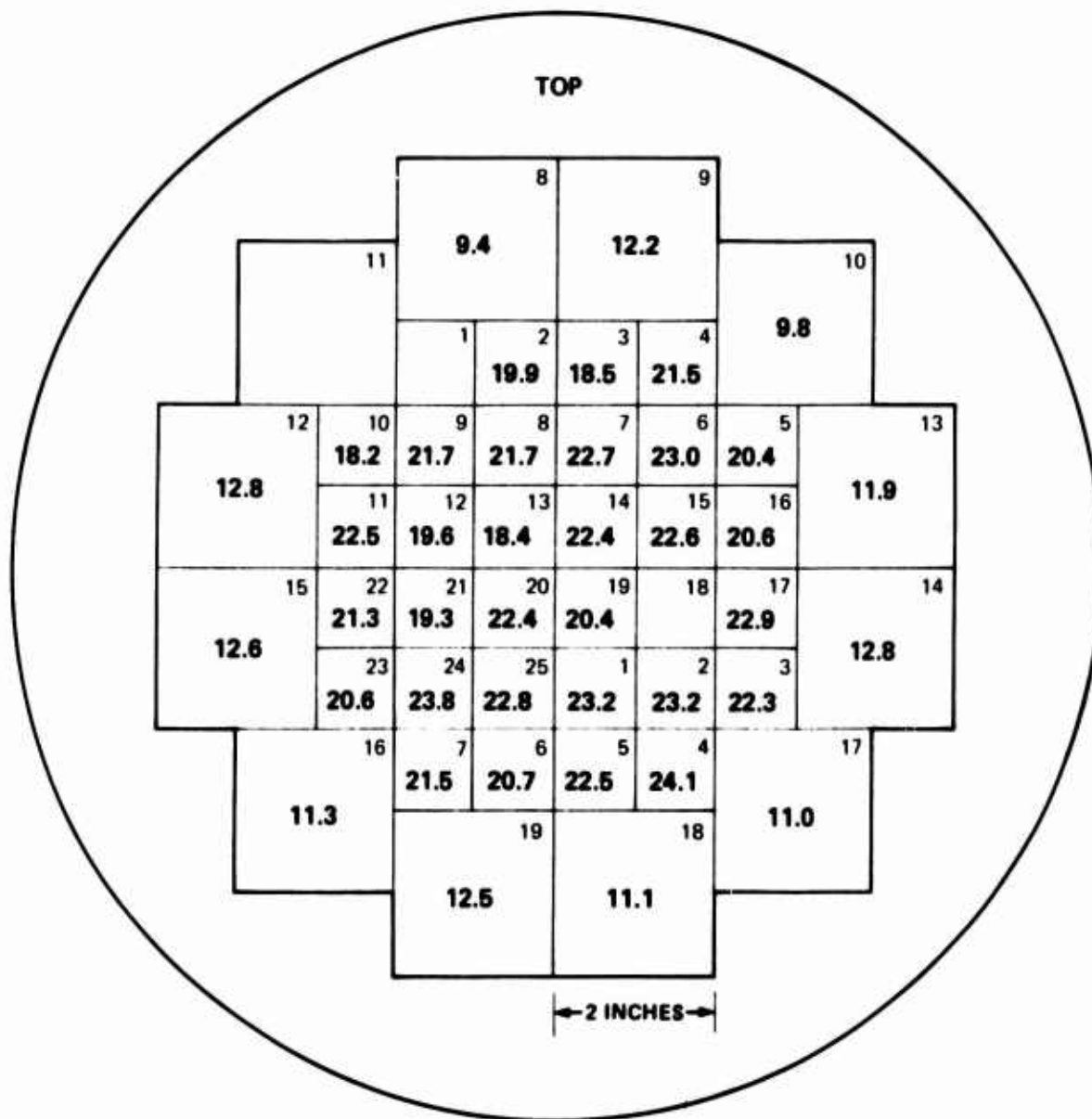
DATE: 6/25/76

1	0.19	9	0.31
2	1.34	10	
3	4.9	11	5.5
4	7.4	12	8.1
5	6.9	13	8.1
6	2.9	14	
7	0.94	15	
8	0.23	16	0.22

1		10	0.22
2	1.67	11	1.63
3	5.4	12	5.3
4	9.8	13	9.1
5	11.4	14	10.6
6	9.8	15	
7	5.8	16	4.6
8	1.55	17	0.71
9	0.23	18	

SHOT NO. 2858

DATE: 6/25/76



PULSE NO. 2859

DATE: 6/25/76

1	0.53	9	0.58
2	4.8	10	3.2
3	11.7	11	10.7
4	14.9	12	14.4
5	16.0	13	14.5
6	6.8	14	
7	3.1	15	
8	0.56	16	0.48

1		10	0.22
2	5.0	11	2.59
3	10.6	12	12.0
4	16.7	13	16.1
5	16.6	14	18.4
6	16.9	15	
7	10.9	16	11.1
8	4.8	17	2.41
9	0.51	18	

PULSE NO. 2860

DATE: 6/25/76

1	0.53	9	0.67
2	5.8	10	3.8
3	11.7	11	12.1
4	17.1	12	18.3
5	17.2	13	18.3
6	7.8	14	
7	3.4	15	
8	0.71	16	0.54

1		10	0.27
2	5.0	11	3.0
3	17.1	12	15.8
4	19.6	13	19.9
5	21.7	14	24.7
6	19.6	15	
7	12.8	16	12.9
8	4.9	17	3.2
9	0.58	18	



PULSE NO. 2861

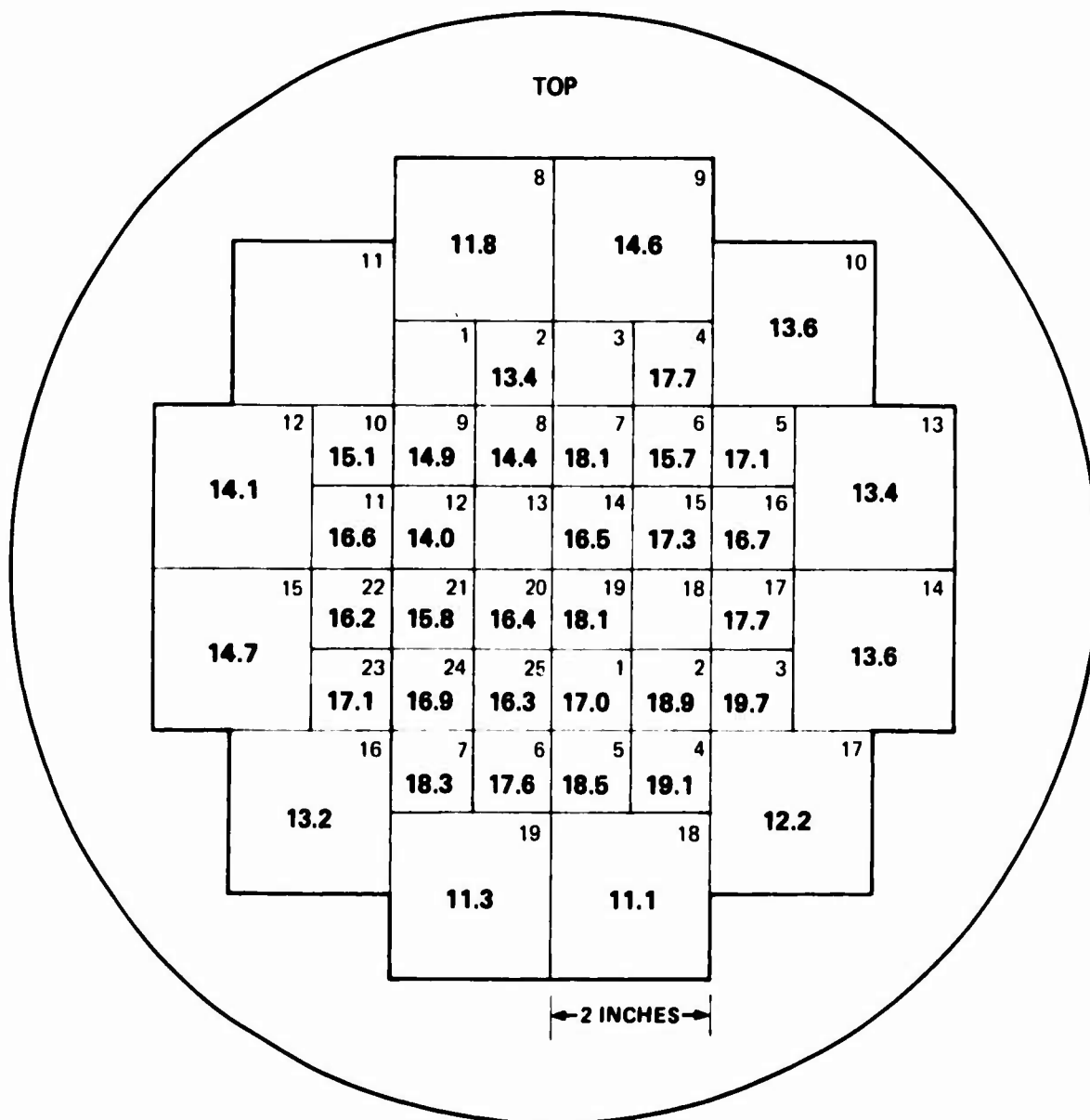
DATE: 6/25/76

1	0.60	9	0.45
2	4.1	10	
3	9.4	11	10.3
4	14.2	12	14.8
5	13.9	13	15.7
6	6.7	14	
7	2.4	15	
8	0.39	16	0.41

1		10	0.56
2	3.3	11	4.7
3	11.2	12	14.0
4	13.6	13	17.5
5	17.9	14	19.3
6	18.4	15	
7	10.7	16	10.4
8	3.7	17	2.1
9	0.31	18	

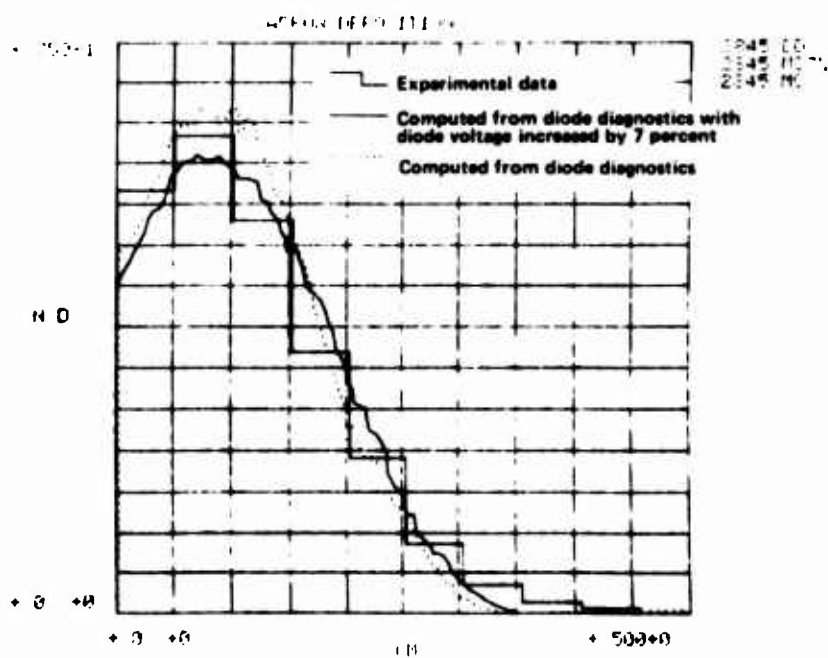
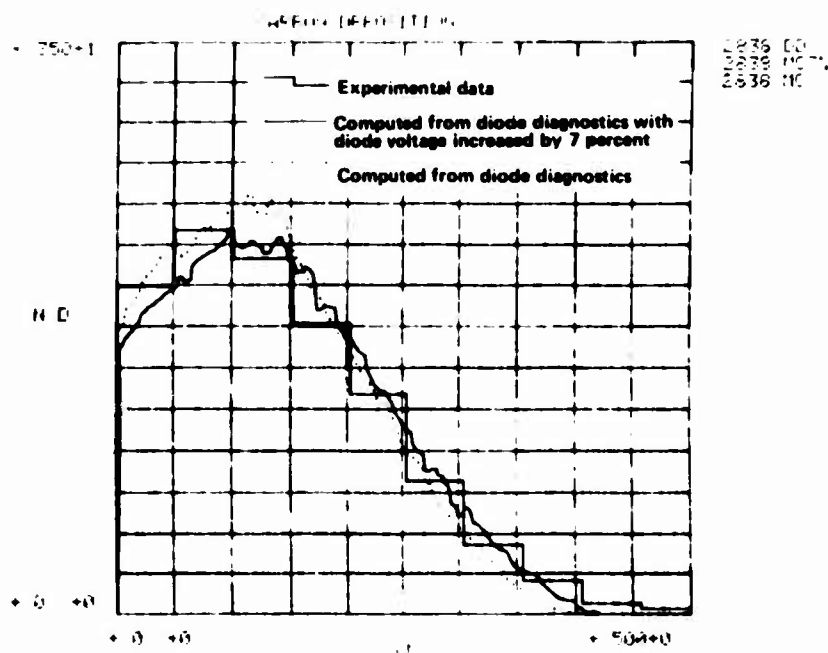
SHOT NO. 2862

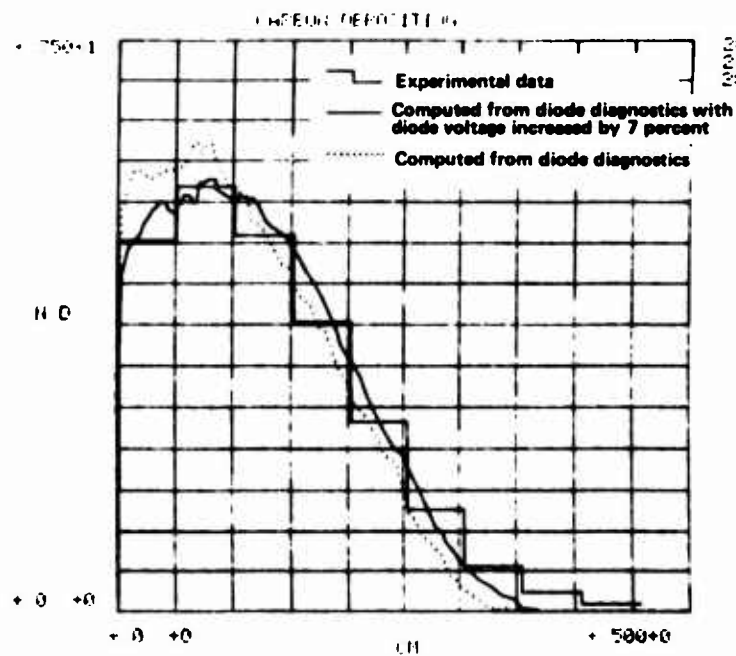
DATE: 6/25/76



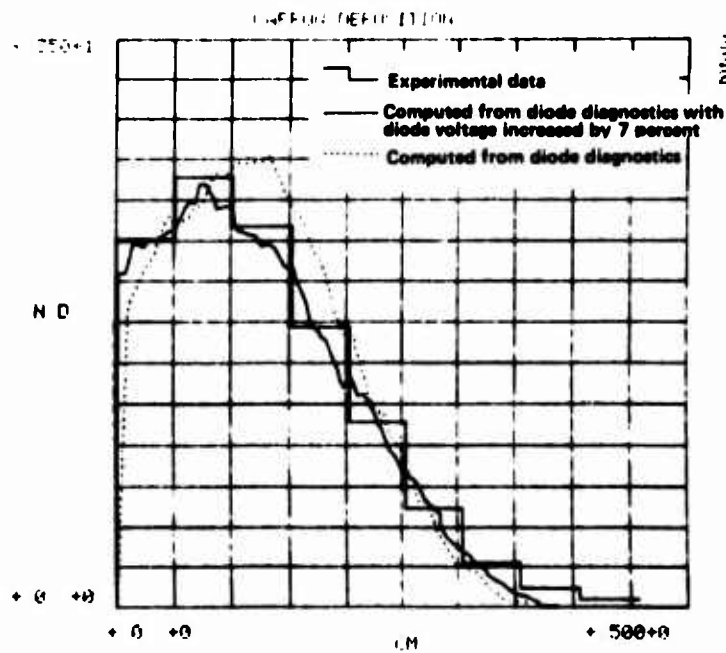
APPENDIX B

MEASURED AND CALCULATED DEPOSITION PROFILES IN CARBON





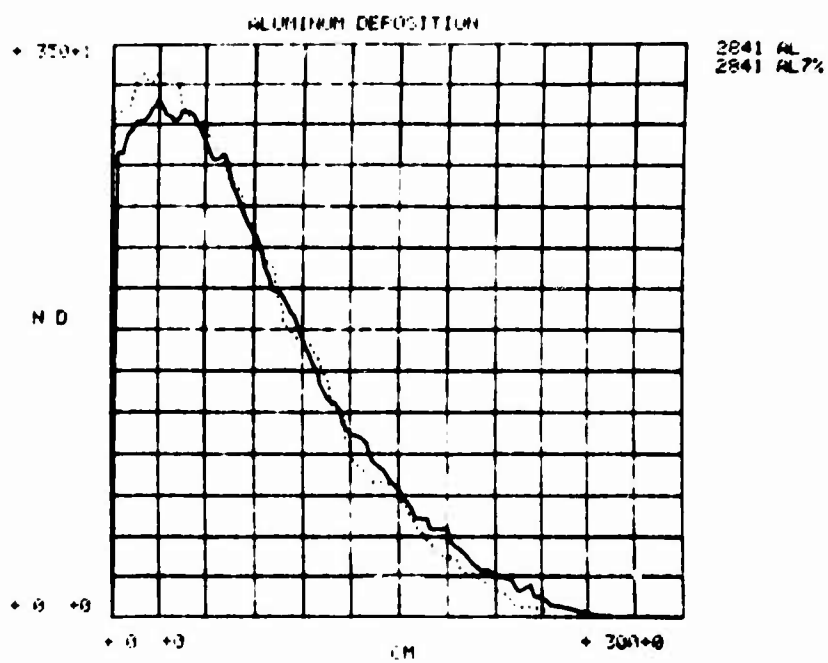
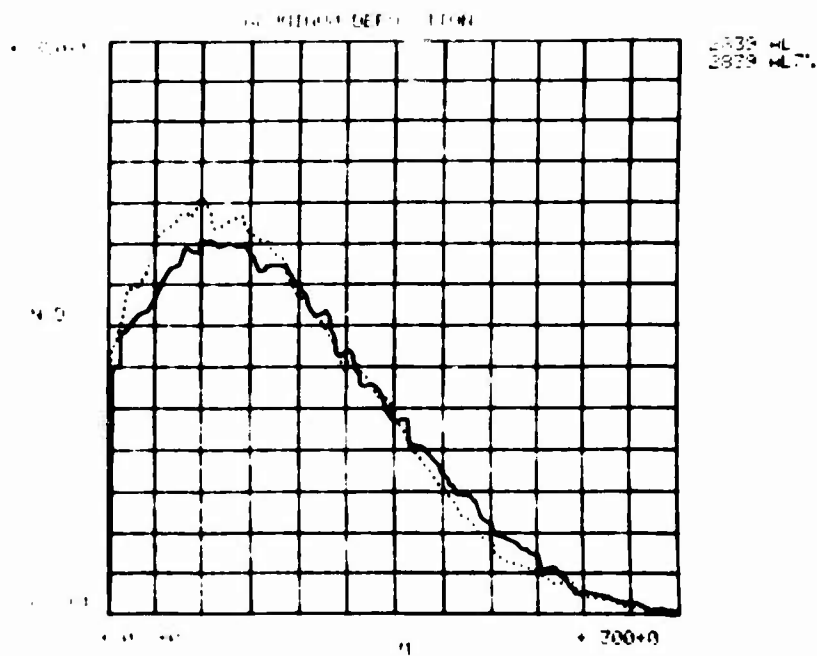
2846 DD  
2846 MC7  
2846 MC

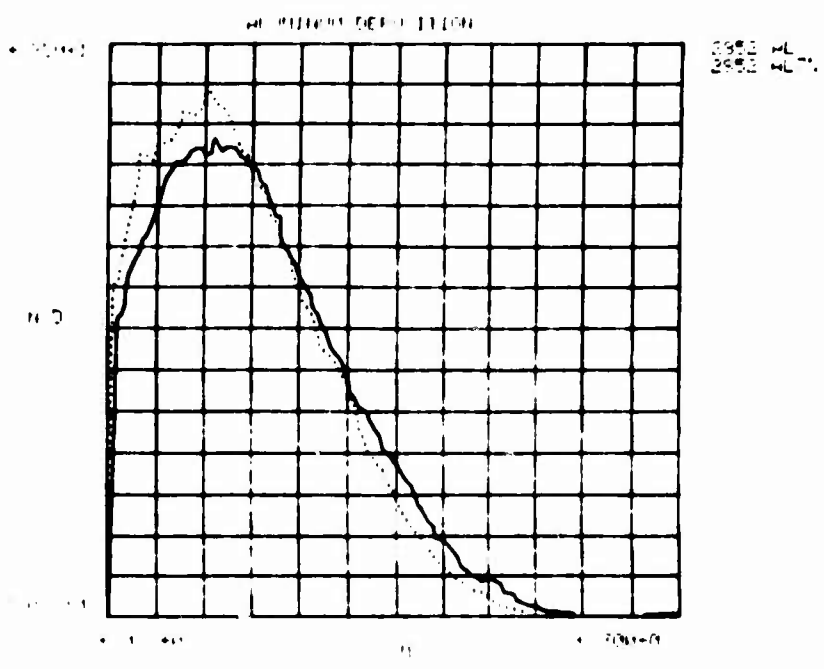
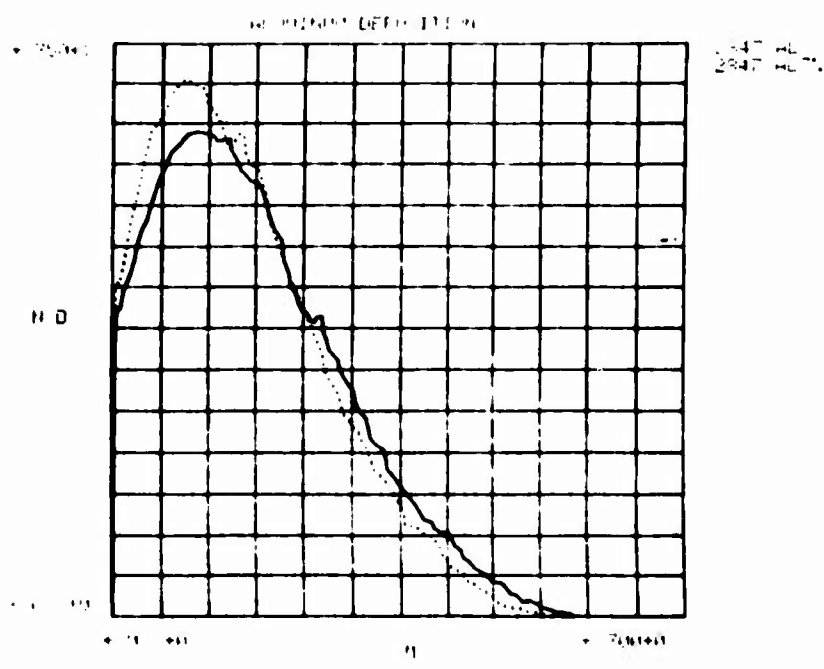


2856 DD  
2856 MC7  
2856 MC

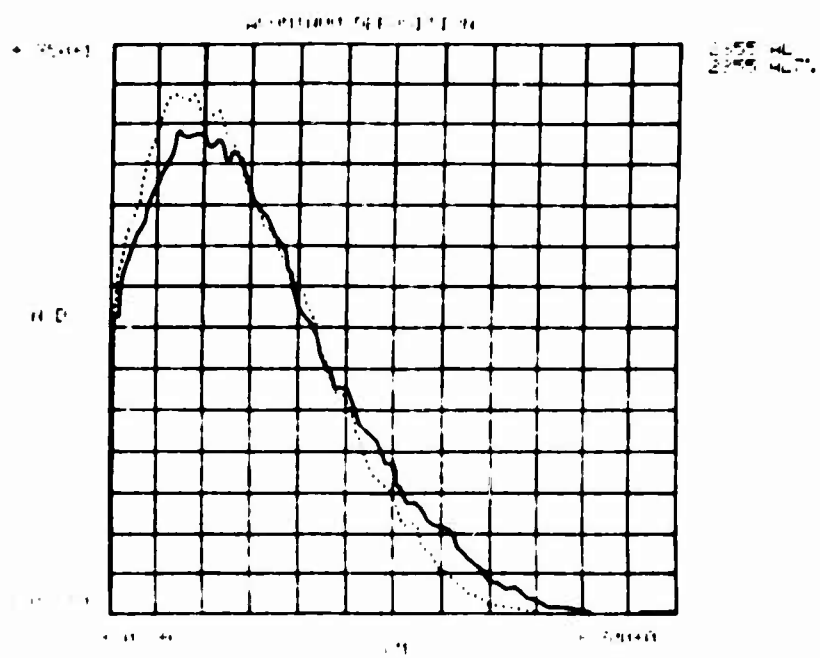
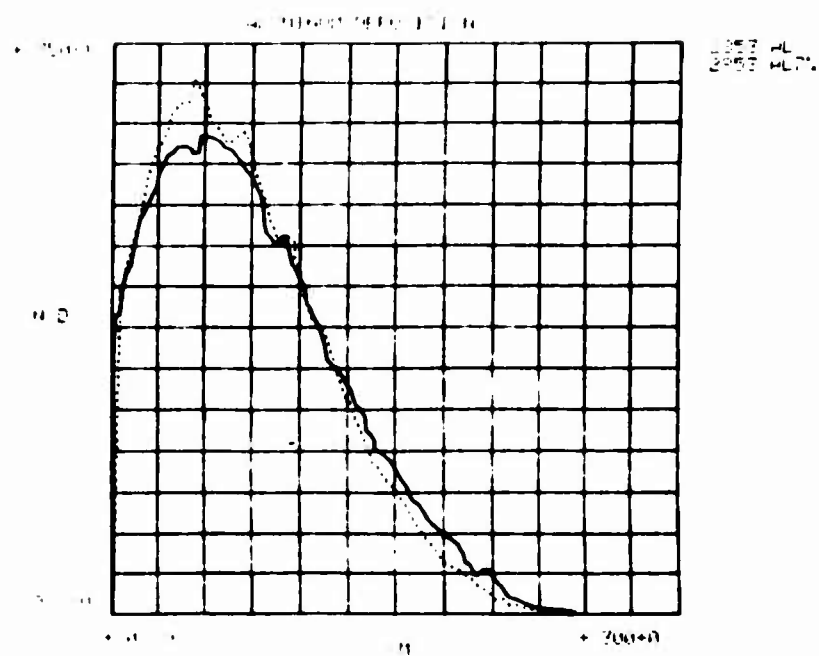
APPENDIX C-1  
CALCULATED DEPOSITION PROFILES IN ALUMINUM  
NORMAL INCIDENCE

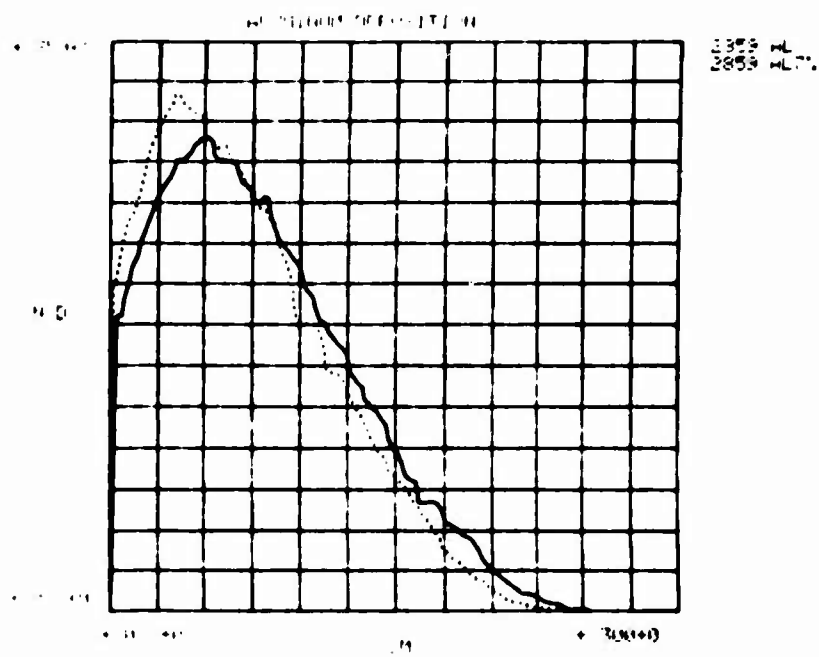
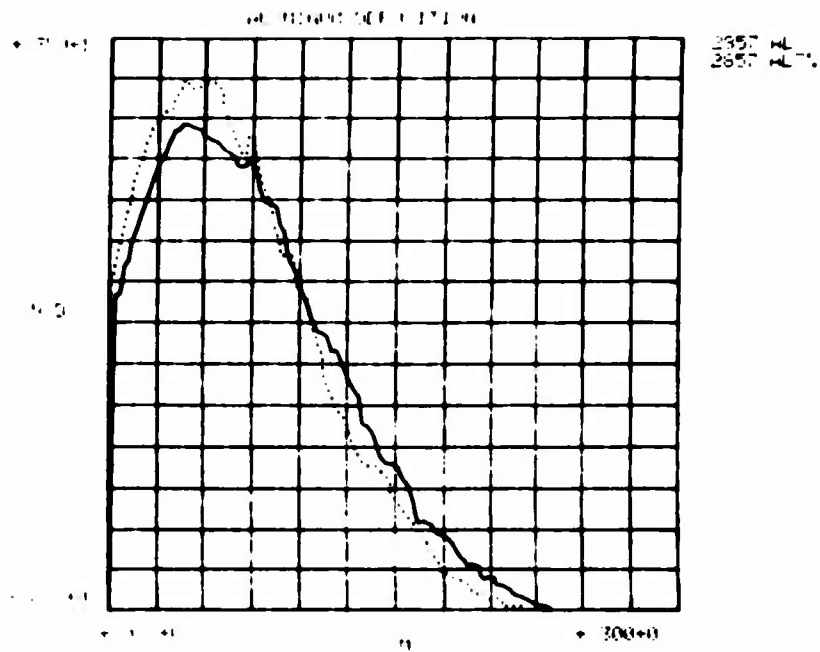
*Preceding Page BLANK*

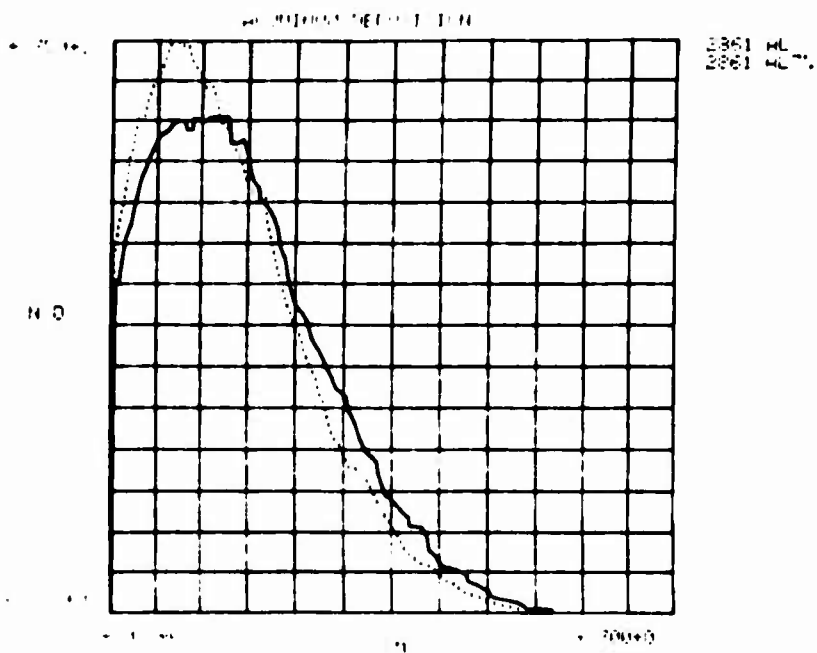
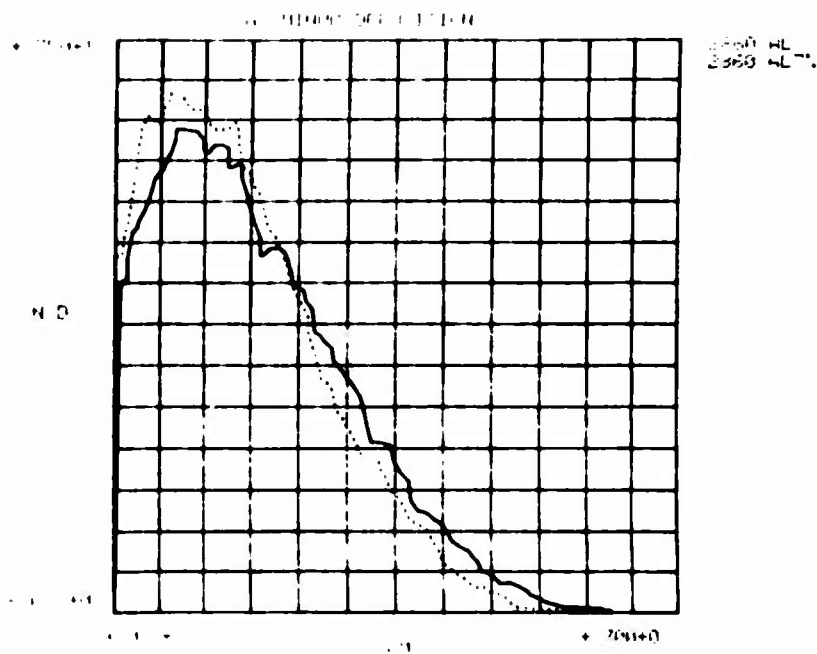








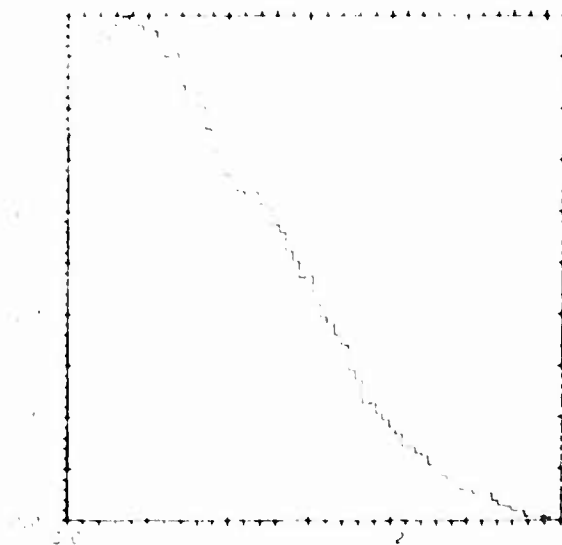




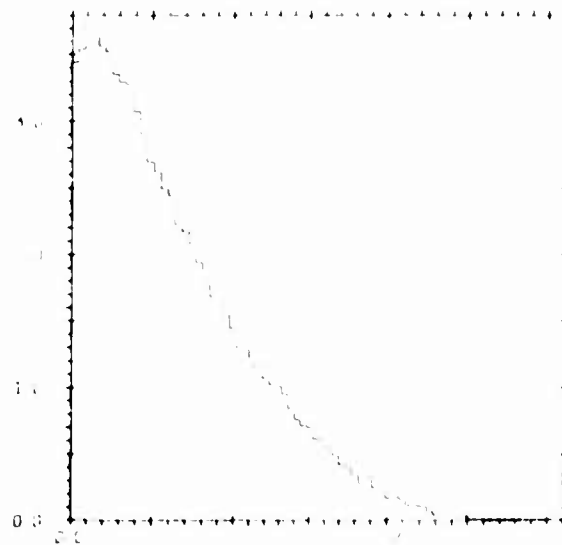
APPENDIX C-2

CALCULATED DEPOSITION PROFILES IN ALUMINUM  
ASSUMING 30° ANGLE OF INCIDENCE AND TUBE  
VOLTAGE INCREASED BY 7 PERCENT

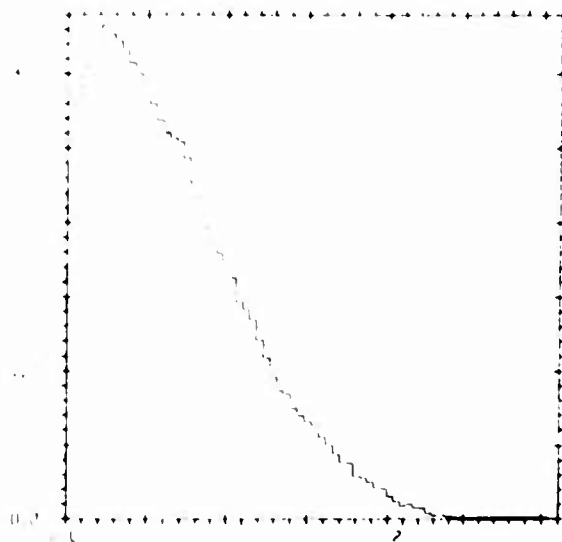
REGIMEN 1 (POLY 1943)



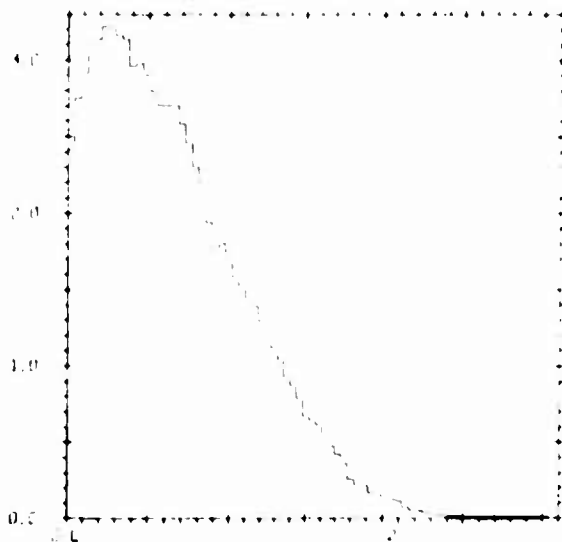
REGIMEN 1 (POLY 1943)



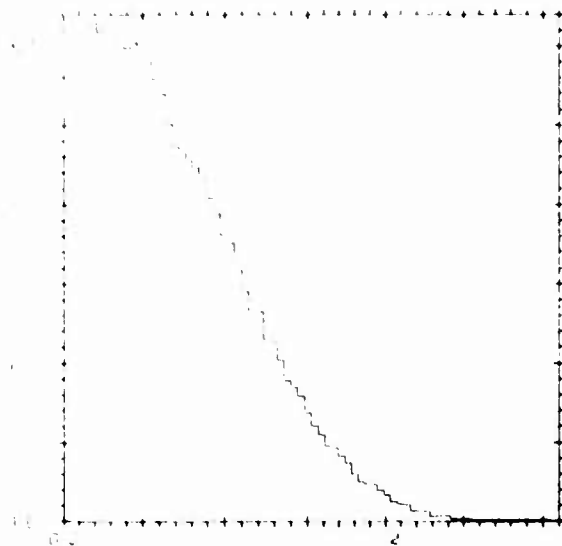
REGIMEN 1 (POLY 1943)



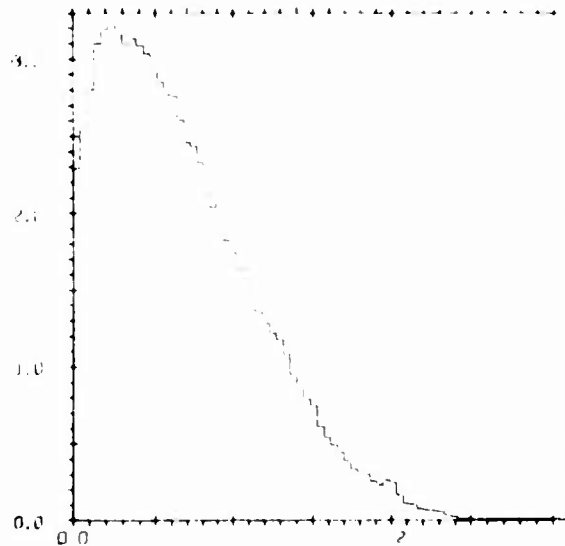
REGIMEN 1 (POLY 1943)



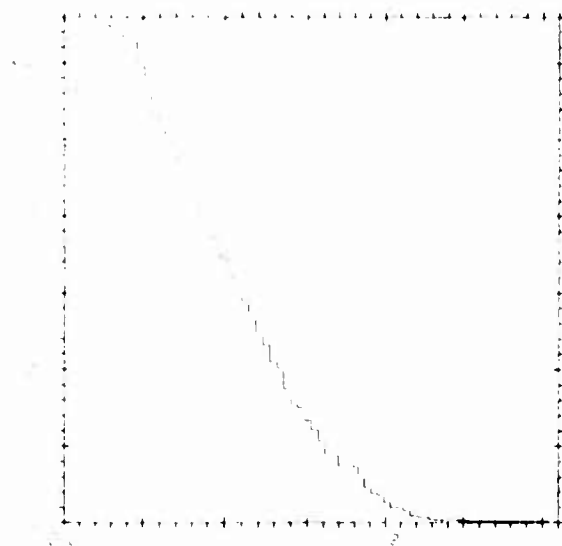
ALUMINUM - Figure 8-13



ALUMINUM - Figure 8-15



ALUMINUM - Figure 8-17



ALUMINUM - Figure 8-18

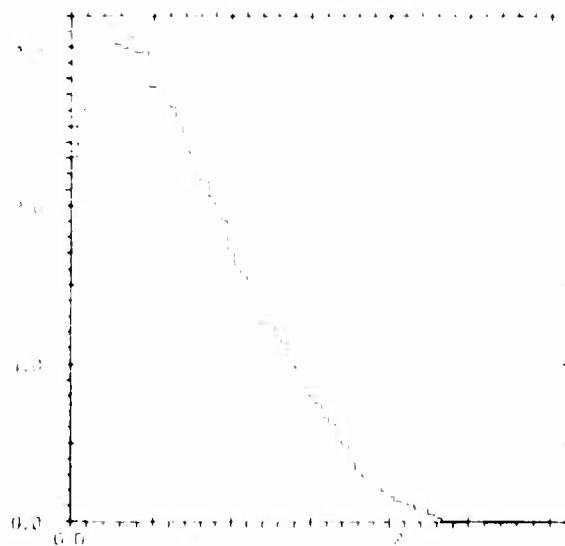


Figure 1. (a)  $\rho_{\text{eff}}(r)$  vs  $r$

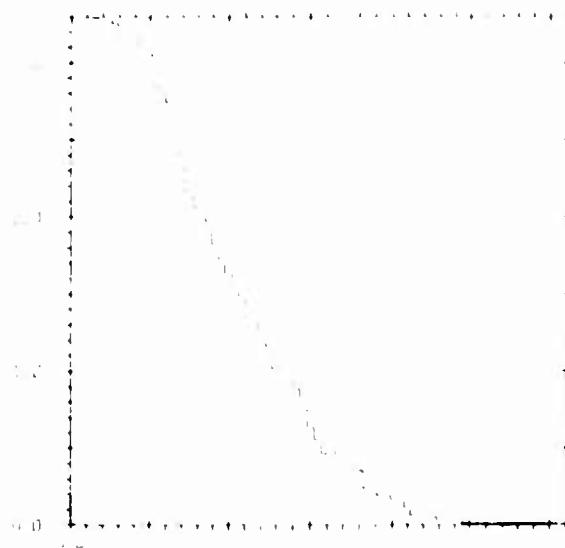
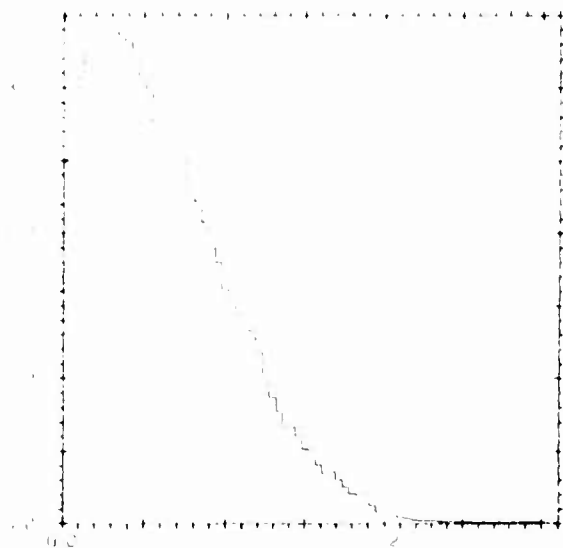


Figure 1. (b)  $\rho_{\text{eff}}(r)$  vs  $r$

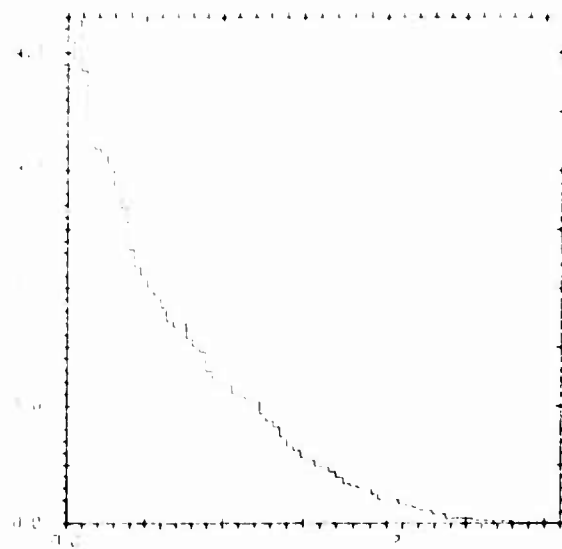


### APPENDIX C-3

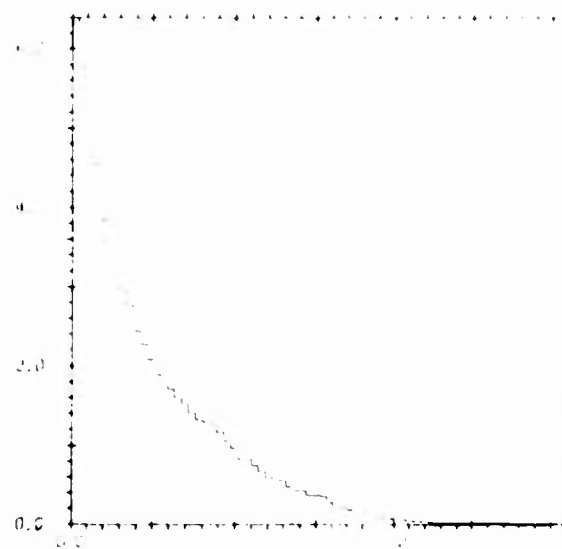
CALCULATED DEPOSITION PROFILES IN ALUMINUM  
ASSUMING 60° ANGLE OF INCIDENCE AND  
TUBE VOLTAGE INCREASED BY 7 PERCENT



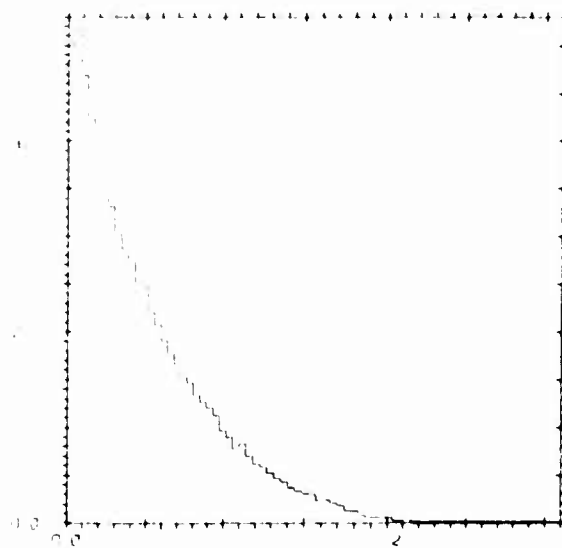
ALUMINUM-FLUORIDE (H4)



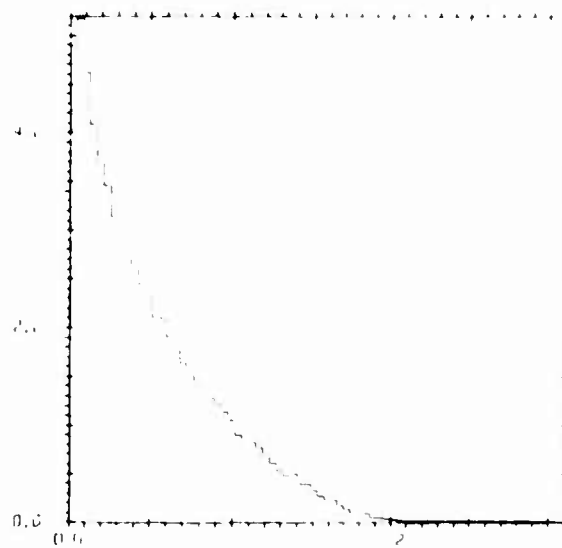
ALUMINUM-FLUORIDE (H4)



ALUMINUM-FLUORIDE (H4)



ALUMINUM-FLUORIDE (H4)



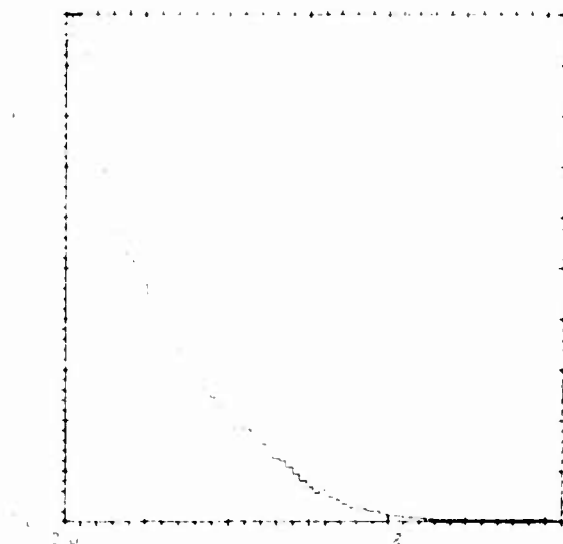
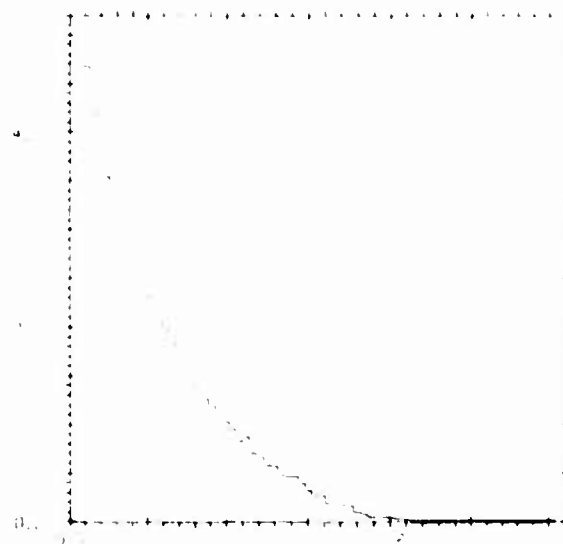
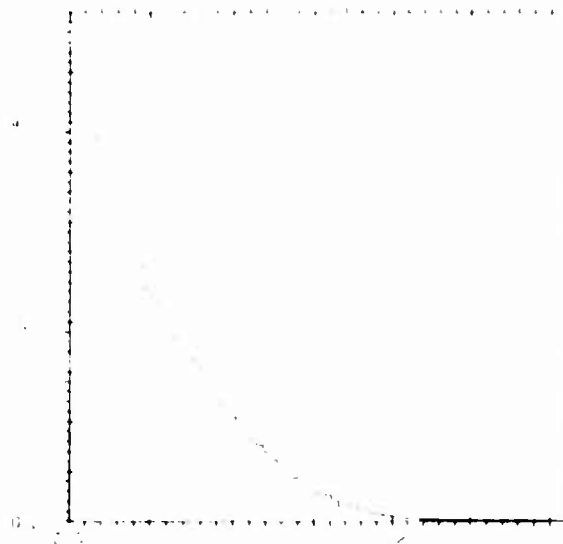
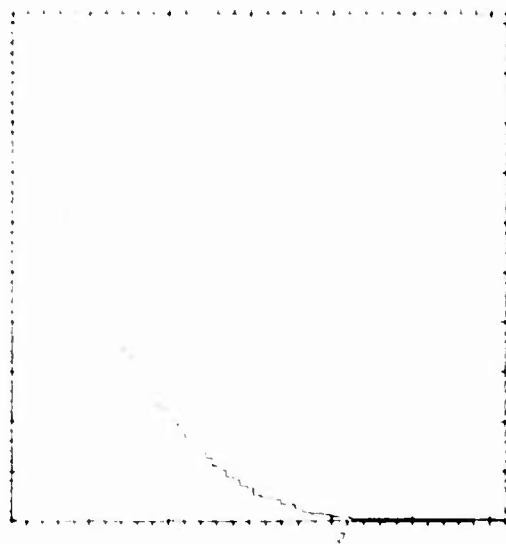


Figure 1. Plot of  $\log_{10} \frac{1}{1 - \rho}$  vs.  $\rho$ .

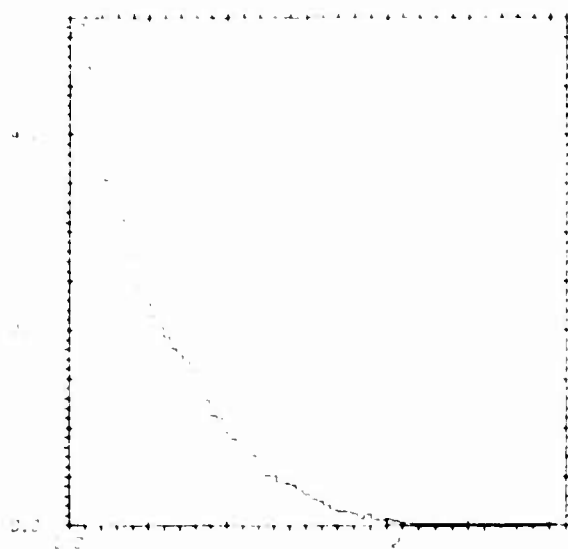
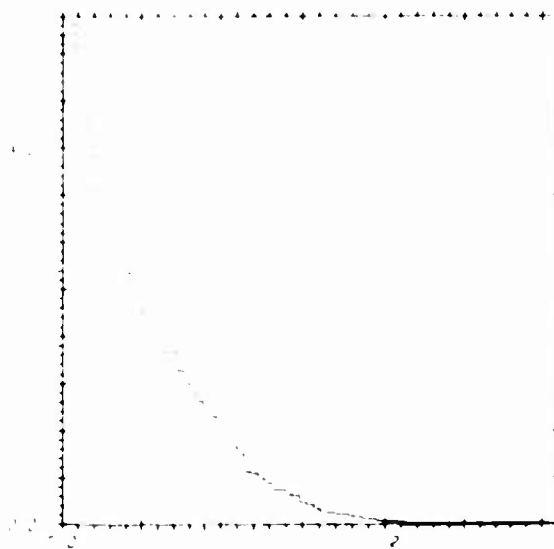


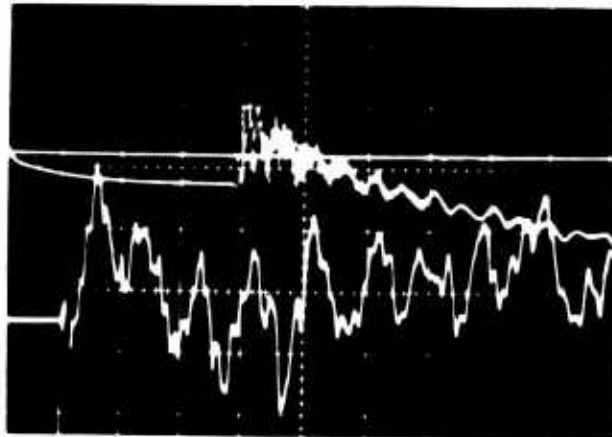
Figure 2. Plot of  $\log_{10} \frac{1}{1 - \rho}$  vs.  $\rho$ .



APPENDIX D

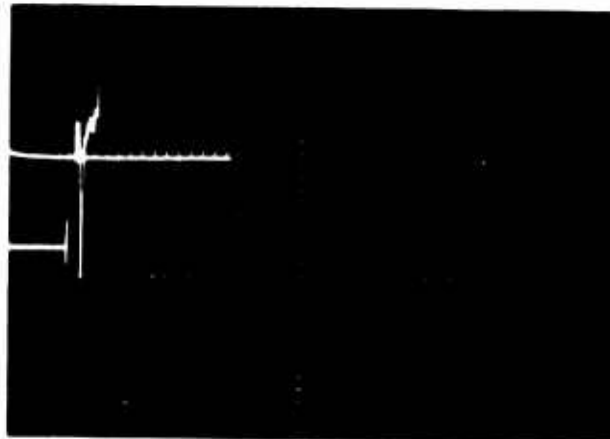
STRAIN GAUGE RECORDS--OSCILLOSCOPE DATA

Pulse 2839



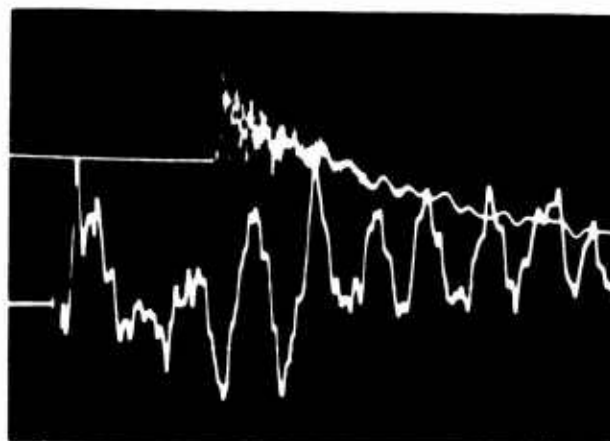
-45°  
860  $\mu$ /division  
5 msec/division

860  $\mu$ /division  
100  $\mu$ sec/division



0°  
2070  $\mu$ /division  
5 msec/division

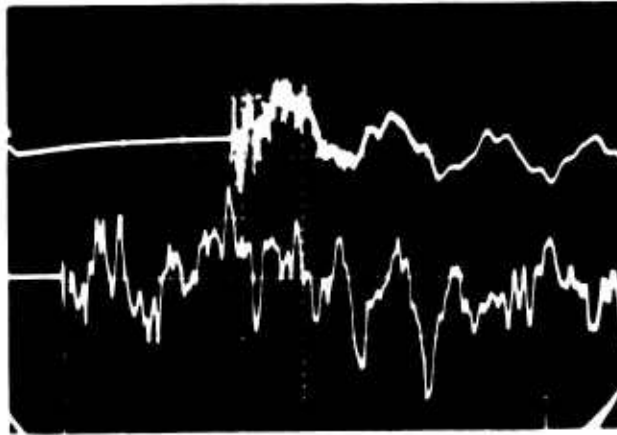
2070  $\mu$ /division  
100  $\mu$ sec/division



45°  
860  $\mu$ /division  
5 msec/division

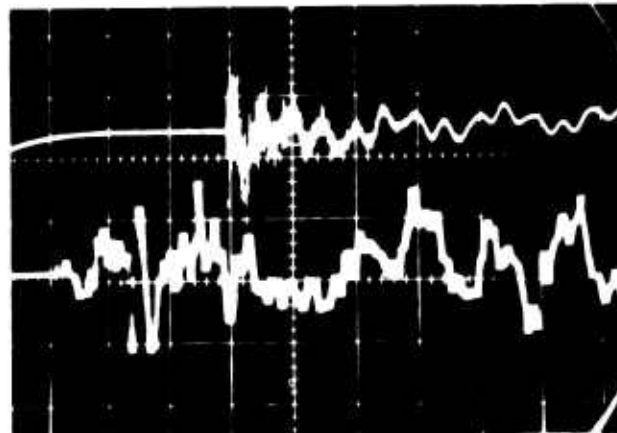
860  $\mu$ /division  
100  $\mu$ sec/division

Pulse 2839



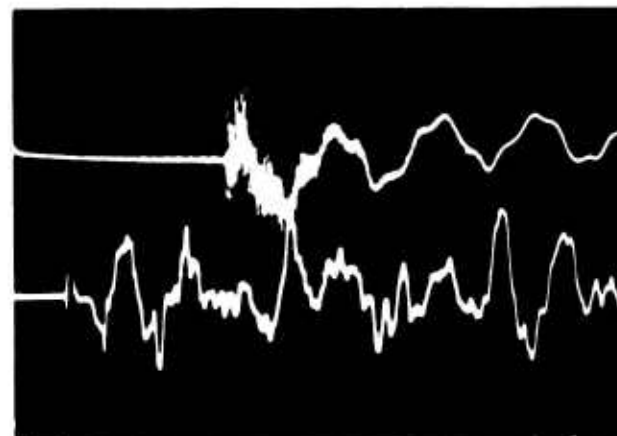
90°  
820  $\mu$ E/division  
5 msec/division

830  $\mu$ E/division  
100  $\mu$ sec/division



135°  
860  $\mu$ E/division  
5 msec/division

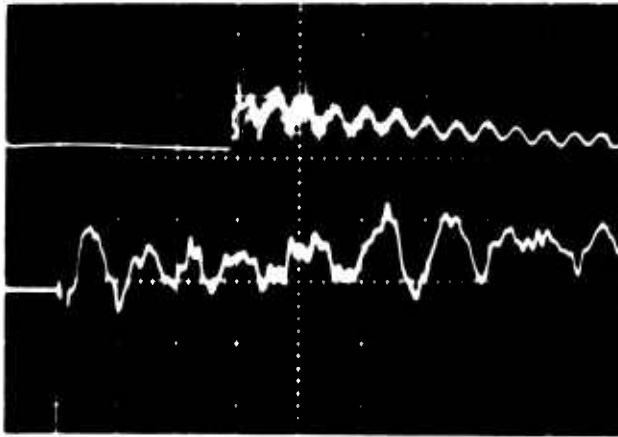
850  $\mu$ E/division  
100  $\mu$ sec/division



170°  
840  $\mu$ E/division  
5 msec/division

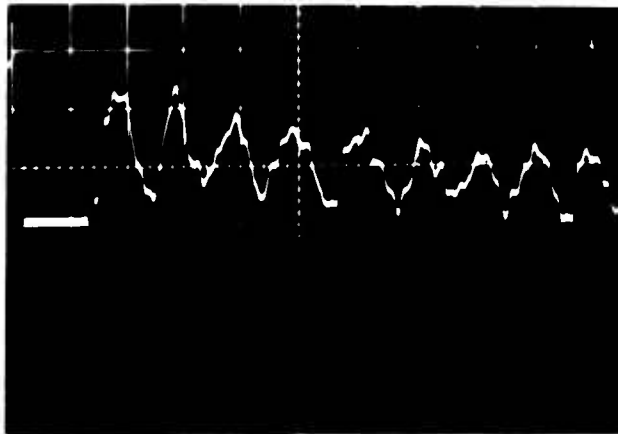
870  $\mu$ E/division  
100 msec/division

Pulse 2841

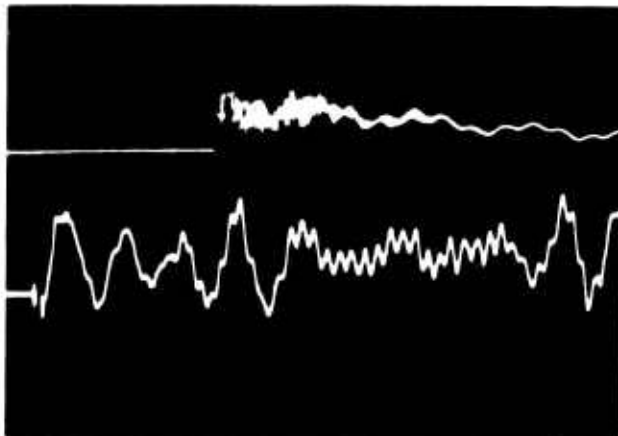


-45°  
860  $\mu$ c/division  
5 msec/division

860  $\mu$ c/division  
100  $\mu$ sec/division



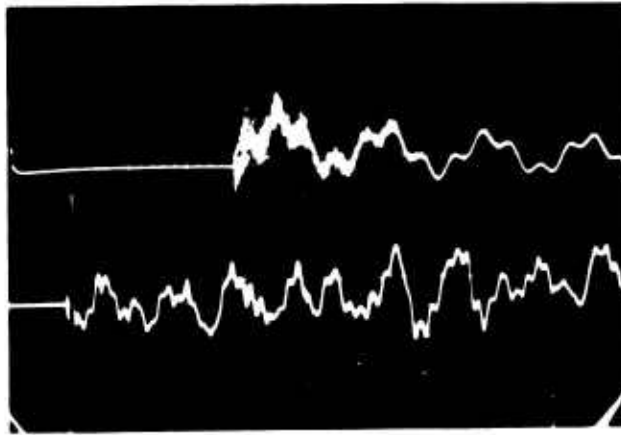
0°  
1040  $\mu$ c/division  
100  $\mu$ sec/division



45°  
860  $\mu$ c/division  
5 msec/division

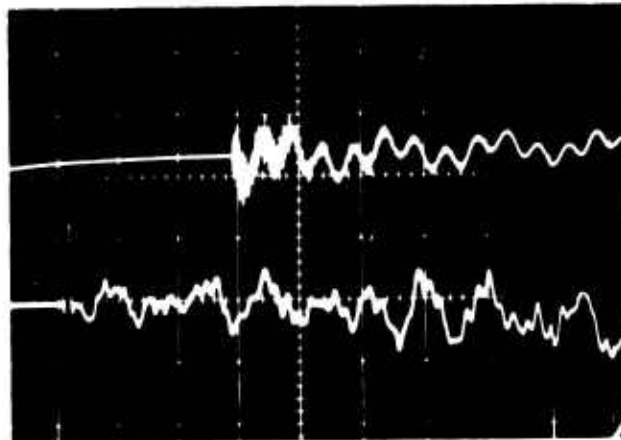
860  $\mu$ c/division  
100  $\mu$ sec/division

Pulse 2841



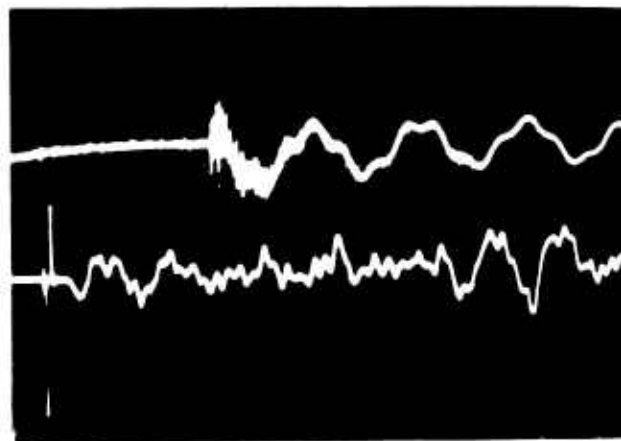
90°  
820  $\mu$ c/division  
5 msec/division

830  $\mu$ c/division  
100  $\mu$ sec/division



135°  
860  $\mu$ c/division  
5 msec/division

850  $\mu$ c/division  
100  $\mu$ sec/division

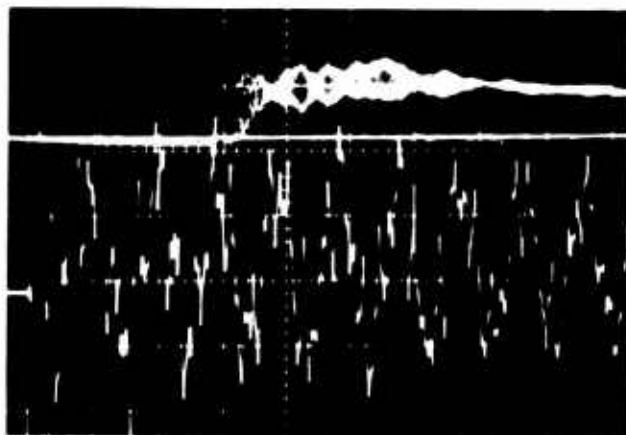


170°  
840  $\mu$ c/division  
5 msec/division

870  $\mu$ c/division  
100  $\mu$ sec/division

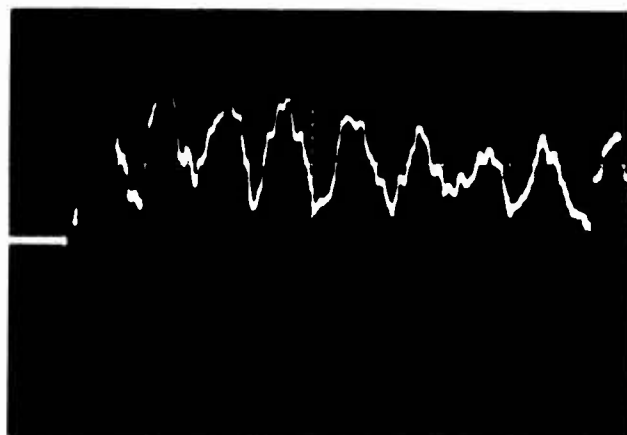


Pulse 2847

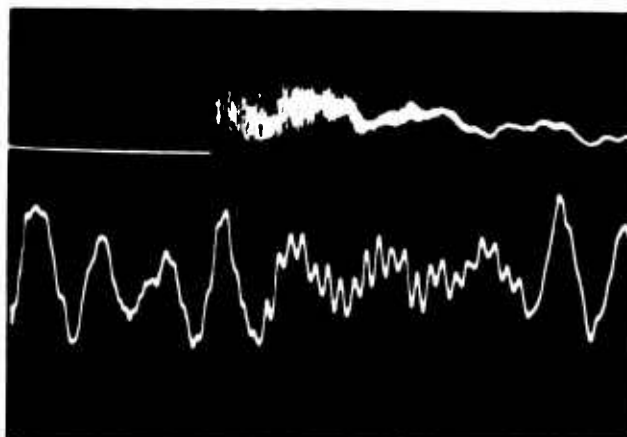


-10° Transverse  
1070  $\mu\epsilon$ /division  
5 msec/division

1070  $\mu\epsilon$ /division  
100  $\mu\text{sec}$ /division



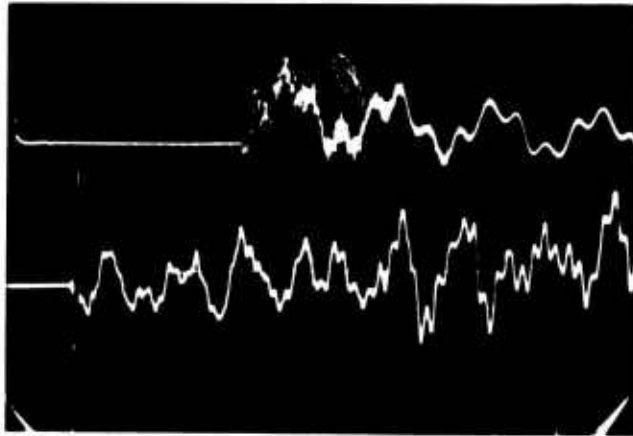
0°  
1040  $\mu\epsilon$ /division  
100  $\mu\epsilon$ /division



45°  
860  $\mu\epsilon$ /division  
5 msec/division

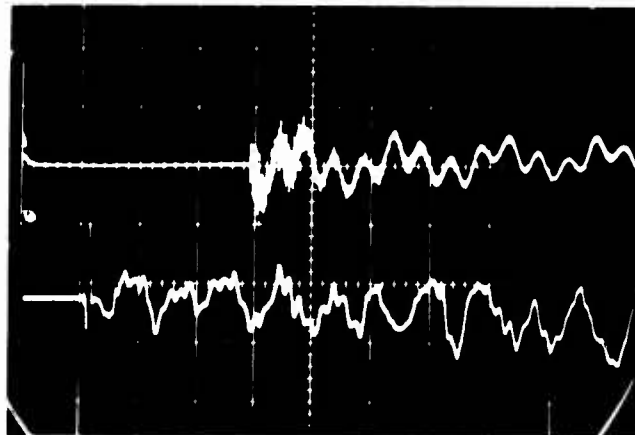
860  $\mu\epsilon$ /division  
100  $\mu\text{sec}$ /division

Pulse 2847



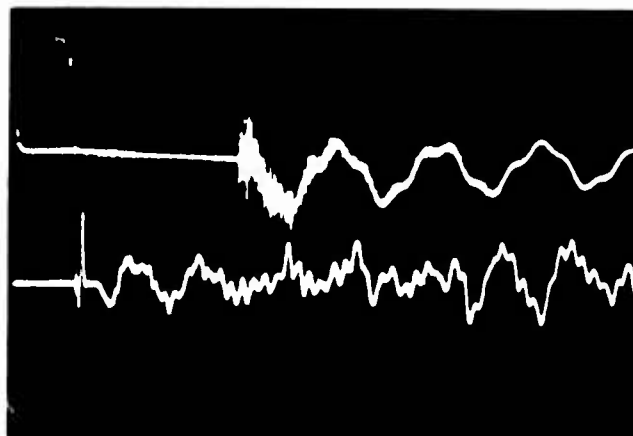
90°  
820  $\mu\text{E}/\text{division}$   
5 msec/division

830  $\mu\text{E}/\text{division}$   
100  $\mu\text{sec}/\text{division}$



135°  
860  $\mu\text{E}/\text{division}$   
5 msec/division

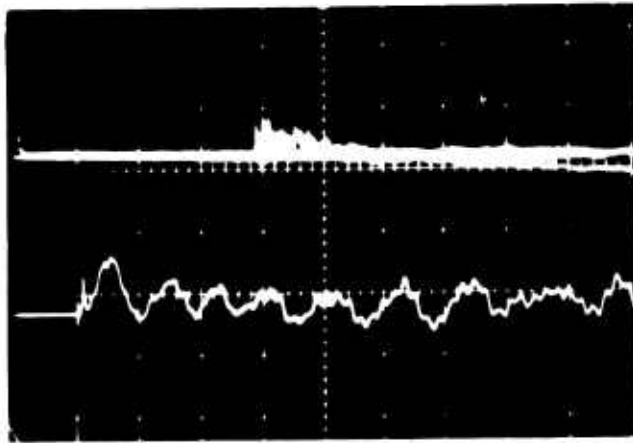
850  $\mu\text{E}/\text{division}$   
100  $\mu\text{sec}/\text{division}$



170°  
840  $\mu\text{E}/\text{division}$   
5 msec/division

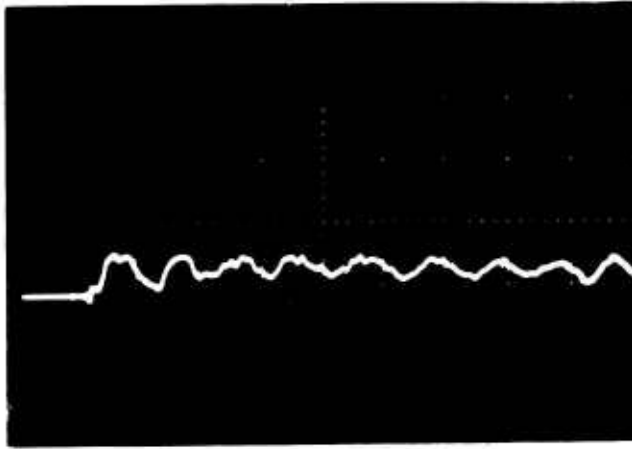
870  $\mu\text{E}/\text{division}$   
100  $\mu\text{sec}/\text{division}$

Pulse 2852

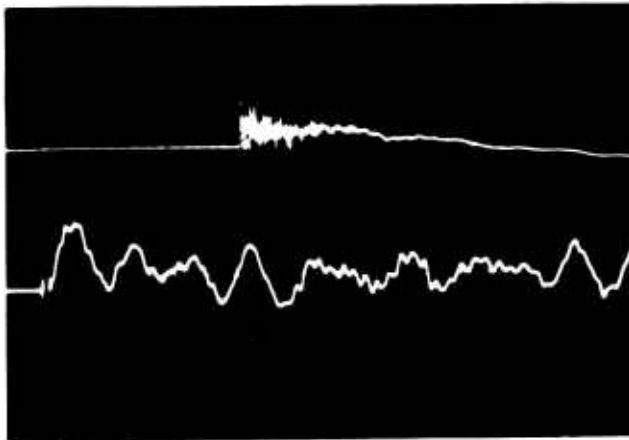


-45°  
2140  $\mu\epsilon$ /division  
5 msec/division

2140  $\mu\epsilon$ /division  
100  $\mu\epsilon$ /division



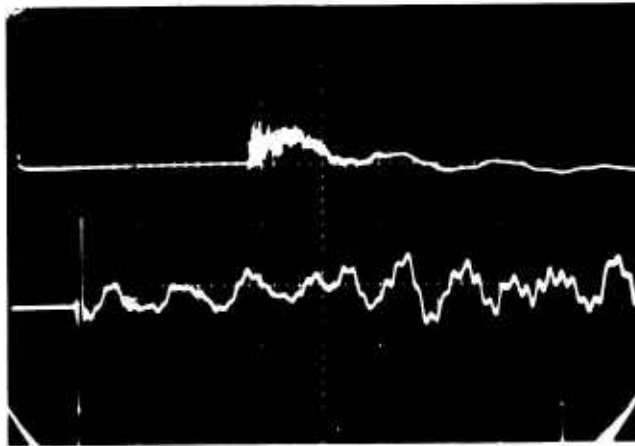
0°  
4100  $\mu\epsilon$ /division  
100  $\mu\epsilon$ /division



45°  
2150  $\mu\epsilon$ /division  
5 msec/division

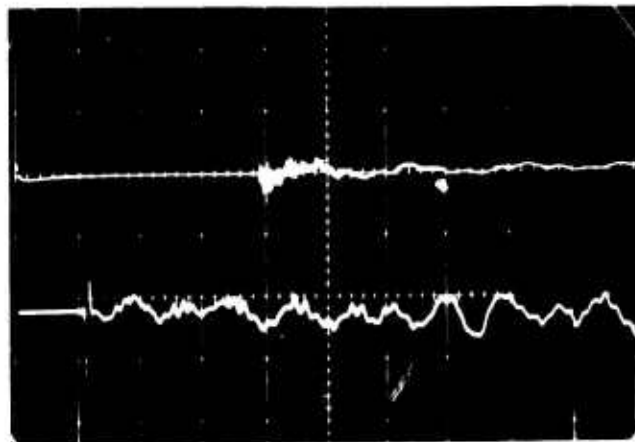
2140  $\mu\epsilon$ /division  
100  $\mu\text{sec}$ /division

Pulse 2852



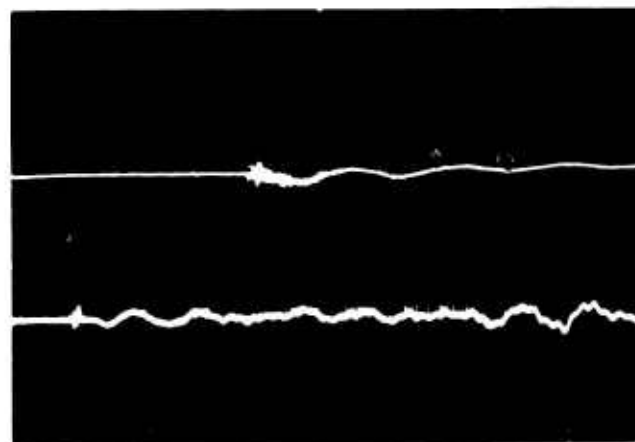
90°  
2060  $\mu\text{E}$ /division  
5 msec/division

2060  $\mu\text{E}$ /division  
100  $\mu\text{sec}$ /division



135°  
2160  $\mu\text{E}$ /division  
5 msec/division

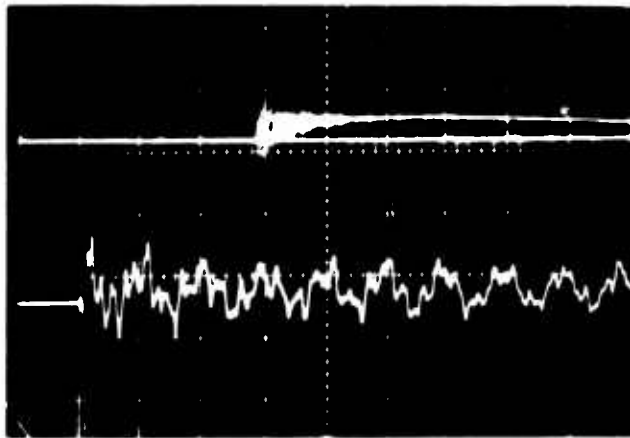
2120  $\mu\text{E}$ /division  
100  $\mu\text{sec}$ /division



170°  
4200  $\mu\text{E}$ /division  
5 msec/division

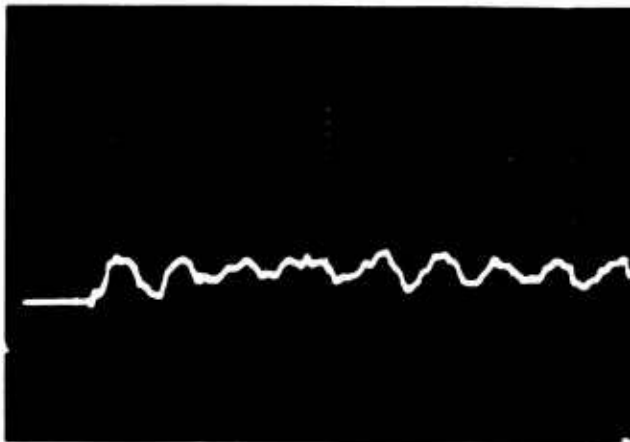
4400  $\mu\text{E}$ /division  
100  $\mu\text{sec}$ /division

Pulse 2853

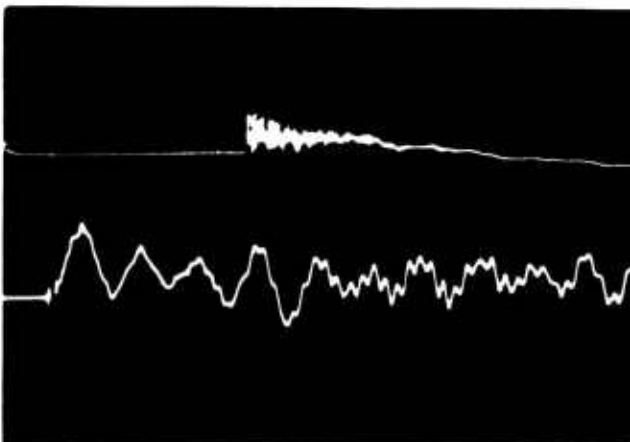


-10° Transverse  
4300  $\mu\epsilon$ /division  
5 msec/division

4300  $\mu\epsilon$ /division  
100  $\mu\epsilon$ /division



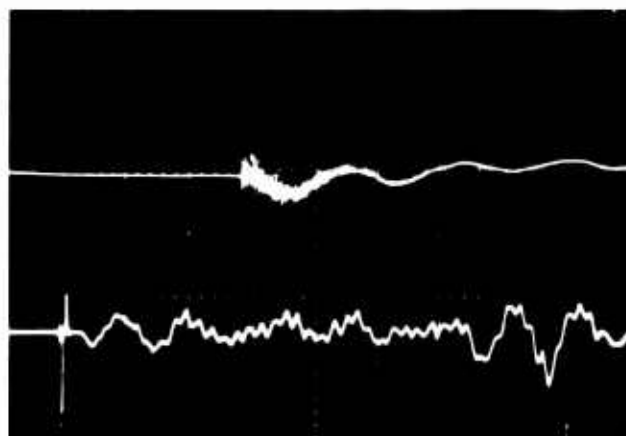
0°  
4100  $\mu\epsilon$ /division  
100  $\mu\text{sec}$ /division



45°  
2150  $\mu\epsilon$ /division  
5 msec/division

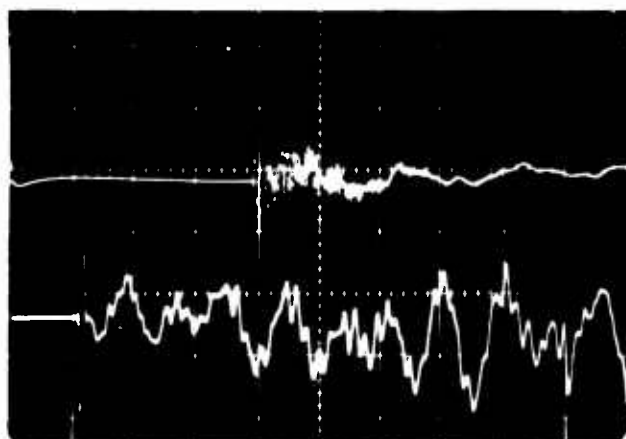
2140  $\mu\epsilon$ /division  
200  $\mu\epsilon$ /division

Pulse 2853



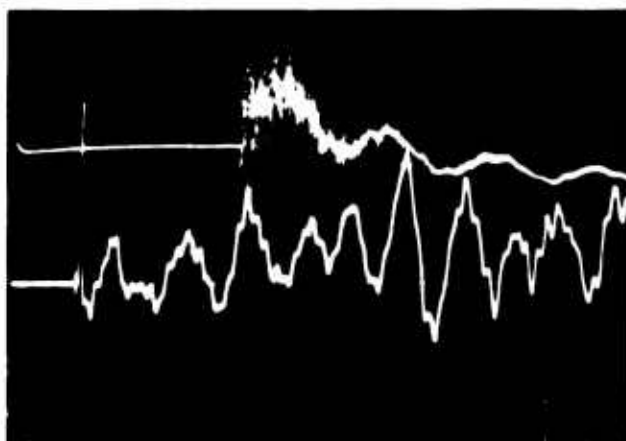
90°  
2060  $\mu\text{E}/\text{division}$   
5 msec/division

2060  $\mu\text{E}/\text{division}$   
100  $\mu\text{sec}/\text{division}$



135°  
860  $\mu\text{E}/\text{division}$   
5 msec/division

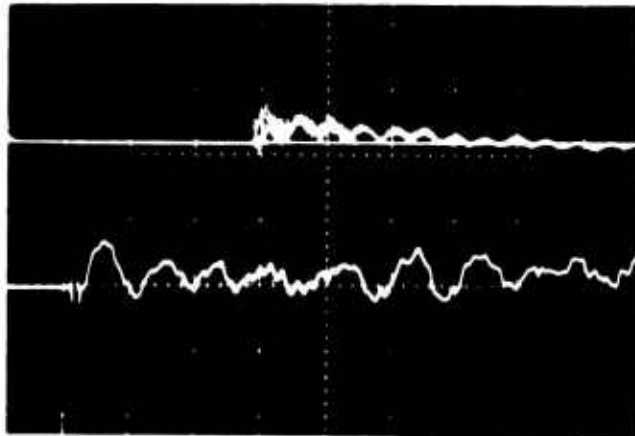
850  $\mu\text{E}/\text{division}$   
100  $\mu\text{sec}/\text{division}$



170°  
840  $\mu\text{E}/\text{division}$   
5 msec/division

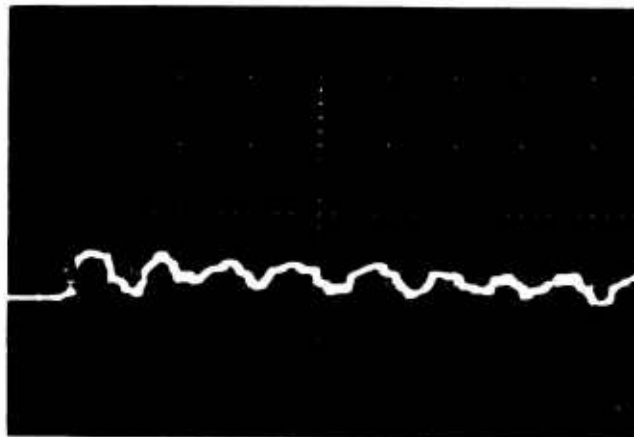
870  $\mu\text{E}/\text{division}$   
100  $\mu\text{sec}/\text{division}$

Pulse 2855

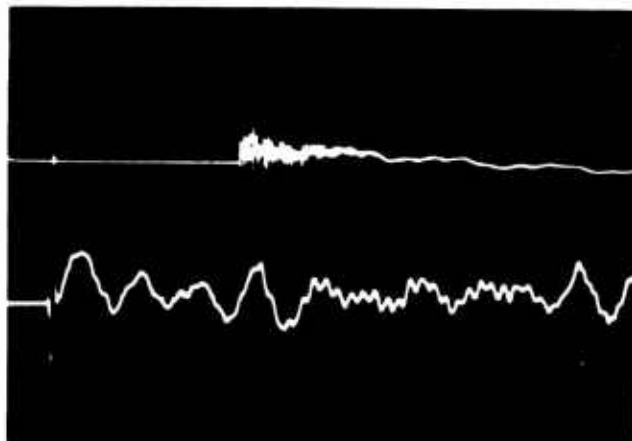


-45°  
2140  $\mu\epsilon$ /division  
5 msec/division

2140  $\mu\epsilon$ /division  
100  $\mu\text{sec}$ /division



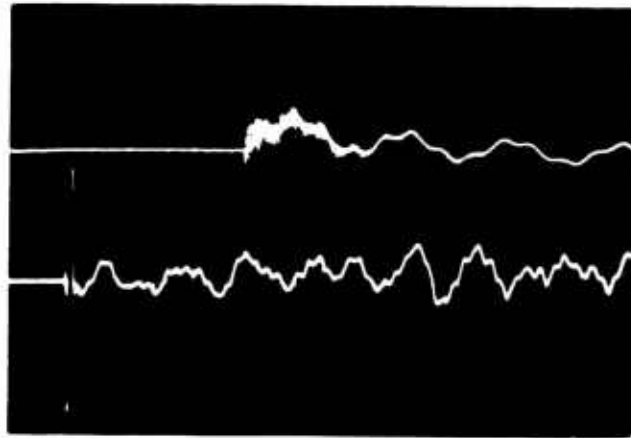
0°  
4100  $\mu\epsilon$ /division  
100  $\mu\text{sec}$ /division



45°  
2150  $\mu\epsilon$ /division  
5 msec/division

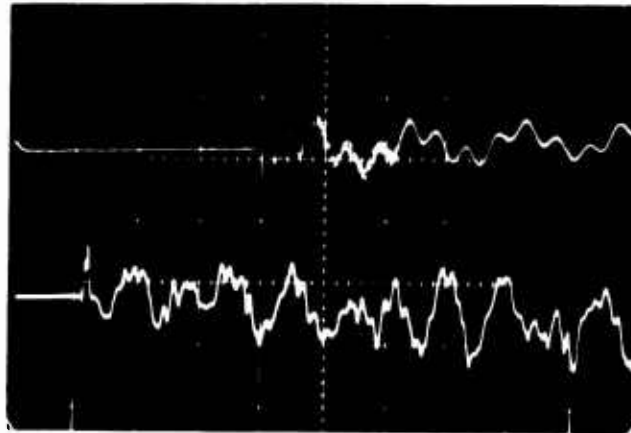
2140  $\mu\epsilon$ /division  
100  $\mu\text{sec}$ /division

Pulse 2855



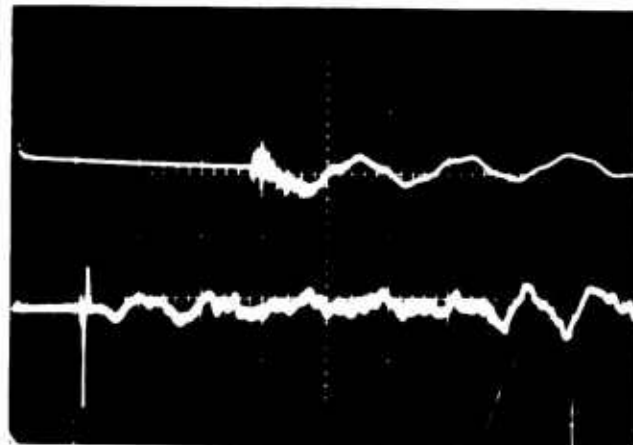
90°  
2060  $\mu\text{V}$ /division  
5 msec/division

2060  $\mu\text{V}$ /division  
100  $\mu\text{V}$ /division



135°  
860  $\mu\text{V}$ /division  
5 msec/division

850  $\mu\text{V}$ /division  
100  $\mu\text{V}$ /division

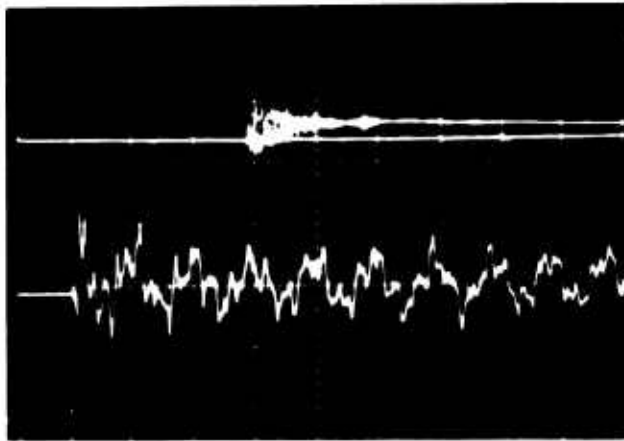


170°  
2100  $\mu\text{V}$ /division  
5 msec/division

2180  $\mu\text{V}$ /division  
100  $\mu\text{V}$ /division

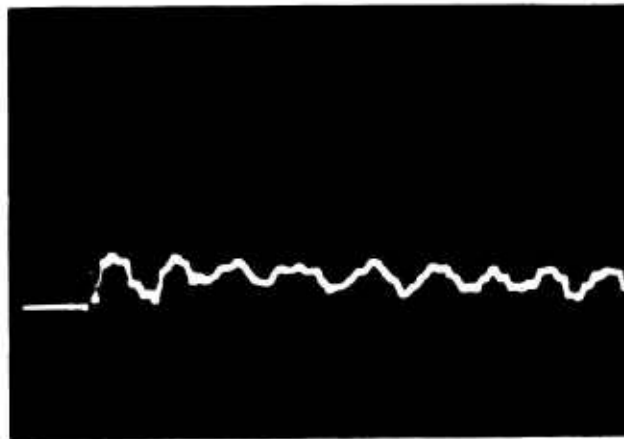


Pulse 2857

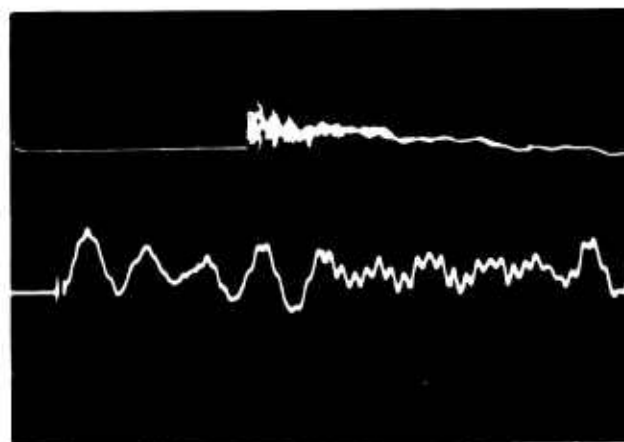


-10° Transverse  
4300  $\mu\epsilon$ /division  
5 msec/division

4300  $\mu\epsilon$ /division  
100  $\mu\text{sec}$ /division



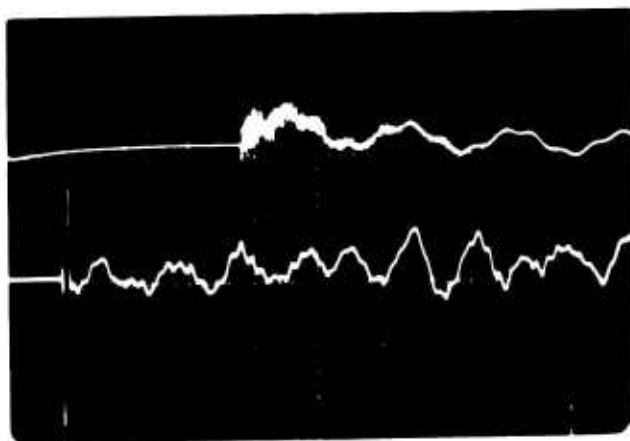
0°  
4100  $\mu\epsilon$ /division  
100  $\mu\text{sec}$ /division



45°  
2150  $\mu\epsilon$ /division  
5 msec/division

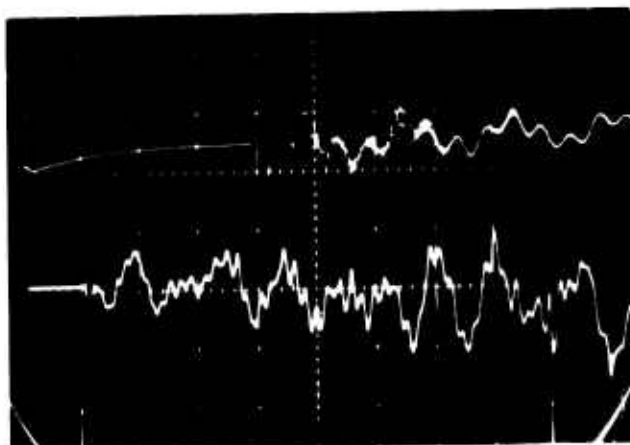
2140  $\mu\epsilon$ /division  
100  $\mu\text{sec}$ /division

Pulse 2857



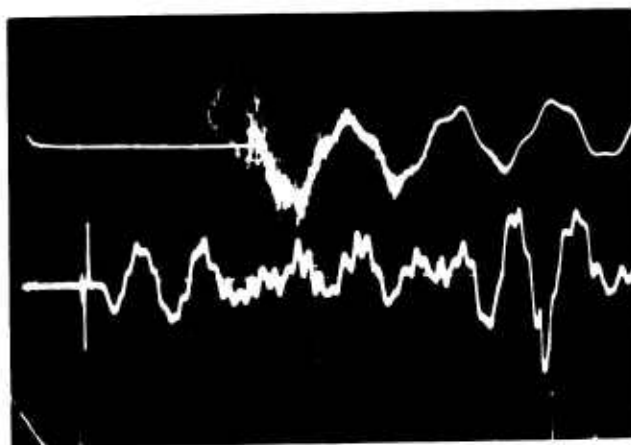
90°  
2060  $\mu\epsilon$ /division  
5 msec/division

2060  $\mu\epsilon$ /division  
100  $\mu\text{sec}$ /division



135°  
860  $\mu\epsilon$ /division  
5 msec/division

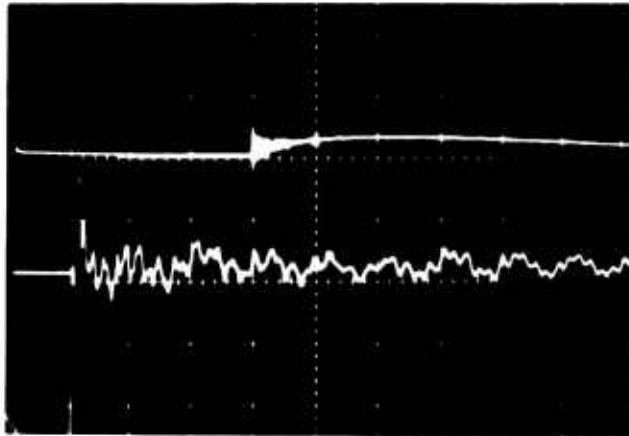
850  $\mu\epsilon$ /division  
100  $\mu\text{sec}$ /division



170°  
840  $\mu\epsilon$ /division  
5 msec/division

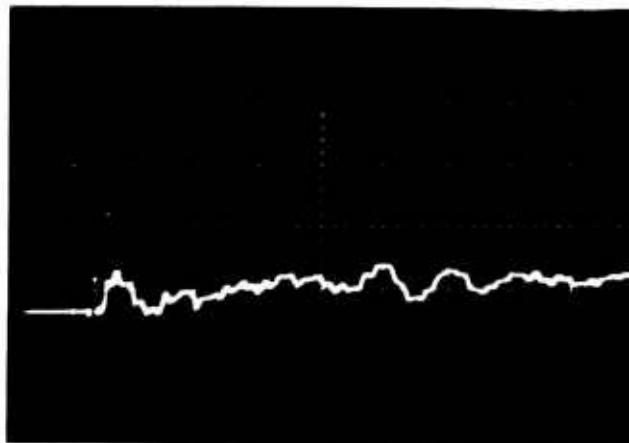
870  $\mu\epsilon$ /division  
100  $\mu\text{sec}$ /division

Pulse 2860

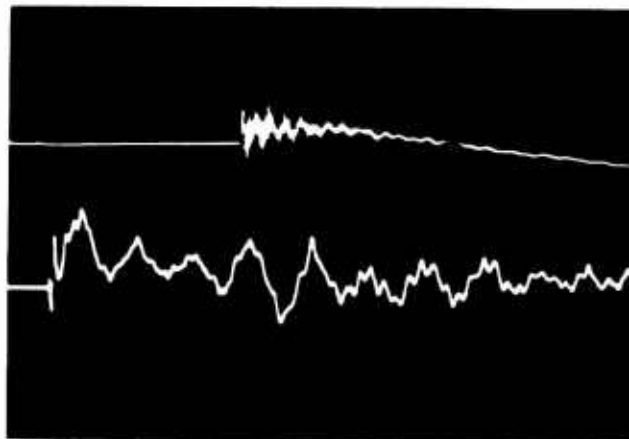


-10° Transverse  
4300  $\mu\epsilon$ /division  
5 msec/division

4300  $\mu\epsilon$ /division  
100  $\mu\text{sec}$ /division



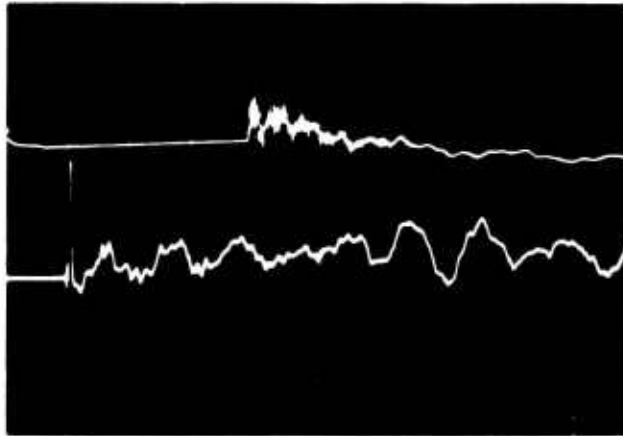
0°  
4100  $\mu\epsilon$ /division  
100  $\mu\text{sec}$ /division



45°  
2150  $\mu\epsilon$ /division  
5 msec/division

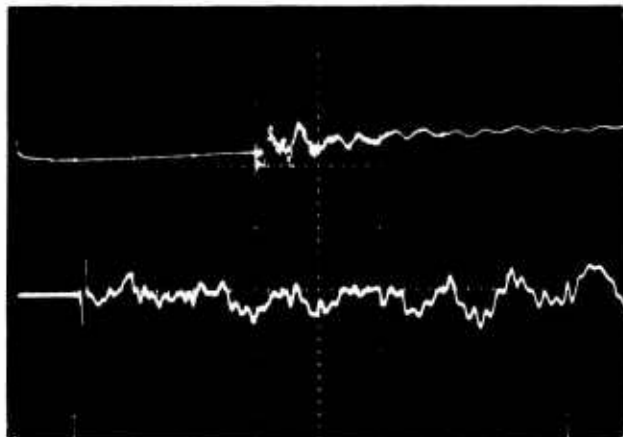
2140  $\mu\epsilon$ /division  
100  $\mu\text{sec}$ /division

Pulse 2860



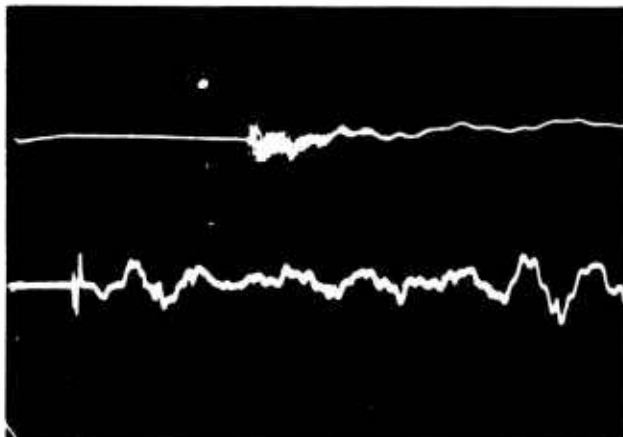
90°  
2060  $\mu\epsilon$ /division  
5 msec/division

2060  $\mu\epsilon$ /division  
100  $\mu\text{sec}$ /division



135°  
2160  $\mu\epsilon$ /division  
5 msec/division

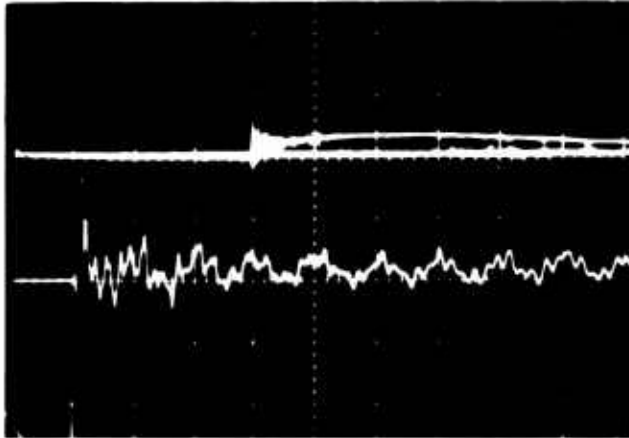
2120  $\mu\epsilon$ /division  
100  $\mu\text{sec}$ /division



170°  
2100  $\mu\epsilon$ /division  
5 msec/division

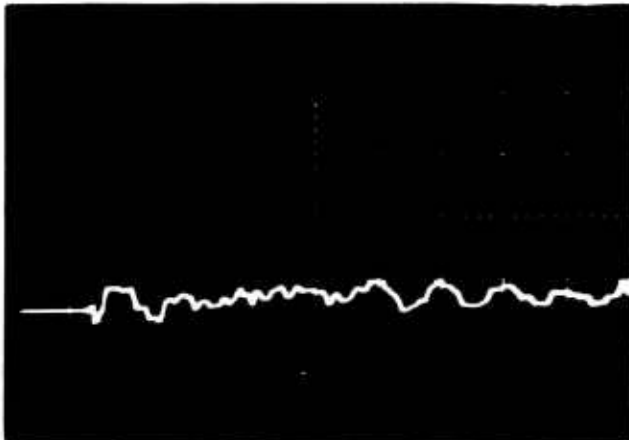
2180  $\mu\epsilon$ /division  
100  $\mu\text{sec}$ /division

Pulse 2861

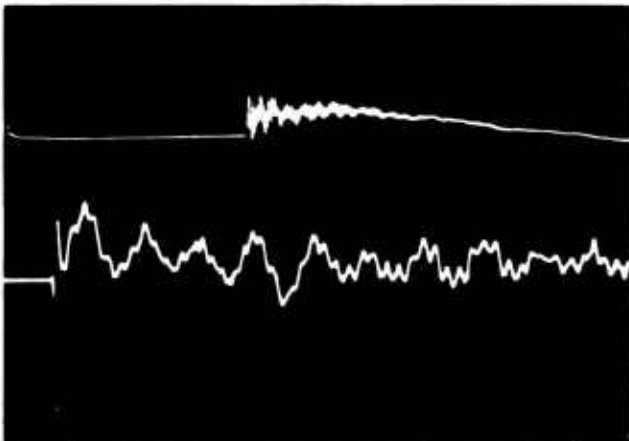


-10° Transverse  
4300  $\mu\epsilon$ /division  
5 msec/division

4300  $\mu\epsilon$ /division  
100  $\mu\text{sec}$ /division



0°  
4100  $\mu\epsilon$ /division  
100  $\mu\text{sec}$ /division



45°  
2150  $\mu\epsilon$ /division  
5 msec/division

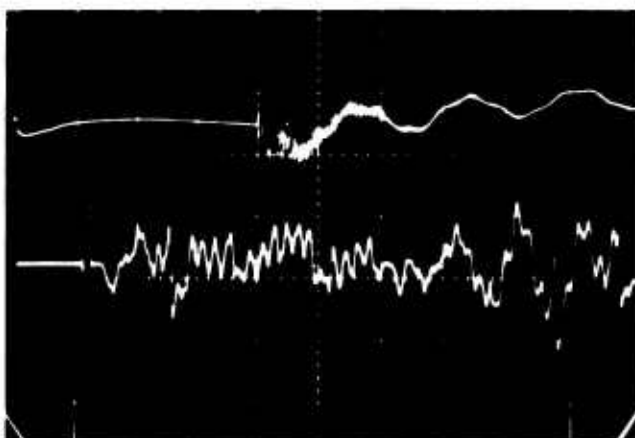
2140  $\mu\epsilon$ /division  
100  $\mu\text{sec}$ /division

Pulse 2861



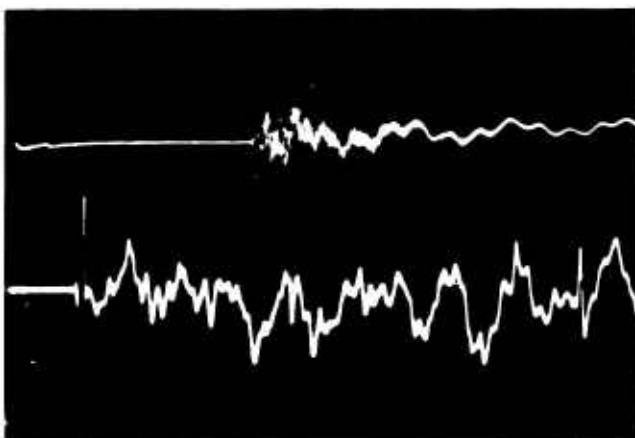
90°  
2060  $\mu\epsilon$ /division  
5 msec/division

2060  $\mu\epsilon$ /division  
100  $\mu\text{sec}$ /division



135°  
860  $\mu\epsilon$ /division  
5 msec/division

850  $\mu\epsilon$ /division  
100  $\mu\text{sec}$ /division



170°  
840  $\mu\epsilon$ /division  
5 msec/division

870  $\mu\epsilon$ /division  
100  $\mu\text{sec}$ /division

APPENDIX E  
QUARTZ GAUGE RECORDS

*Preceding Page BLANK -*

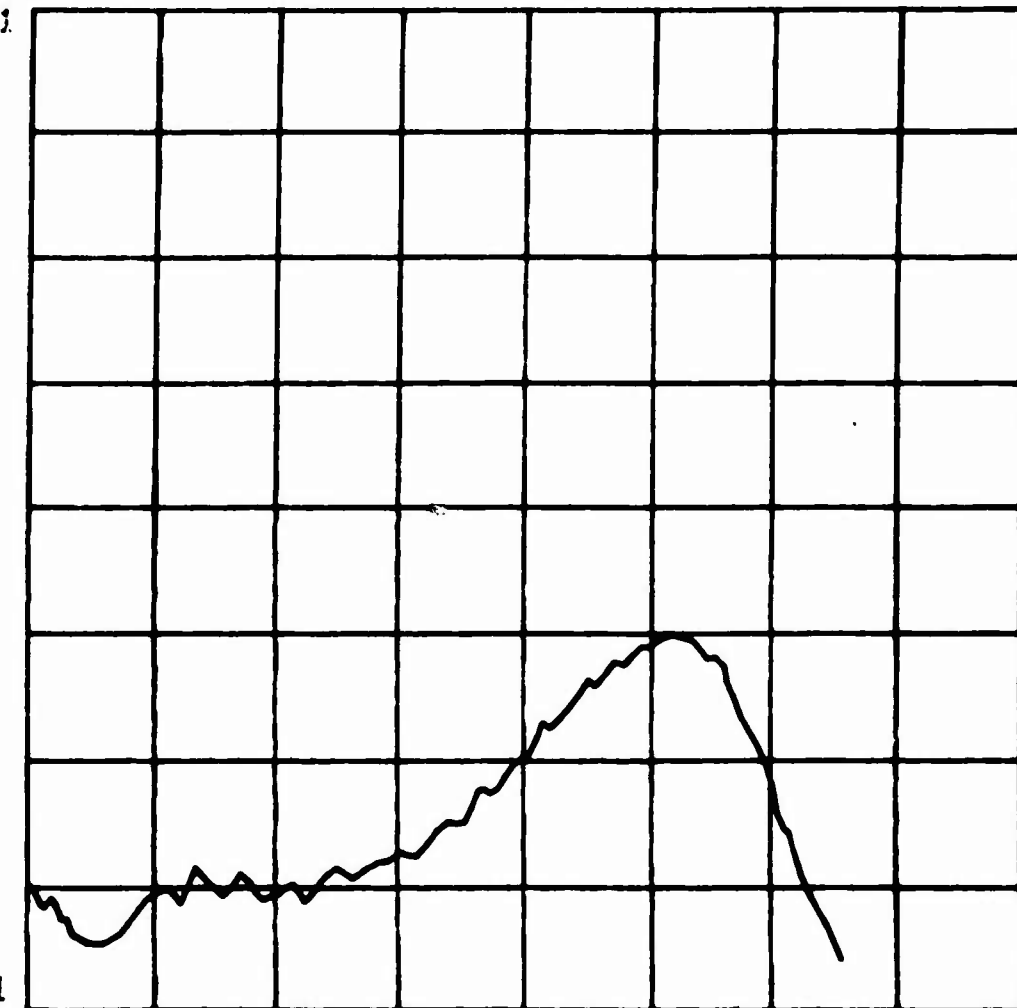
QUARTZ GAUGE

2841 QG

+ .780+01

VOLT

- .100+01



+ .000+00

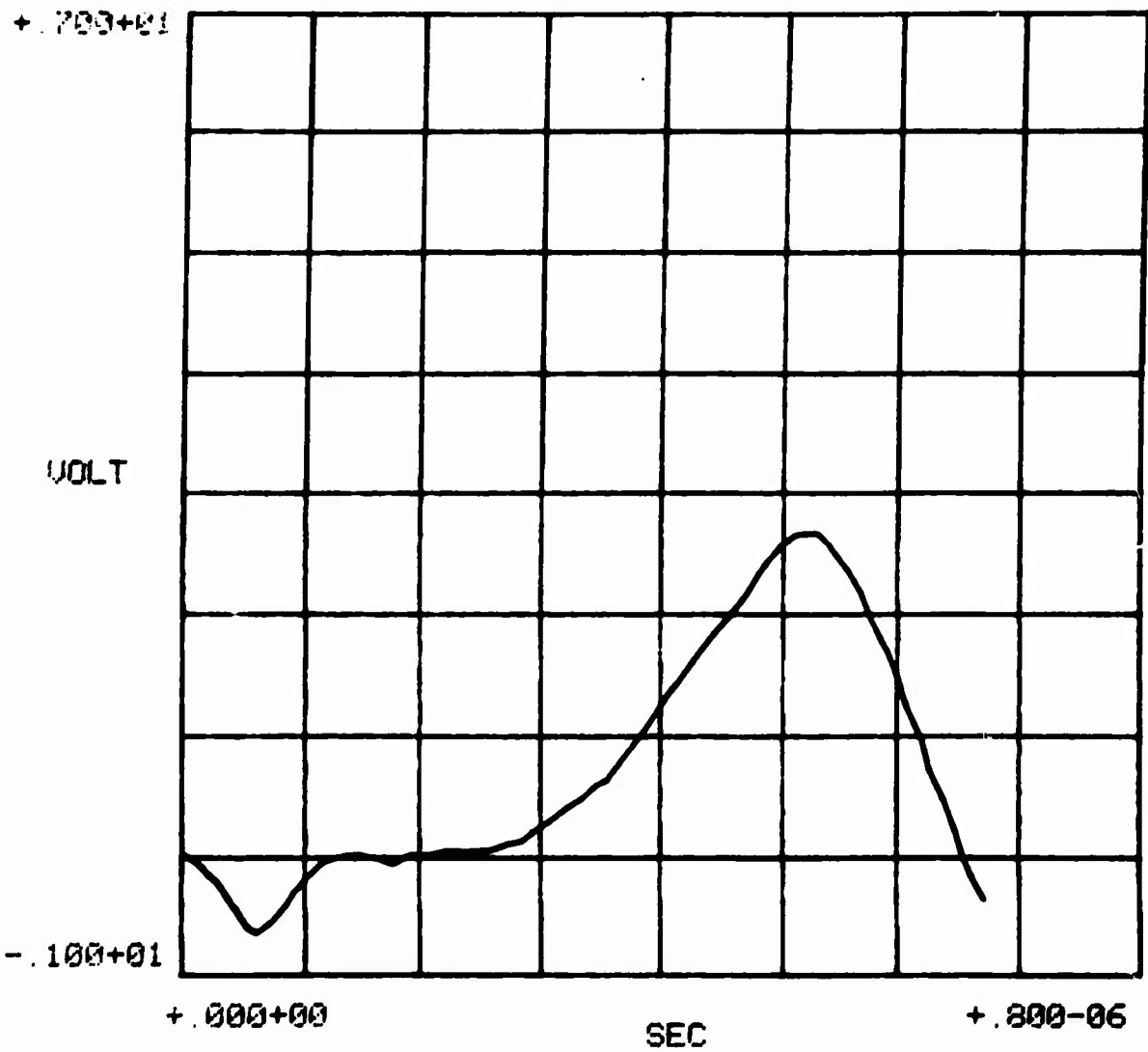
SEC

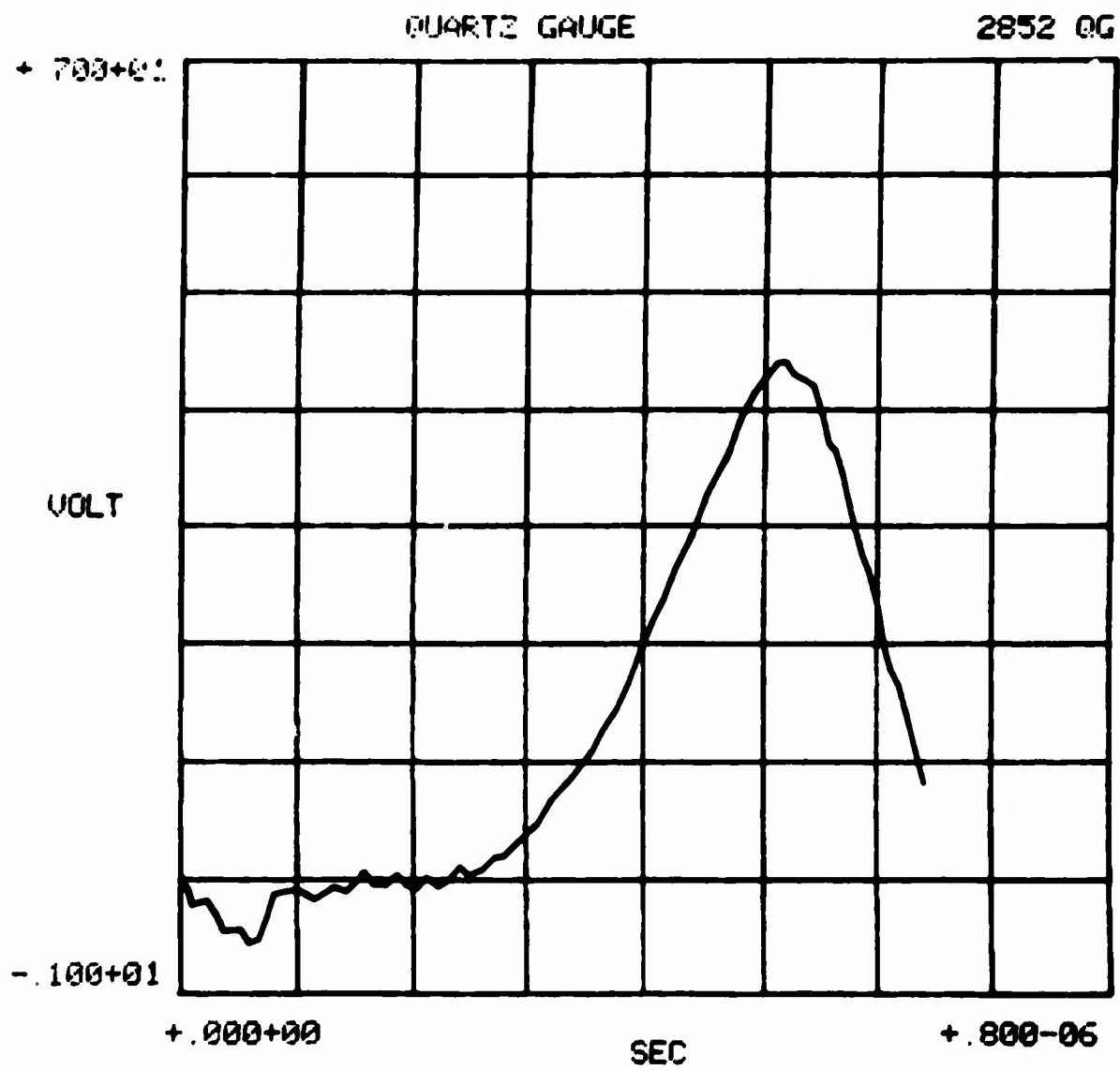
+ .800-06

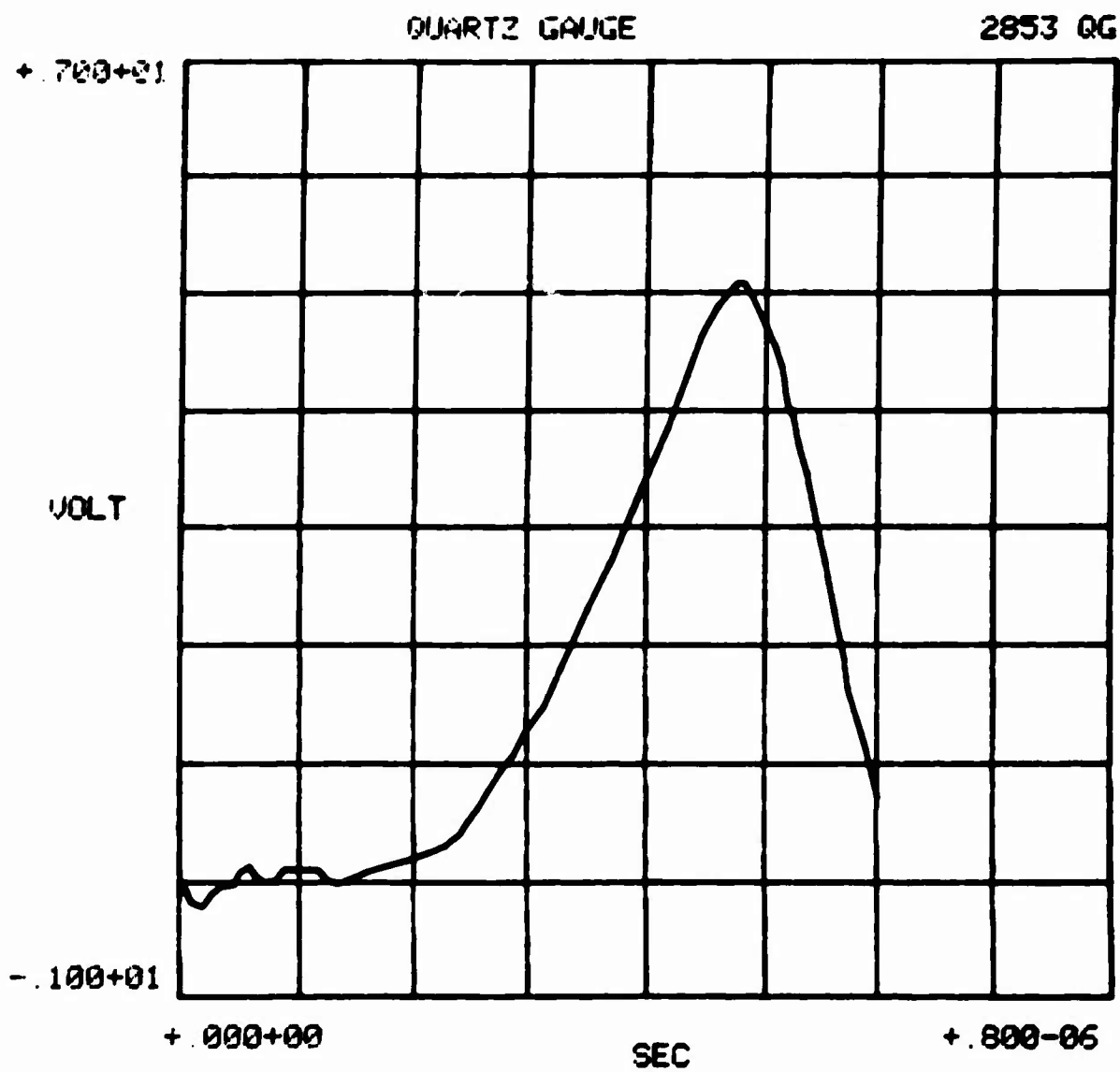


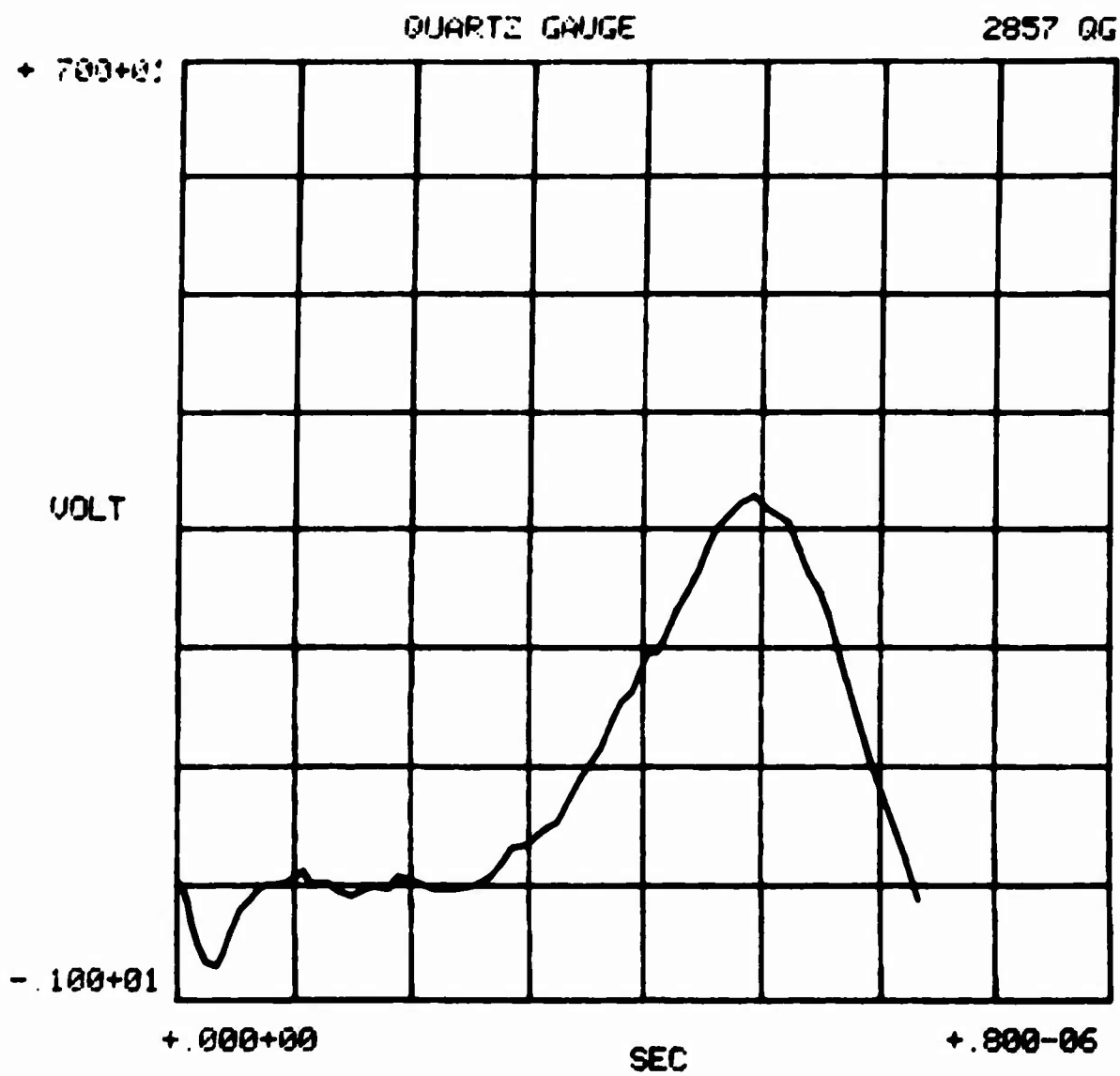
QUARTZ GAUGE

2847 QG



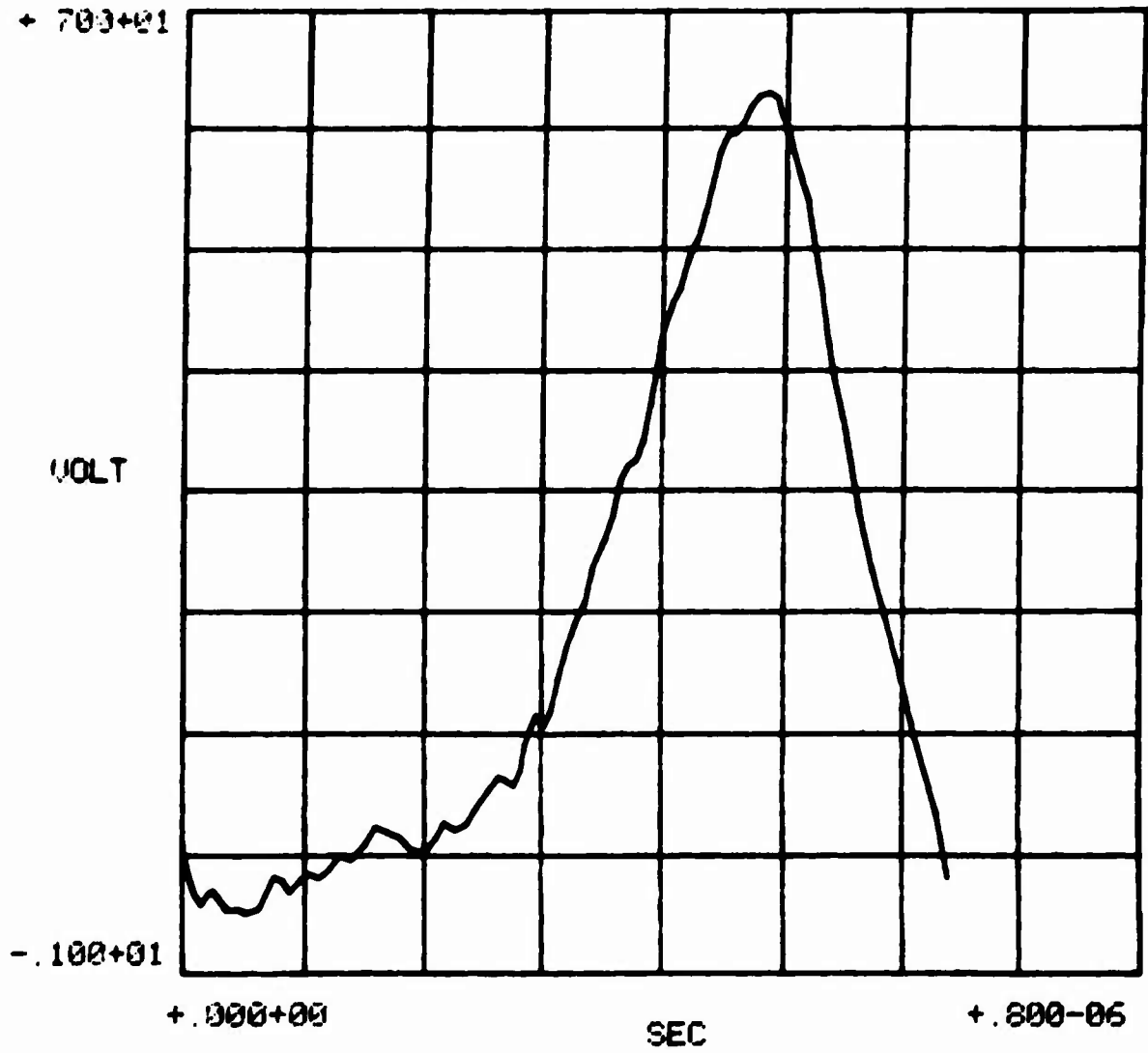


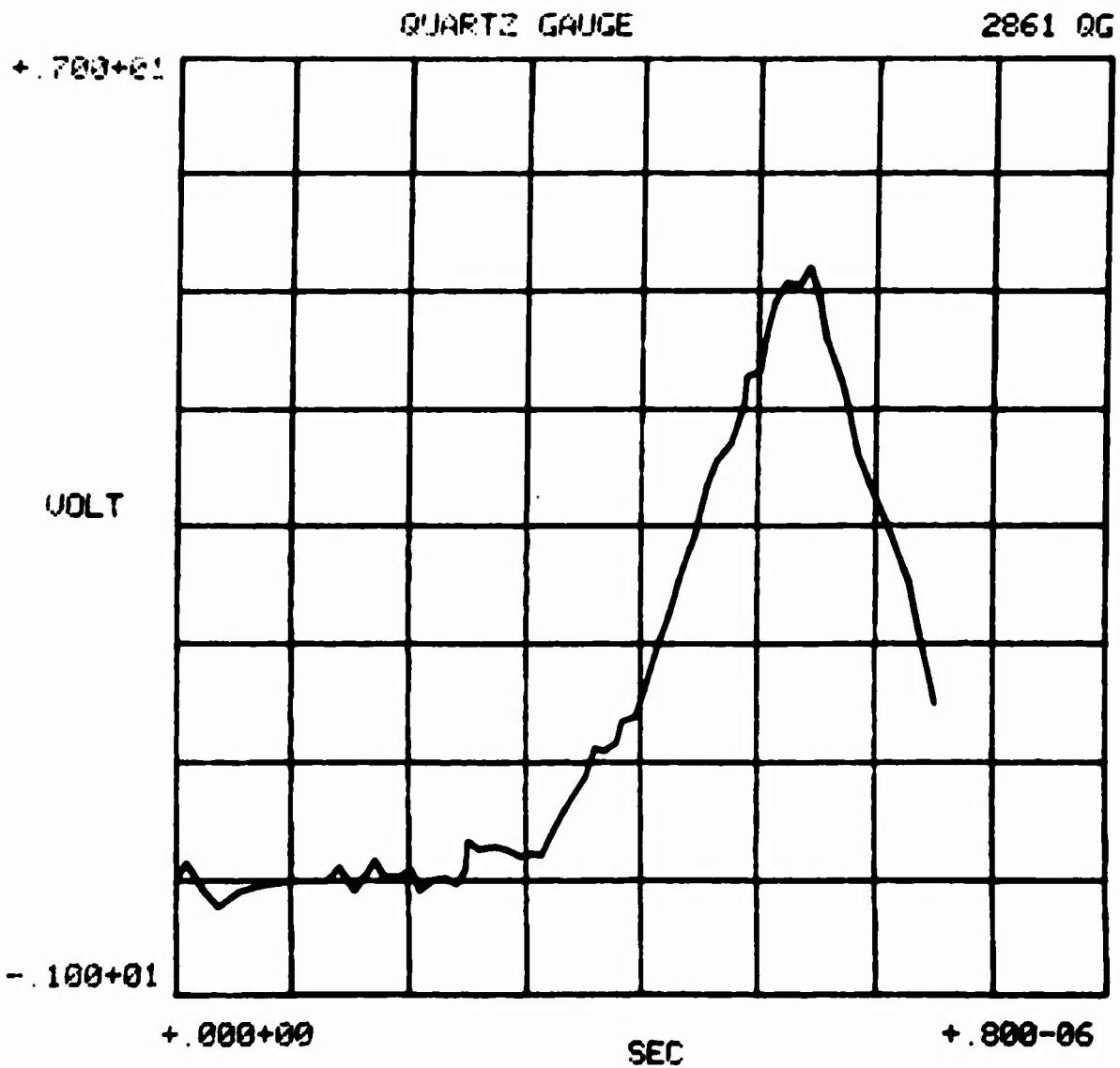




QUARTZ GAUGE

2859 OG





## DISTRIBUTION LIST

### DEPARTMENT OF DEFENSE

Director  
Defense Advanced Rsch. Proj. Agency  
ATTN: Strategic Tech. Office

Defense Documentation Center  
Cameron Station  
12 cy ATTN: TC

Director  
Defense Intelligence Agency  
ATTN: DT-2, Wpns. & Sys. Div.  
ATTN: DI-7D  
ATTN: DT-1C, Nuc. Eng. Branch

Director  
Defense Nuclear Agency  
ATTN: SPAS  
ATTN: DOST  
ATTN: TISI, Archives  
ATTN: SPSS  
3 cy ATTN: TITL, Tech. Library  
ATTN: SPTD  
ATTN: STSP

Commander, Field Command  
Defense Nuclear Agency  
ATTN: FCTMOF  
ATTN: FCTMD  
ATTN: FCPR  
ATTN: FCTMOT

Chief  
Livermore Division, Field Command, DNA  
Lawrence Livermore Laboratory  
ATTN: FCPRL

Under Secretary of Def. for Rsch. & Engr.  
ATTN: S&SS (OS)

### DEPARTMENT OF THE ARMY

Director  
BMD Advanced Tech. Ctr.  
Huntsville Office  
ATTN: ATC-T, Melvin T. Capps  
ATTN: Marcus Whitfield

Program Manager  
BMD Program Office  
ATTN: DACS-BMZ  
ATTN: DACS-BMT, John Shea  
ATTN: DACS-BMZ-D, Julian Davidson  
ATTN: DACS-BMT, Clifford E. McLain

Commander  
BMD System Command  
ATTN: BDMSC-TEN, Noah J. Hurst

Dep. Chief of Staff for Rsch. Dev. & Acq.  
ATTN: NCB Division

### DEPARTMENT OF THE ARMY (Continued)

Commander  
Harry Diamond Laboratories  
ATTN: DRXDO-TF, Robert B. Oswald, Jr.  
ATTN: DRXDO-RBH, James H. Gwaltney  
ATTN: DRXDO-NP

Commander  
Picatinny Arsenal  
ATTN: SARPA-FR-E, Louis Avrami  
ATTN: SARPA-ND-C-T, Donald Miller  
ATTN: SMUPA-MD, Henry Opat  
ATTN: Al Loeb

Director  
U.S. Army Ballistic Research Labs.  
ATTN: Richard Vitali  
ATTN: J. H. Keefer, DRDAR-BLE  
ATTN: William J. Schuman, Jr., DRXRD-BVL  
ATTN: J. T. Frasier, DRXBR-TB  
ATTN: Julius J. Meszaros, DRXBR-X  
ATTN: Robert E. Eichelberger

Commander  
U.S. Army Mat. & Mechanics Rsch. Ctr.  
ATTN: DRXMR-HH, John F. Dignam

Commander  
U.S. Army Materiel Dev. & Readiness Cmd.  
ATTN: DRCDE-D, Lawrence Flynn

Commander  
U.S. Army Missile Command  
ATTN: DRS-RKP, W. B. Thomas  
ATTN: DRSMI-RRR, Bud Gibson  
ATTN: DRSMI-XS, Chief Scientist

Commander  
U.S. Army Nuclear Agency  
ATTN: MONA-SA  
ATTN: ATCA-NAW  
ATTN: CDC-NVA  
ATTN: MONA-WE

### DEPARTMENT OF THE NAVY

Chief of Naval Material  
ATTN: Mat. 0323, Irving Jaffe

Chief of Naval Research  
ATTN: Code 464, Thomas P. Quinn

Director  
Naval Research Laboratory  
ATTN: Code 2600, Tech. Lib.  
ATTN: Code 5180, Mario Persechino  
ATTN: Code 7770, Gerald Cooperstein

Commander  
Naval Sea Systems Command  
ATTN: 0333A, Marlin A. Kinna

DEPARTMENT OF THE NAVY (Continued)

Officer-in-Charge  
Naval Surface Weapons Center  
ATTN: Code WA07, Carson Lyons  
ATTN: Code WR10, Joseph Petes  
ATTN: Code WA501, Navy Nuc. Prgms. Off.

Commanding Officer  
Naval Weapons Evaluation Facility  
ATTN: Lawrence R. Oliver

Director  
Strategic Systems Project Office  
ATTN: NSP-272

DEPARTMENT OF THE AIR FORCE

Commandant  
AF Flight Dynamics Laboratory, AFSC  
ATTN: FXG

AF Materials Laboratory, AFSC  
ATTN: MAS  
ATTN: MBC, Donald L. Schmidt  
ATTN: MBE, George F. Schmitt  
ATTN: LPH, Gordon Griffith  
ATTN: T. Nicholas  
ATTN: LTM

AF Rocket Propulsion Laboratory, AFSC  
ATTN: RTSN, G. A. Beale

AF Weapons Laboratory, AFSC  
ATTN: Al Sharp  
ATTN: DYS  
ATTN: DYT  
ATTN: DYV  
ATTN: SAB  
ATTN: Tech. Review  
ATTN: SUL  
ATTN: Dr. Minge  
2 cy ATTN: NTO

Headquarters  
Air Force Systems Command  
ATTN: XRTO  
ATTN: SOSS

Commander  
Foreign Technology Division, AFSC  
ATTN: TDFBD, J. D. Pumphrey  
ATTN: TDPTN  
ATTN: PDBG

Hq. USAF/RD  
ATTN: RDPM  
ATTN: RDQSM

SAMSO/DY  
ATTN: DYS

SAMSO/MN  
ATTN: MNNH  
ATTN: MNNR

SAMSO/RS  
ATTN: RSS  
ATTN: RST  
ATTN: RSSE

DEPARTMENT OF ENERGY

Division of Military Application  
Department of Energy  
ATTN: Doc. Con. for Res. & Dev. Branch

University of California  
Lawrence Livermore Laboratory  
ATTN: Joseph E. Keller, Jr., L-125  
ATTN: L. Woodruff  
ATTN: Joseph B. Knox, L-216  
ATTN: D. Hanner

Los Alamos Scientific Laboratory  
ATTN: Doc. Con. for John McQueen  
ATTN: Doc. Con. for J. W. Taylor  
ATTN: Doc. Con. for R. S. Thurston  
ATTN: Doc. Con. for R. Dingus  
ATTN: Doc. Con. for Robert Skaggs

Sandia Laboratories  
Livermore Laboratory  
ATTN: Doc. Con. for 8131, H. F. Norris, Jr.  
ATTN: Doc. Con. for Tech. Library

Sandia Laboratories  
ATTN: Doc. Con. for Albert Chabai  
ATTN: Doc. Con. for M. Cowan  
ATTN: Doc. Con. for R. R. Boade  
ATTN: Doc. Con. for Thomas B. Cook

DEPARTMENT OF DEFENSE CONTRACTORS

Acurex Corporation  
ATTN: C. Nardo  
ATTN: J. Courtney  
ATTN: J. Huntington  
ATTN: R. Rindal

Aerospace Corporation  
ATTN: W. Mann  
ATTN: Richard Crollius, A2-Rm. 1027  
ATTN: W. Barry  
ATTN: J. McClelland  
ATTN: R. Mortensen  
ATTN: H. Blaes  
ATTN: Robert L. Strickler

Avco Research & Systems Group  
ATTN: George Weber, J230  
ATTN: John E. Stevens, J100  
ATTN: Doc. Control  
ATTN: William Broding  
ATTN: John Gilmore, J400

Battelle Memorial Institute  
ATTN: Technical Library  
ATTN: E. Unger  
ATTN: Merwyn R. Vanderlind

The Boeing Company  
ATTN: Robert Dyrda  
ATTN: Brian Lempiere

California Research & Technology, Inc.  
ATTN: Ken Kreyenhagen

Calspan Corporation  
ATTN: M. S. Holden



DEPARTMENT OF DEFENSE CONTRACTORS (Continued)

University of Dayton  
Industrial Security Super, KL-505  
ATTN: Hallock F. Swift  
ATTN: D. Gerdman

Effects Technology, Inc.  
ATTN: Richard Parisse  
ATTN: Robert Mengler

Ford Aerospace & Communications Operations  
ATTN: P. Spangler

General Electric Company  
Space Division  
ATTN: Daniel Edelman  
ATTN: Carl Anderson  
ATTN: G. Harrison  
ATTN: Phillip Cline  
ATTN: A. Martellucci

General Electric Company  
TEMPO-Center for Advanced Studies  
ATTN: DASIAC

General Research Corporation  
ATTN: T. Stathacopoulos

Institute for Defense Analyses  
ATTN: Joel Bengston  
ATTN: IDA Librarian

Ion Physics Corporation  
ATTN: Robert D. Evans

Kaman Avidyne  
Division of Kaman Sciences Corp.  
ATTN: E. S. Criscione  
ATTN: Ray Reutinick  
ATTN: Norman P. Hobbs

Kaman Sciences Corporation  
ATTN: Thomas Meagher  
ATTN: John Keith  
ATTN: Frank H. Shelton  
ATTN: Donald C. Sachs  
ATTN: John R. Hoffman

Lockheed Missiles & Space Co., Inc.  
ATTN: R. Walz, Dept. 81-14

Lockheed Missiles & Space Co., Inc.  
ATTN: F. G. Borgardt

Lockheed Missiles & Space Co., Inc.  
ATTN: T. R. Fortune

Martin Marietta Corporation  
Orlando Division  
ATTN: James M. Potts, MP-61  
ATTN: William Gray, MP-61  
ATTN: Laird Kinnaid  
ATTN: Gene Aiello

McDonnell Douglas Corporation  
ATTN: H. Hurwicz  
ATTN: R. J. Reck  
ATTN: J. F. Garibotti  
ATTN: H. M. Berkowitz  
ATTN: E. A. Fitzgerald  
ATTN: L. Cohen

DEPARTMENT OF DEFENSE CONTRACTORS (Continued)

National Academy of Sciences  
ATTN: National Materials Advisory Board for  
Donald G. Groves

Northrop Corporation  
ATTN: Don Hicks

Pacific-Sierra Research Corp.  
ATTN: Gary Lang

Physics International Company  
ATTN: Doc. Con. for James Shea  
ATTN: Doc. Con. for V. Buck

Prototype Development Associates, Inc.  
ATTN: John Slaughter  
ATTN: John McDonald

R&D Associates  
ATTN: Cyrus P. Knowles  
ATTN: William R. Graham, Jr.  
ATTN: F. A. Field  
ATTN: Paul Rausch

The Rand Corporation  
ATTN: J. J. Mate

Raytheon Company  
ATTN: Library

Science Applications, Inc.  
ATTN: Dwane Hove  
ATTN: W. Yengst  
ATTN: John Warner  
ATTN: G. Ray  
ATTN: Olan Nance

Science Applications, Inc.  
ATTN: G. Burghart  
ATTN: Carl Swain  
ATTN: Lyle Dunbar

Science Applications, Inc.  
ATTN: William R. Seebaugh  
ATTN: William M. Layson

Southern Research Institute  
ATTN: C. D. Pears

SRI International  
ATTN: Herbert E. Lindberg  
ATTN: Donald Curran  
ATTN: George R. Abrahamson

Systems, Science & Software, Inc.  
ATTN: Russell E. Duff  
ATTN: G. A. Gurtman

Terra Tek, Inc.  
ATTN: Sidney Green

TRW Defense & Space Sys. Group  
6 cy ATTN: R. K. Plebuch, R1-2078/P. Brandt,  
E1-2006/D. H. Baer, R1-2136/P. K.  
Dai, R1/2170/W. W. Wood/T. G. Williams  
2 cy ATTN: I. E. Alber, R1-1008

TRW Defense & Space Sys. Group  
5 cy ATTN: E. Y. Wong, 527/712/V. Blankenship/  
W. Polich/L. Berger/E. W. Allen, 520/141